NUMERICAL SIMULATION OF INFILTRATION AND EVAPORATION FOR UNSATURATED INFINITE SOIL SLOPES

A THESIS SUBMITTED TO

THE GRADUATE SCHOOL OF NATURAL AND APPLIED SCIENCES

OF

MIDDLE EAST TECHNICAL UNIVERSITY

BY

MELİH BİRHAN KENANOĞLU

IN PARTIAL FULLFILLMENT OF THE REQUIREMENTS

FOR

THE DEGREE OF MASTER OF SCIENCE

IN

CIVIL ENGINEERING

FEBRUARY 2017

Approval of the thesis:

NUMERICAL SIMULATION OF INFILTRATION AND EVAPORATION FOR UNSATURATED INFINITE SOIL SLOPES

Submitted by **MELİH BİRHAN KENANOĞLU** in partial fulfillment fo the requirements for the degree of **Master of Science in Civil Engineering Department, Middle East Technical University** by,

Prof. Dr. Gülbin Dural Ünver
Dean, Graduate School of **Natural and Applied Sciences** _____

Prof. Dr. İsmail Özgür Yaman
Head of Department, **Civil Engineering** _____

Asst. Prof. Dr. Nabi Kartal Toker
Supervisor, **Civil Engineering Dept., METU** _____

Asst. Prof. Dr. Nejan Huvaj Sarıhan
Co-Supervisor, **Civil Engineering Dept., METU** _____

Examining Committee Members:

Asst. Prof. Dr. M. Tuğrul Yılmaz
Civil Engineering Dept., METU _____

Asst. Prof. Dr. Nabi Kartal Toker
Civil Engineering Dept., METU _____

Asst. Prof. Dr. Nejan Huvaj Sarıhan
Civil Engineering Dept., METU _____

Asst. Prof. Dr. Onur Pekcan
Civil Engineering Dept., METU _____

Assoc. Prof. Dr. Mehmet Barış Can Ülker
Earthquake Engineering and Disaster Management Institute., ITU _____

Date: 03.02.2017

I hereby declare that all information in this document has been obtained and presented in accordance with academic rules and ethical conduct. I also declare that, as required by these rules and conduct, I have fully cited and referenced all material and results that are not original to this work.

Name, Last name: Melih Birhan Kenanoğlu

Signature:

ABSTRACT

NUMERICAL SIMULATION OF INFILTRATION AND EVAPORATION FOR UNSATURATED INFINITE SOIL SLOPES

Kenanoğlu, Melih Birhan
M. S., Department of Civil Engineering
Supervisor: Asst. Prof. Dr. Nabi Kartal Toker
Co-Supervisor: Asst. Prof. Dr. Nejan Huvaj Sarıhan
February 2017, 130 pages

Rainfall triggered landslides are common threat in many regions of the world and cause loss of lives and properties. These are shallow failures (typically 3-5 m depths from the ground surface) that occur along a plane parallel to the ground surface where the groundwater level is located at significant depths below, and they are triggered after a heavy rainfall in a short time or after days of lower intensity rainfall (Huvaj et al., 2013). Considering a failure plane oriented parallel to the ground surface, infinite slope models are used to analyse stability of these landslides after rainfall infiltration in general.

In this study, a numerical model was developed to simulate the infiltration and evaporation in the unsaturated infinite soil slopes by considering the effect of wetting-drying hysteresis, as well as transitions between the two regimes. The scanning curve model fits the general shape of retention curves found in the literature. The incremental form of Darcy's equation was used to evaluate water flow within the infinite slope in case of both infiltration and evaporation. The proposed numerical model was validated with results of infiltration column test.

The flow model was used with infinite slope analysis (without coupling hydraulic and mechanical behavior at the element scale), and a parametric study was conducted to obtain suction and water content profiles, as well as rainfall intensity-duration thresholds for failure. Three distinct mechanisms that led to instability was observed, depending on soil proporties and rainfall intensity. The understanding of various mechanisms of landslide trigger due to rainfall may eventually pave the road for areal models and early warning systems to mitigate the hazard of such landslides.
The proposed hydraulic model can also be used in incremental form to predict suction in different hydromechanical frameworks for other physical problems.

Keywords: Rainfall-triggered landslides, Darcy's equation, infiltration, soil water characteristic curves, scanning curves.

ÖZ

SUYA DOYGUN OLMAYAN SONSUZ ŞEVLERDE İNFİLTRASYON VE BUHARLAŞMANIN NUMERİK MODELLENMESİ

Kenanoğlu, Melih Birhan
Yüksek Lisans, İnşaat Mühendisliği Bölümü
Tez Yöneticisi: Yrd. Doç. Dr. Nabi Kartal Toker
Ortak Tez Yöneticisi: Yrd. Doç. Dr. Nejan Huvaj Sarıhan
Şubat 2017, 130 sayfa

Yağmur tarafından tetiklenen heyelanlar dünyanın birçok bölgesinde yaygın olup, birçok can ve mal kaybına sebep olmaktadır. Bu sığ heyelanlar yeraltı su seviyesinin önemli derecede aşağıda kaldığı yer yüzeyine paralel doğrultuda, tipik olarak 3-5 m derinlikte gerçekleşmekte olup kısa süreli şiddetli yağmurlar ile veya birkaç gün süren düşük şiddetli yağmurlar ile tetiklenirler (Huvaj vd., 2013). Yağmur suyunun infiltrasyonu ile tetiklenen bu heyelanların stabilitesi, kayma yüzeyinin yer yüzeyine paralel olması düşünülerek genellikle sonsuz şev modelleri ile incelenir.

Bu çalışmada, suya doygun olmayan sonsuz bir şevdeki infiltrasyon ve buharlaşmanın simulasyonun yapılabildiği ve ıslanma-kuruma sırasındaki histeresis etkisinin ve de bu iki rejim arası geçişlerinde dahil edildiği bir numerik model geliştirilmiştir. Geçiş eğrisi modeli literatürde bulunan geçiş eğrilerinin şekilleri ile uyumlu olmuştur. Histeresis modellemesi için önerilen ilişkiler farklı modellerde (örneğin, elastoplastisite modelleri) veya diğer fiziksel problemler için artımlı formda emmeyi tahmin etmek üzere kullanılabilir. Darcy denklemi artımlı formda düşünülerek sonsuz şevde infiltrasyon ve buharlaşma durumlarındaki su akışını değerlendirmede kullanılmıştır. Önerilen nümerik model infiltrasyon kolonu deneyi sonuçları kullanılarak doğrulanmaya çalışılmıştır.

Akış modeli sonsuz şev analizinde (eleman düzeyinde hidrolik ve mekanik davranışı birbirine bağlamadan) kullanılmıştır. Yine yenilme için yağmur şiddeti-süre sınır eğrileri elde etme ve matrik emme ve su muhtevası profillerini belirleme amacıyla parametrik çalışma yürütülmüştür. Burada zemin özelliklerine ve yağmur şiddetine bağlı olarak çok çeşitli yenilme mekanizmaları gözlenmiştir. Yağmur nedeniyle tetiklenen heyelanlar arkasındaki çeşitli mekanizmaları anlamak, heyelandan kaynaklı tehlikeleri azaltacak alansal modellerin ve erken uyarı sistemlerinin geliştirilmesinin yolunu açacaktır.
Geliştirilen hidrolik model farklı fiziksel problemlerde için hidromekanik yapının artımlı olarak modellenmesinde kullanılabilir.

Anahtar Kelimeler: Yağmurla tetiklenen heyelanlar, Darcy denklemi, infiltrasyon, su tutma eğrileri, geçiş eğrileri.

Dedicated to my beloved father,

Ali Rıza Kenanoğlu

ACKNOWLEDGEMENTS

I would like to express my greatest gratitude to my dear advisor, Asst. Prof. Dr. Nabi Kartal Toker for his theoretical support, precious guidance, encouragement and kind attitude throughout our study. He led me to accomplish this study and his intelligence and technical advices shaped my mind. I consider myself hugely privileged to have worked with him.

The most difficult part in this study is to write this passage. Because, I don't have any idea about how can I express my gratitude to my dear co-advisor, Asst. Prof. Dr. Nejan Huvaj.

I would like to express my gratitude to my thesis committee members: Assoc. Prof. Dr. Mehmet Barış Can Ülker, Asst. Prof. Dr. Onur Pekcan and Asst. Prof. Dr. M. Tuğrul Yılmaz for being a part of review of my work.

I would like to express my deepest gratitude to Assoc. Prof. Dr. Sami Oğuzhan Akbaş and Assoc. Prof. Dr. Yüksel Yılmaz for all their instructions, support and making geotechnical engineering courses appealing to me.

I would like to express my very special thanks to Dr. Mohammad Ahmadi-adli and Dr. Reza-Ahmadi Naghadeh for all their support, technical guidance and precious friendship.

I also would like to extend my gratitude to the METU soil mechanics laboratory experts, Mr Ulaş Nacar and Mr Kamber Bölgen for their kind attitude and supports.

I would like to present my special thanks and fellowship to my friends from METU Geotehnical Engineering Division, Burak Akbaş, Emir Ahmet Oğuz, Yılmaz Emre Sarıçiçek, Berkan Söylemez, Muharrem Can Şimşek, Yağızer Yalçın for all their kind friendship and supports.

I also would like to express my particular thanks to academic members of Atılım University Civil Engineering Department. I present my gratitude to Asst. Prof. Dr. Ebru Akış for her tolerance during my delays. I express my sincere regards to my

colleagues Pınar Bilgin, Ulaş Ozan Ceyhan, Tunç Gökdemir, Barış Küçük, Berhan Melek, Cumhur Özbey and İnci Ünver.

After these appreciations, I could finally express my gratitude to my best friends,
Nazım Erbağ, for killing all of us with his details during our meetings,
İhsan Celal Sevimli, for all his humbleness, tolerance and supports,
Ömer Yavuz Şahin, for answering all my questions about extraordinary judicial cases,
Ömercan Yılmaz, for his kind friendship and high-quality jokes,
and Melih Koçak (out of alphabetic order exclusively), for being a brother and, of course, for all of our joyfull memories.
And i would like to express my deepest gratitude to my beloved family,
my mother Hülya Kenanoğlu, for all her supports and everything
my beloved, joyfull, warm-hearted sister Sümeyra Kenanoğlu, for all her precious support and everything. I consider myself extremely fortunate and grateful to have a sister like her.
my beloved, sweet, adorable sister Şeyda Kenanoğlu, for all her precious support, encouragement and motivation during my studies. I will always be proud of her.
And my father Ali Rıza Kenanoğlu. It is impossible to describe my gratitude and my love to him. His unmeasurable devotion will always warm my heart in all my life.

TABLE OF CONTENTS

LIST OF TABLES

TABLES

LIST OF FIGURES

FIGURES

LIST OF SYMBOLS

SYMBOLS

CHAPTER 2

π ..... Osmotic suction

n ..... Mols of solute

V ..... Volume of solvent

R ..... Universal gas constant

T ..... Temperature

ψ_m ..... Matric suction

u_a ..... Pressure of air

u_w ..... Pressure of water

ψ_{AE} ..... Air-entry pressure

$\overline{s}$ ..... Image suction

α ..... Projection centre

β ..... Material parameter

Q ..... Flow rate

i ..... Hydraulic gradient

k ..... Hydraulic conductivity

A ..... cross-section area of flow

q ..... Flux

h ..... Head

θ ..... Volumetric water content

θ_s ..... Saturated volumetric water content

θ_r ..... Residual volumetric water content

ψ_r ..... Suction corresponding to residual water content

λ ..... Pore size distribution parameter

k_{sat} ..... Saturated hydraulic conductivity

τ ..... shear strength

c' ..... Effective cohesion

σ' ..... Effective stress

ϕ' ..... Angle of internal friction

σ ..... Total stress

χ ..... Bishop's stress parameter

S ..... Degree of saturation

S_e ..... Effective degree of saturation

θ_e ..... Effective volumetric water content

c ..... Apparent cohesion

c'' ..... Capillary cohesion

CHAPTER 3

I_{rain} ..... Rainfall intensity

α ..... Slope base angle

θ ..... Volumetric water content

V_w ..... Volume of water in the pores of the slice

i ..... Hydraulic gradient

Δz ..... Slice height

Δu ..... Difference of matric suction of successive slices

γ_w ..... Unit weight of water

$q_{i,j}$ ..... Water flux between the i^{th} slice and the $i+1^{th}$ slice in the j^{th} time step

$k_{i,j}$ ..... Hydraulic conductivity of the i^{th} slice in the j^{th} time step

$\psi_{i,j}$ ..... Matric suction of the i^{th} slice in the j^{th} time step

$\theta_{i,j}$ ..... Volumetric water content of the i^{th} slice in the j^{th} time step

Δt ..... Time step size

ψ ..... Total suction

ρ_w ..... Density of water

R ..... Universal gas constant

T ..... Temperature

MW_{water} ..... Molecular weight of the water

RH ..... Relative humidity

θ_{target} ..... Target value of volumetric water content

$\theta_{sat,w}$ ..... Wetting saturated volumetric water content

$\theta_{sat,d}$ ..... Drying saturated volumetric water content

θ_{res} ..... Residual volumetric water content

$\theta_{initial}$ ..... Volumetric water content at the begining of wetting

K ..... Power type parameter

CHAPTER 4

α ..... Slope base angle

W ..... Vertical force due to the weight of the soil column

τ ..... Resistive force along the potential failure surface

σ ..... Normal force that acts on the potential failure surface

γ_{bulk} ..... Bulk unit weight of soil

Z .....Depth of the soil column

D.....Driving force

R ..... Resistive force

γ_{dry} .....Dry unit weight of soil

ρ_{dry} .....Dry density

c ..... Effective cohesion

LIST OF ABBREVIATIONS

ABBREVIATIONS

SWCC.....Soil water characteristic curve

SWRC .....Soil water retention curve

DSR .....Desaturation rate

HCF .....Hydraulic conductivity function

TNS ..... Tensiometer

AEV.....Air entry value

M .....Moisture propagation

W ..... Sharp wetting front

E ..... Surface erosion

I-D .....Rainfall intensity-duration threshold

CHAPTER 1

INTRODUCTION

Landslides are the natural phenomena that change the surface of the Earth. These massive movements result in loss of lives and property damage in many regions of the world. According to Turkish General Directorate of Natural Disasters, 25 percent of Turkey's lands, which amount to 194 000 km2 are exposed to landslide hazard. There are approximately 8 million people in Turkey who live in these areas (Ersoy, 2013). Actually, landslides are the most devastating natural hazard after earthquakes in Turkey (Ildır 1995, Reis and Yomralıoğlu 2005).

"A large amount of statistical data shows that most of landslides occur after a rainfall or during a rainfall", (Zhang et al., 2014). It is reported that most landslides that occured in Turkey have typically been associated with rainfall (Okalp and Akgün, 2016).

Landslides have harmful consequences on society and its economy. It is not possible to prevent such a natural disaster from happening but it is wise to take precautions in order to avoid the natural disasters becoming human tragedies.

1.1.Problem Statement

In this study, physical-based numerical model was developed to accomplish required hydraulic calculations and stability analyses for rainfall-induced landslides. It is aimed to use this model to establish rainfall intensity-duration thresholds (I-D thresholds), which are defined as the critical amount of rainfall that triggers a landslide (Reihenbach et al., 1998) as an alternative to empirical methods. In the physical modelling and prediction of a landslide, the assessment of the spatial and temporal distribution of water content and water pressure within the slope is crucial.

The hysteretic nature of the soil water pressure complicates the hydraulic modelling. Also, each numerical model suffers from the numeric problems and they must be enchanced to minimize errors and to obtain correct solutions.

Numerical algorithms can be developed by considering the afore-mentioned requirements to simulate the natural process that results in a landslide and such tools might be used in the early warning systems to protect people and proporties.

1.2. Aims of the Research

The ultimate aim of this research is to develop a numerical algorithm that can be used in the prediction and mitigation of landslides. To do this, an algorithm that is capable of carrying out one dimensional seepage and infinite slope stability calculations was developed. The proposed code was written in MATLAB. For this purpose, the following problems and their solutions were investigated.

- The physical model for the landslide prediction algorithm should be devised by considering the natural failure mechanism. The appropriate geometry and boundary conditions for the problem should be defined.
- The hydraulic modelling of the infiltration and evaporation through soil medium is difficult due to hysteresis of the soil-water characteristic function. The hysteretic behaviour of hydraulic functions can be captured by developing a seperate model for the hysteresis.

1.3. Outline of the Thesis

The successive chapter 2 gives essence information mainly about the unsaturated soil mechanics to provide theoretical background for the readers. In chapter 3, the stages for the generated numerical algorithm for flow model has been described. The verification of the proposed numerical models were presented. In chapter 4, stability analysis has been described and a parametric study for various soils has been presented. Chapter 5 summarizes the findings in this study and includes plannings for the future works.

CHAPTER 2

LITERATURE BACKGROUND

2.1. Potential of Soil Water

In classical physics, mechanical energy emerges from two components; kinetic energy and potential energy. In the case of soil water, kinetic energy is negligible since its movement is quite slow; therefore, the difference in the potential energy within the soil induces water movement. Hillel (2003) had explained the phenomenon as follows: “the spontaneous and universal tendency of all matter in nature is to move from where the potential energy is higher to where it is lower and for each parcel of matter to equilibrate with its surroundings. Soil water obeys the same universial tendency toward that elusive state known as equilibrium, definable as a condition of uniform potential energy throughout. In the soil, water moves constantly in the direction of decreasing potential energy. The rate of decrease of potential energy with distance is in fact the moving force causing flow”.

In soil science, the level of potential energy of soil water is described with respect to a reference state of water, that is, an imaginary pool of pure water at same elevation, atmospheric pressure and temperature as that of soil water (Aitchison, 1965).

2.1.1. Components of Soil Water Potential

The potential energy includes different components resulting from the various type of forces in the nature. The gravitational potential energy (the potential energy

caused by gravity force) of soil water depends on the elevation difference with respect to the reference level.

The dissolved solutes cause osmotic effects in the soil because sharing energy with nearby solute molecules reduces the energy of water molecules. The difference in solute concentration generates non-uniform potential energy distribution within the soil. The soil water moves to the higher concentration regions where the potential energy is lower. The pure water contains no solutes, then the potential energy of the soil water, which mostly includes dissolved solutes, might be considered negative with respect to the reference state. In soil science, the positive of the osmotic potential value is defined as the osmotic suction. Osmotic suction can be expressed as

$$\pi = \frac{n}{V} \times R \times T \qquad (2.1)$$

Where is the $\frac{n}{V}$ is total ion concentration (molar), R is the universial gas constant, T is the absolute temperature (K) (Petrucci, 1989).

When the soil is unsaturated, different type of forces start to control the soil water movement. In classical soil mechanics theory, it is assumed that the soil contains the solids and one fluid phase (only air or only water); but both air and water phase often exist in the soil together (e.g. soil layers above the ground water table). Then unsaturated soil is defined as having three phases (1) solids, (2) water and (3) air. Beyond this consideration, Fredlund and Morgernstern (1977) introduce a fourth phase, namely, air-water interface or contractile skin and it is defined as a thin layer of water molecules at the interface, which behaves differently due to the surface tension of water.

In saturated soil, the pressure of soil water is hydrostatic and it is usually positive compared to the reference state of water. But, in unsaturated soil matrix, air at atmospheric pressure occupies the concave side of the air-water interface and the soil water is held in the convex side because water is the wetting phase compared to air. Therefore the pressure of soil water is less than the ambient air pressure (i.e. it is negative compared to the reference state of water). The pressure of water becomes

more negative with increasing curvature of the interface. “The potential energy due to the physics of the curved interface is defined as the matric potential of the soil water”, (Toker, 2007). The positive of the matric potential value is called matric suction. Matric suction is the difference between the air pressure and water pressure and it is expressed as

$$\psi_m = u_a - u_w \tag{2.2}$$

where, ψ_m is the matric suction, u_a is the pressure of air and u_w is the pressure of water.

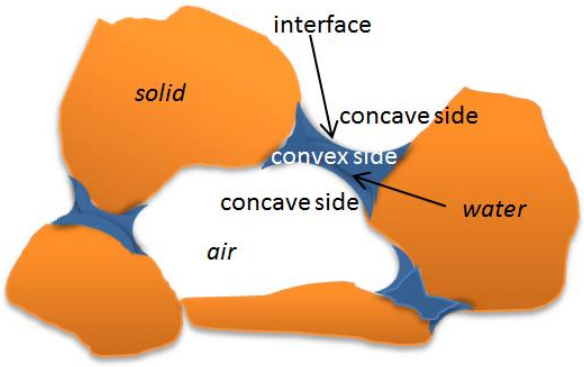

Figure 2. 1. Illustration of condition of water in unsaturated soil.

In most of geotechnical engineering problems, significant changes in osmotic suction are not observed (Nelson and Miller, 1992). Consequently, the mechanical behaviour of the unsaturated soil primarily depends on the matric suction.

In soil science, the sum of osmotic suction and matric suction is called total suction. Soil suction often causes unsaturated soil to have higher strength, lower compressibility and lower hydraulic conductivity compared to saturated soil.

2.2. Soil Water Characteristic Curve (SWCC)

Soil water characteristic curve (SWCC) (also, soil water retention curve, SWRC) is a soil property that defines the relation between the amount of soil water that occupies the pores and the associated suction. SWCC is critical in modelling and interpreting unsaturated soil behaviour. SWCCs are generally S-shaped curves, which consist of three distinct stages depending on the state of water (see Fig. 2.2). For the initially

saturated porous media, the progress of drying is described as follows: approximately constant water content values are observed up to a certain threshold value of suction that is called air-entry pressure (ψ_{AE}). The bulk water is held in the pores throughout this stage. Beyond the ψ_{AE}, the bulk of the water in the pores starts to drain, in response to a relatively small increase in suction. After all the bulk water is drained, the remaining water is held between the particles in the form of liquid brigdes or pendular rings. The pendular water can be drained gradually if enough suction is applied. But, a few molecule-thick layer of adsorbed residual water still remain on the solid surface even if suction increases furthermore.

In the direction of wetting, absorbed water films around particles begin to rise and join each other to form pendular rings. As the suction decreases, the surface of pendular rings start to touch their neighbors. Below a certain threshold value of suction, that is called water-entry, the inscribed circle between connected pendular rings is spontanenously filled with water, if the air in the pore is still connected to the athmosphere by a continuous phase of air.

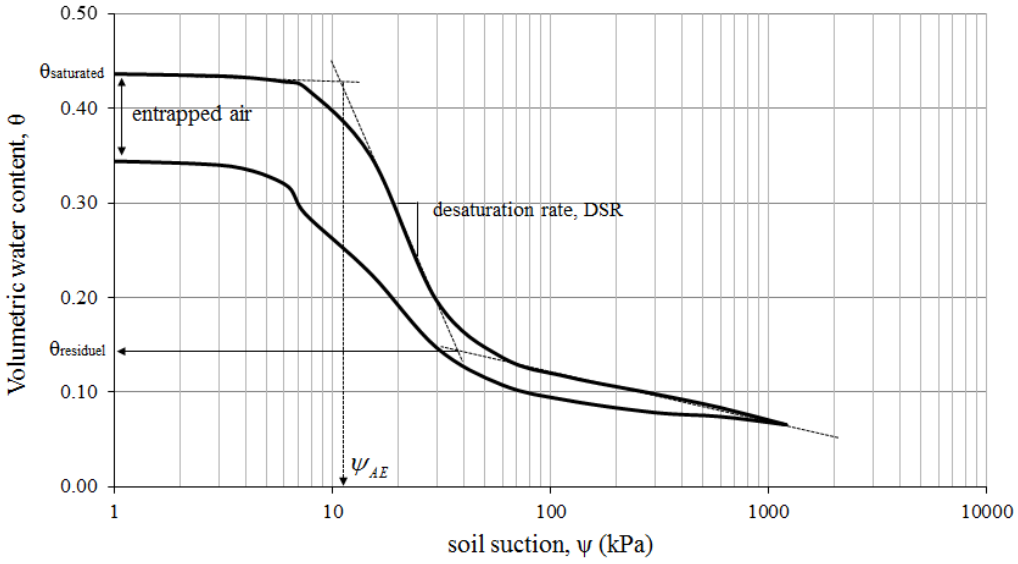

Figure 2. 2. Illustration of various stages in the SWCC (volumetric water content, θ: ratio of water volume to total volume).

Soil water characteristic curve is not unique, the drying path differs from wetting path and this is called hysteresis. According to this phenomenon, different values of

suction may correspond to a single value of water content depending on the drying-wetting history. Several hysteresis mechanisms have been proposed in the literature with the consensus of many researchers. Likos and Lu (2004) pointed out these mechanisms as "(1) the effects of nonhomogeneous pore size distribution(ink-bottle effect), (2) capillary condensation, which is related to adsorbed water films on the surfaces of fine-grained particles, (3) entrapped air, which refers to the formation of occluded air bubbles during wetting, (4) swelling and shrinkage, which alter soil fabric differently during drying and wetting, and (5) contact angle hysteresis, which is related to the difference between drying and wetting contact angles at solid and liquid interface".

Different approaches can be prefered for obtaining SWCC,

- Grain size distribution of given soil can be used to produce SWCC (Arya & Paris, 1981, Sattari & Toker, 2016).
- Number of data points can be obtained on the SWCC by using standart testing techniques such as hanging column, pressure plate extractor, chilled mirror hygrometer (ASTM D6836-02(2008)e2). To obtain several data points on the SWCC takes 1-2 weeks. Then, regression equations (Brooks and Corey, 1964, Van Genuchten, 1980, Fredlund et al., 1994) can be fitted to these data points in order to obtain entire SWCC.
- A continuous SWCC measurement can be carried out on a single specimen by the syringe pump method (Znidarcic et al., 1991), by mercury intrusion porosimetry (Kong & Tan, 2000), or by the MIT evaporation technique (Toker et al., 2004).

2.2.1. Scanning Curves

The experimental studies have shown the transition between the drying and wetting branches of the SWCC constitutes a closed hysteresis loop (Miller et al., 2008, Lins et al., 2007, Hammervold et al., 1998, Viane et al., 1994, Watson et al., 1975, Topp, 1971). These transition curves between the drying and wetting curve are defined as scanning curves in the literature.

The influence of hysteretic behaviour on the water flow in the unsaturated soil zone becomes essential in case of numerical simulations that aim to capture the real field conditions (Beese and Van Der Ploeg, 1976).

Pham (2001) reported extensive review of related literature and showed that most of hysteresis models proposed in the literature require main drying and wetting branches of the SWCC.

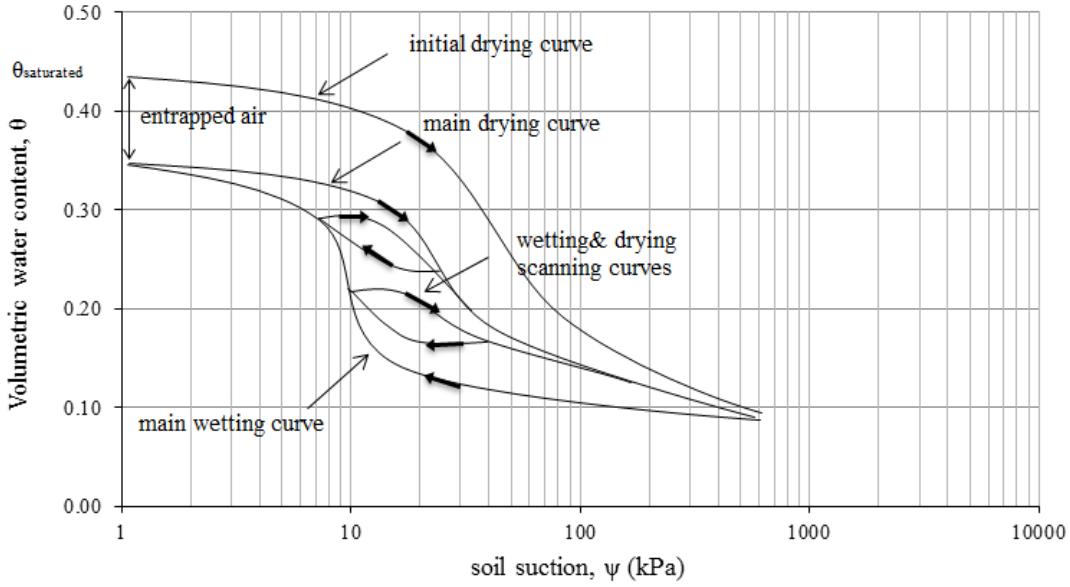

Figure 2. 3. Schematic illustration of hysteresis loops and scanning curves.

In the hysteresis model proposed by Li (2005), the parameter of image suction, ($\bar{s}$) that is the corresponding suction on the wetting or drying branch of the SWCC for given water content, the parameter of projection centre (α) that is the reference suction at the begining of wetting or drying and a material parameter (β) which controls the flatness of the hysteresis loop, were introduced. In this model, scanning curves are obtained by integrating suction and water content increments by using following formula,

$$s^* = \alpha^* \pm \left(\left| \bar{s}^* - \alpha^* \right|^{\beta+1} - \left| \bar{s}_0^* - \alpha^* \right|^{\beta+1} \right)^{1/(\beta+1)} \qquad (2.3)$$

where $\bar{s}^* = \ln(\bar{s})$, $\alpha^* = \ln(\alpha^*)$ and $\bar{s}_0^*$ is the value of $\bar{s}^*$ at the beginning of the scanning curve. ' $\pm$ ' on the right hand side is to define the process of either drying or wetting.

Pedroso et al. (2010) developed another incremental form approach based on geometrical observations on the SWCC and defined a few model parameters to describe shape of scanning curves.

2.3. Water Flow Through Unsaturated Soil

Darcy's law is used to explain the flow through saturated soil and it is given in following equation,

$$Q = i\ k\ A \tag{2.4}$$

Where, Q is the flow rate (L^3/T), i is the hydraulic gradient (unitless), k is the hydraulic conductivity (L/T) and A is the cross-section area normal to the direction of flow (L^2). The hydraulic gradient term is the spatial derivative of hydraulic head, which is the potential energy of water within the soil per unit weight of water . The hydraulic conductivity is a state dependent characteristic property of soil. According to equation above, there is a linear relationship between the hydraulic gradient and the amount of water flow within a saturated soil.

In the case of unsaturated soils, Darcy's law is again valid; but, hydraulic conductivity is no longer constant and it varies depending on the degree of saturation (or other measures of the amount of water, e.g. gravimetric water content or volumetric water content, which varies over time and space as the flow is no longer continuous).

The Eq. 2.4 can be generalized in the following differential form to determine the flow when the hydraulic gradient or the conductivity is variable over time and space.

$$q = -k(\theta)\,.\,\nabla h \tag{2.5}$$

where q is the flux, ∇h is the gradient vector of hydraulic head and $k(\theta)$ is the hydraulic conductivity as a function of the volumetric water content $(\theta = \frac{V_{water}}{V_{total}})$. The minus sign is necessary because flow is in the inverse direction of the gradient.

The conservation of mass principle can be used to express the water flow through unsaturated soils. In this case, the conserved mass is the volume of soil water.

$$\frac{d\theta}{dt} = -\nabla . \vec{q} \tag{2.6}$$

The combination of Eq. 2.5 and Eq. 2.6 yields the equation known as Richards equation (1931);

$$\frac{d(\theta)}{dt} = \nabla . (k(\theta) . \nabla h) \tag{2.7}$$

or,

$$\frac{d(\theta)}{dt} = \nabla . (k(\theta) . \nabla (z - \frac{u_a - u_w}{\gamma_w})) \tag{2.8}$$

In the case of one dimensional flow,

$$\frac{d\theta}{dt} = \frac{d}{dL} . \left[k(\theta) . \frac{d}{dL} (z - \frac{u_a - u_w}{\gamma_w}) \right] \tag{2.9}$$

where $d\theta$ is equal to $d\left(\frac{V_{water}}{V_{total}}\right)$, z is the elevation head component and L is the distance travelled by the flow.

The Eq. 2.9 can be solved by applying various numerical methods (e.g. finite difference).

2.4. Soil Water Characteristic and Hydraulic Conductivity Models

2.4.1. Soil Water Characteristic Curve Models

Soil water characteristic curve is usually obtained by fitting a curve onto data points which are measured by commonly used experimental techniques (hanging column, pressure plate, filter paper, chilled mirror hygrometer etc., ASTM D6836-02(2008)e2). There are a number of fitting equations proposed in the literature (see Table 2.1 for most commonly used ones). The characteristic of these equations is they use fixed data points at specific conditions (e.g., saturated condition, residual condition, air entry), and a couple of fitting parameters to capture the shape of the

curve between these points (Likos et al., 2013). Among these equations, the model proposed by Fredlund and Xing (1994) is the most widely accepted approach. It generally yields better prediction of experimental results and is being more realistic about the residual state of soil water (Vanapalli et al.,1998). Fredlund and Xing (1994) approach uses residual or finite value of suction instead of residual value of water content. The use of finite value of residual water content results in unrealistical representation of SWCC and stability problems in numerical modelling (Likos and Yao, 2014).

Table 2. 1. Mostly used closed form SWCC equations

Reference	Equation	parameters
Brooks & Corey (1964)	$\theta = \theta_s$, $\psi < \psi_{AE}$ $\frac{\theta - \theta_r}{\theta_s - \theta_r} = \left(\frac{\psi}{\psi_{AE}} \right)^{\lambda}$, $\psi > \psi_{AE}$	ψ_{AE} : Air entry pressure λ : pore size distribution index
Van Genuchten (1980)	$\frac{\theta - \theta_r}{\theta_s - \theta_r} = \left(1 + \left(\frac{\psi}{a} \right)^n \right)^{-m}$	a , m, n: fitting parameters
Fredlund & Xing (1994)	$\frac{\theta}{\theta_s} = C_\psi \left(\ln \left(e + \left(\frac{\psi}{a} \right)^n \right) \right)^{-m}$	C_ψ : correction function $C_\psi = 1 - \frac{\ln\left(1 + \frac{\psi}{\psi_r}\right)}{\ln\left(1 + \frac{(10^6\ kPa)}{\psi_r}\right)}$ a , n, m : fitting parameters

where, θ is the volumetric water content, θ_s is the saturated volumetric water content (or porosity), θ_r is the residual volumetric water content, ψ_r is the suction corresponding to the residual water content.

2.4.2. Hydraulic Conductivity Function (HCF)

The experimental methods in determining hydraulic conductivity function of the unsaturated soil are too time-consuming, obviously not preferable in geotechnical

engineering practice (Richards and Weeks, 1953, Corey, 1957, Bruce and Klute, 1956, Hamilton et al., 1981, Daniel, 1983, Meerdink et al., 1996, Chiu and Shackelford, 1998). The approach of utilizing the soil water characteristic curve, which is routinely obtained, is, therefore, a prominent way of determining the hydraulic conductivity function. For example, the empirical hydraulic conductivity model proposed by Brooks and Corey (1964) directly uses the pore size distribution parameter (λ), which is obtained from the soil water characteristic curve and the relationship is given in following Eq. 2.10.

$$k(\psi) = k_{sat} \text{ for } \psi \le \psi_{AE}$$

$$k(\psi) = k_{sat}\left(\frac{\psi_{aev}}{\psi}\right)^{(2+3\lambda)} \text{ for } \psi > \psi_{AE} \tag{2.10}$$

where k_{sat} is the hydraulic conductivity of the saturated soil.

The empirical equation proposed by Averjanov (1950) uses the effective degree of saturation in a power function for determining the hydraulic conductivity function.

$$k(S) = k_{sat} S_e^n \tag{2.11}$$

where $S_e = \frac{S - S_r}{1 - S_r}$ and S_r is the degree of saturation at residual condition. The fitting parameter n is 3.5 for most soils.

Statistical hydraulic conductivity models are alternative to the empirical equations. These models are based on the fact that the hydraulic conductivity is mainly related to the pore-size distribution of the soil under consideration and the hydraulic conductivity function is estimated by assuming random variation of pore size. The pore-size distribution can be determined by an interpretation of soil water characteristic curve, via numerous models that have been reported in the literature to describe the pore-size distribution function (Childs and Collis-George, 1950, Burdine, 1953, Mualem, 1978).

Fredlund et al. (1994) have used the SWCC equation proposed by Fredlund and Xing (1994) (see Table 2.1) to predict hydraulic conductivity function.

$$k(\psi) = \frac{\int_{\ln(\psi)}^{b} \frac{\theta\left(e^{y}\right) - \theta(\psi)}{e^{y}} \theta'\left(e^{y}\right) dy}{\int_{\ln(\psi_{aev})}^{b} \frac{\theta\left(e^{y}\right) - \theta_{sat}}{e^{y}} \theta'\left(e^{y}\right) dy} \tag{2.12}$$

where $k(\psi)$ is the hydraulic conductivity as a function of suction, b is equal to $\ln(10^6)$, ψ_{AEV} is the air-entry pressure (kPa), e is the natural number 2.71828, y is a dummy variable of integration representing the natural logarithm of suction, θ_{sat} is the saturated volumetric water content, θ' denotes the first derivative of equation proposed by Fredlund and Xing (1994) with respect to suction ψ (i.e. $\theta' = \frac{d\theta}{d\psi}$).

2.5. Shear Strength of Unsaturated Soils

In most of geotechnical engineering problems, the ultimate loads are restricted by the shear strength of the soil rather than the compressive and tensile strength and therefore its evalution is quite significant. The Mohr-Coulomb relationship is the most accepted approach for describing shear strength of saturated soils.

$$\tau = c' + \sigma' \tan\left(\phi'\right) \tag{2.13}$$

where τ is the shear strength (or shear stress acting on the failure plane), c' is the effective cohesion, σ' is the effective stress normal to the failure plane and ϕ' is the angle of internal friction. In this equation, the component of shear strength due to friction forces along the shear surface is captured by the second term on the right hand side and the cohesion term captures the contribution of attraction forces between soil particles (Van der Walls forces, cementation, etc.).

In unsaturated soils, the tension in the water draws the soil particles to each other and causes increase in the normal stresses at the particle contacts, thus effective stress also increases. Bishop (1959) proposed following equation to include the

contribution of suction to the effective stress in unsaturated soils and extended the definition of the Terzaghi's effective stress (Terzaghi, 1943).

$$\sigma' = (\sigma - u_a) + \chi (u_a - u_w) \tag{2.14}$$

where σ' is the effective stress, σ is the total stress, u_a is the pressure in the air and if the air phase is continuous, it is equal to zero gage pressure, u_w is the pressure in the water and χ is Bishop's effective stress parameter. It should be noted that not all matric suction contributes to the effective stress; actually, χ is a highly non-linear function, it is equal to 1 at saturated condition and 0 at residual condition. Bishop and Donald (1961) reported that there is an inconsistency in the degree of saturation and effective stress parameter χ relationship for different type of soils.

Öberg and Sällfors (1995) suggested that χ parameter can be considered equal to degree of saturation for engineering purposes.

Karube et al. (1996) used effective degree of saturation (S_e) in order to describe χ parameter:

$$\chi = S_e = \frac{S - S_r}{1 - S_r} \tag{2.15}$$

where S is the degree of saturation and S_r is the degree of saturation at residual condition.

Vanapalli et al. (1996) used effective volumetric water content (θ_e) in order to describe χ parameter:

$$\chi = \theta_e = \frac{\theta - \theta_r}{\theta_{sat} - \theta_r} \tag{2.16}$$

where θ is the volumetric water content, θ_r is the volumetric water content at residual condition and θ_{sat} is the saturated volumetric water content. Note that $\theta_e = S_e$ unless soil volume changes with changing water content.

Khalili and Khabbaz (1998) proposed an empirical equation based on data from a large number of soils:

$$\chi = \left(\frac{\psi_m}{\psi_{AE}} \right)^{-0.55}, \ R^2 = 0.94 \tag{2.17}$$

where ψ_w is the matric suction in water and ψ_{AE} is the air-entry pressure of the soil.

As a result, the shear strength equation (Eq. 2.13) can be extended into the following form for unsaturated soils.

$$\tau = c' + (\sigma - u_a)\tan(\phi') - \chi(u_w - u_a)\tan(\phi') \tag{2.18}$$

Lu and Likos (2006) proposed different approach to define the effective stress in unsaturated soils. They defined a new stress variable called as suction stress (σ_S), which is the unified tensile stress caused by various type of forces such as capillary forces, van der Walls forces, cementation, etc.

$$\sigma' = \sigma - \sigma_S \tag{2.19}$$

Lu and Likos (2006) defined the suction stress as "the work done by the matric suction in soil water per unit soil volume" ,

$$\sigma_S = -\frac{\theta - \theta_r}{\theta_s - \theta_r}(u_a - u_w) = -\Theta_e(u_a - u_w) \tag{2.20}$$

where θ=volumetric water content, θ_r=residual volumetric water content, θ_s =saturated volumetric water content and Θ_e=effective volumetric water content. That definition of suction stress was used in the closed-form equation called suction stress characteristic curve (SSCC) by relating effective saturation term with the soil water characteristic curve (e.g. van Genuchten, 1980) (Lu et al., 2010).

The other approach is proposed by Fredlund and Morgenstern (1977) and they introduce the following equation:

$$\tau = c' + (\sigma - u_a)\tan(\phi') - (u_w - u_a)\tan(\phi^b) \tag{2.21}$$

where $\tan(\phi^b)$ parameter controls the contribution of matric suction to the shear strength.

The Eq. 2.18 and Eq. 2.21 can be used together and following relationship is obtained:

$$\tan\left(\phi^{b}\right) = \chi \tan\left(\phi'\right) \tag{2.22}$$

In literature, the approaches that are generalized in Eq. 4.5 and Eq. 4.6 are called "effective stress approach" and "independent state variable approach" respectively. Both approaches state that the failure line moves upwards due to the contribution of suction to the shear strength, without changing slope. More clearly, the intercept of the failure line or cohesion term changes and the slope of the failure line or angle of internal friction remains almost constant. As a result, the effect of suction on the shear strength can be concluded in the following general equation,

$$\tau = c + (\sigma - u_a)\tan\left(\phi'\right) \tag{2.23}$$

where c is the apparent cohesion and it equals to $c' + c''(\theta \, or \, \psi)$ where c' is the effective cohesion and $c''(\theta \, or \, \psi)$ is the capillary cohesion, which is a function of water content and/or suction.

Naghadeh (2016) introduced the following exponential equation in order to evaluate the apparent cohesion.

$$c'' = c''_{\max} \times \left(1 - \exp^{(-\psi \times \tan\phi')/(c''_{\max})}\right) \tag{2.24}$$

In this equation, ψ is the suction, ϕ' is the effective angle of internal friction and $c''_{\max}$ is the maximum value of the apparent cohesion that could be achieved due to suction. The maximum value of apparent cohesion is expressed in the following Eq. 2.25.

$$c''_{\max} = \psi_t \tan\phi' \tag{2.25}$$

where ψ_t is the transition suction and it is determined by using SWCC.

2.6. Instability of Unsaturated Soil Slopes due to Rainfall Infiltration

Rainfall triggered landslides are common threat in many regions of the world and cause loss of lives and properties. These are shallow failures (less than 5 m depth

from the ground surface) that occur along a plane parallel to the ground surface where the groundwater level is located at significant depths below, and they are triggered after a heavy rainfall in a short time or after a longer period of lower density rainfall (Huvaj et al., 2013).

The mechanism behind the slope failure is that the matric suction starts to decrease due to infiltration into the unsaturated soil. The decreasing matric suction results in loss of shear strength of the soil. In addition to the loss of shear strength, the soil weight as a destabilizing force in the slope increases because of increasing water content (Lepore et al., 2013). This advancement of the wetting front triggers the slope failure when the depth of potential slip surface is reached.

Considering that a failure plane oriented parallel to the ground surface, infinite slope models are used to analyse stability of these landslides after rainfall infiltration in general (Cho and Lee, 2002, Iverson, 2000, Li et al. 2013, Tsai, 2008, Tsai and Yang, 2006, White and Singham, 2012, Zhan and Ng, 2004).

The propagation of wetting front in the slope is assumed to be in the direction normal to the slope surface since the flow normal to the slope is much higher than the flow parallel to the slope at a given time interval due to existing gradient vector (White and Singham, 2012). This allows to analyze the rainfall infiltration as one-dimensional flow problem in the models.

2.7. Previous Research at METU

Ahmadi-adli (2014) investigated physical mechanism of the rainfall-induced landslides and aimed to develop rainfall-intensity thresholds (I-D thresholds) based on two dimensional (2-D) numerical analyses. A methodology for numerical analysis was used to estimate I-D thresholds. He used wetting and drying hydraulic functions (i.e. SWCCs, HCFs) and unsaturated shear strength parameters in his analyses to simulate natural process. He carried out flume tests in order to experimentally validate his approach. He also performed numerical sensitivity analyses to investigate the effect of unsaturated soil properties on the I-D thresholds. His previous studies provide the most important basis for this study.

CHAPTER 3

FLOW MODEL

The main goal of this study is to simulate rainfall induced landslides by means of a numerical model that is based on the physical mechanism of the natural process.

An unsaturated infinite soil slope was considered in order to model the general mechanism of rainfall-induced landslides. The first stage is to perform seepage calculations in order to evaluate the water pressures within soil. The problem of infiltration of rain water and evaporation of soil water was modelled by considering the water flow in the direction of advancing wetting front, the component of water flow that is parallel to the slope surface was ignored. Therefore, the seepage problem becomes one-dimensional.

3.1. Geometry

In the case of seepage calculations, the following unit model geometry was used since the wetting front propagation within the soil is assumed to be perpendicular to the slope surface (see Section 2.6) and the coordinate system is adjusted according to the direction of the wetting front. Figure 3.1 illustrates the geometry used in hydraulic calculations. In Fig. 3.1, I_{rain} denotes the rainfall and it limits the amount of the water flux entering through the upper boundary of the soil due to rainfall (i.e.infiltration) as

$$q_{boundary} \leq I_{rain} \cos\alpha \qquad (3.1)$$

where I_{rain} is the intensity of rainfall (mm/hr). In the seepage calculations, the considered portion of the infinite slope model is divided into small-thickness slice elements so that the spatial discretization of the problem is established. The thickness of the slices is denoted by "Δz". The volumetric water content, θ of each slice is expressed in the Eq. 3.2.

$$\theta = \frac{V_w}{area \times \Delta z} \tag{3.2}$$

where V_w is the volume of water in the pores of the slice. The hydraulic gradient between successive slices is given in the following Eq. 3.3.

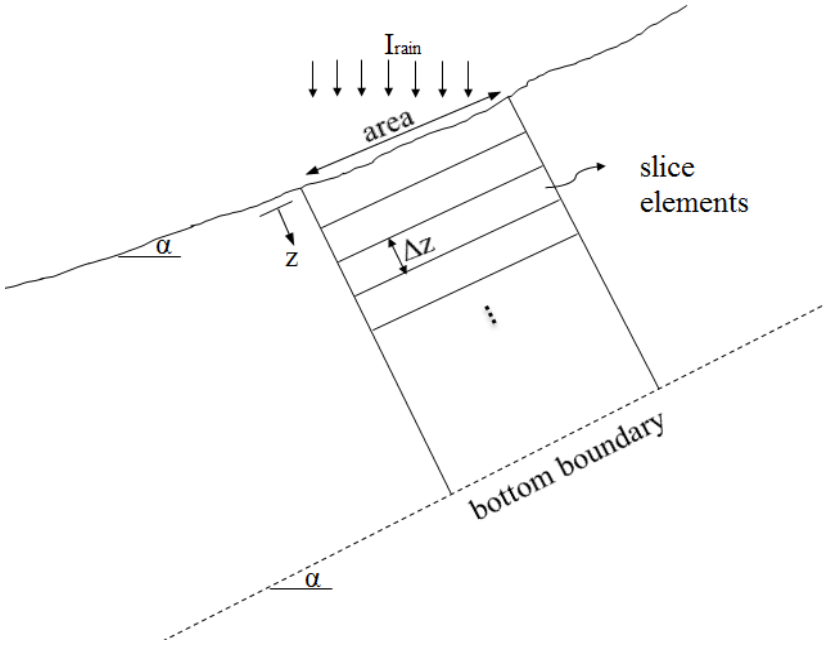

Figure 3. 1. The sketch of the geometry used in hydraulic calculations.

$$i = \frac{\left(\Delta z \cos\alpha + \frac{\Delta u}{\gamma_w} \right)}{\Delta z} \tag{3.3}$$

where i is the hydraulic gradient, the term $dz\cos\alpha$ is the difference in the elevation head between the midpoints of succesive slices, Δu is the difference of suction of

successive slices, γ_w is the unit weight of the water, which is 9.8 kN/m^3 and the term $\frac{\Delta u}{\gamma_w}$ is the difference in the pressure head.

3.2. Numerical Modelling

In the numerical modelling of water flow (e.g. infiltration and evaporation), the initial conditions are defined by assigning initial values of either volumetric water content, θ or matric suction, Ψ to each slice. The soil water characteristic curve (SWCC) is used to convert the volumetric water content values to the matric suction values. The hydraulic conductivity function (HCF) is used to convert either volumetric water content or matric suction values to the hydraulic conductivity values. Next, the incremental form of Darcy's equation (section 2.3 Eq. 2.5) is used to evaluate the water flux between the successive slices. In this study, the subscript *i* refers to the spatial variation and the subscript *j* refers to the temporal variation.

$$q_{i,j} = \left(\frac{2\, k_{i,j}\, k_{i+1,j}}{k_{i,j} + k_{i+1,j}} \right) \frac{\left(\Delta z \cos(\alpha) + \frac{\psi_{i,j} - \psi_{i+1,j}}{\gamma_w} \right)}{\Delta z} area \qquad (3.4)$$

where $q_{i,j}$ denotes the water flux between the ith slice and the i+1th slice in the jth time step, ψ denotes the value of suction within the slices. In this equation, the first term is the harmonic mean of two successive slices between which the flow is represented, similar to the equivalent value of hydraulic conductivity in case of flow perpendicular to soil layers.

The volumetric water content values of each slices in the next time step t_{j+1} can be evaluated by considering the mass-conservation principle (Eq.2.6). The time derivative is solved numerically as an initial value problem (e.g. Euler Method, Heun's Method), by converting the equation to an incremental form:

$$\theta_{i,j+1} = \theta_{i,j} + \left(q_{i+1,j} - q_{i,j} \right) \frac{\Delta t}{\Delta z \times area} \qquad (3.5)$$

Then the values of matric suction and hydraulic conductivity for the next time step t_{j+1} can be determined and the water flux between the slices is calculated.

In the algorithm, the SWCC and HCF data points are used to calculate the matric suction and hydraulic conductivity values by applying linear interpolation technique rather than using SWCC and HCF models (see Section 2.4.1 and 2.4.2). The flow chart of hydraulic calculations is illustrated in Fig. 3.2.

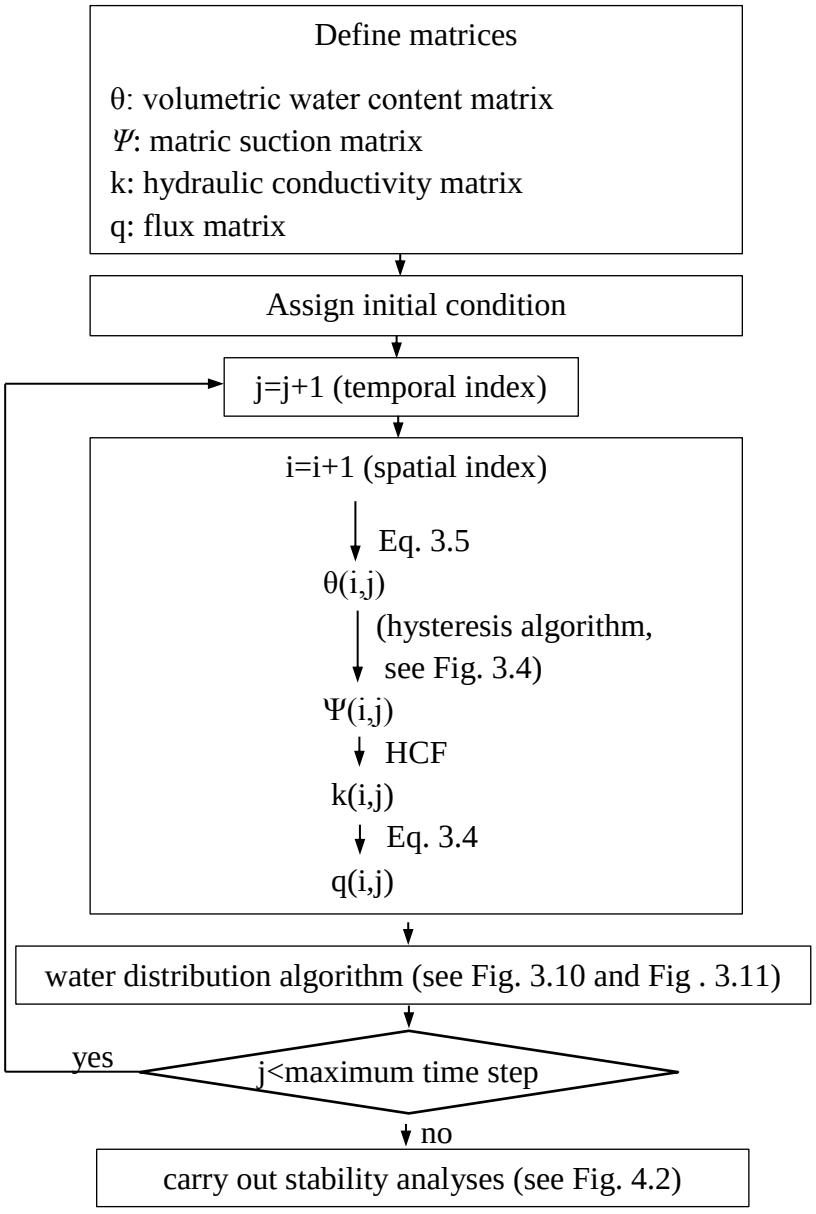

Figure 3. 2. Flow chart of proposed numerical model.

3.3. Boundary Conditions

In the developed numerical model of the hydraulic stage, different types of boundary conditions can be assigned to top and bottom layer on the model geometry.

In case of infiltration of rain water, the top boundary is considered to be flux value that is equal to the rainfall intensity times cosine of slope angle (see Eq. 3.1).

The upper boundary condition is considered as pressure value rather than flux value in the simulation of evaporation. It is known that the total suction exerted by the atmophere causes evaporation of soil water. The total suction exerted by the atmosphere can be estimated by using Kelvin's equation as a function of temperature and it is given in the following equation.

$$\psi = -\frac{\rho_w \times R \times T}{MW_{water}} \times \ln(RH) \qquad (3.6)$$

In this equation, ψ is the total suction (MPa), ρ_w is the density of water (g/cm^3), R is the universial gas constant (J.mol/K), MW_{water} is the molecular weight of the water (gr/mol) and RH is the relative humidity. When realistic numbers are entered in the Kelvin's equation, total suction can be expressed as the function of only relative humidity in the following equation.

$$\psi \cong -(135\,MPa) \times \ln(RH) \qquad (3.7)$$

Even if the higher values of relative humidity closer to 1 are put into Eq. 3.7., this equation yields large amount of total suction acts on the specimen compared to matric suction within it. Then this causes numerical error in the calculations since large amount of potential difference between the atmosphere and the soil elements causes drawing large amount of water and empties the the uppermost slice. However, even the total suction exerted by the atmosphere demands drawing large amount of water from uppermost slice, there is a limit for the amount of drained water, that is, rate of evaporation. In this study, an empirical formula for the lake evaporation proposed by USBR (*water management manual*) is used to roughly estimate the evaporation rate from the soil surface. The amount of rate of evaporation obtained by

using empirical formula is reduced by means of a constant coefficient to convert the rate of lake evaporation to rate of soil surface evaporation. As a result, the flux values due to evaporation exceed the rate of evaporation, the flux value that comes out from the uppermost slice is restricted by the rate of evaporation. The formula used in algorithm is in the following Eq. 3.8.

$$E = c \times 0.833 \times (4.57 \times T + 43.3) / 2.592 / 10^6 \quad (3.8)$$

where E is the rate of evaporation in (m/sec), T is the mean annual temperature in °C and c is the constant coefficient that is used to convert the rate of lake evaporation to rate of soil surface evaporation.

Two different types of bottom boundary conditions are considered, i) impervious boundary condition and ii) drained boundary condition. The impervious boundary condition is defined by equating the value of flux out of bottom slice to zero. The drained boundary condition is defined by linearly extrapolating the volumetric water content values of the two slices immediately above the bottom slice in order to calculate its volumetric water content.

$$\theta_{i,j} = 2 \times \theta_{i-1,j} - \theta_{i-2,j} \quad (3.9)$$

3.4. Modelling Hysteresis

The hysteretic nature of soil water characteristic curves (SWCC) complicate the modelling of hydraulic framework in the algorithm. The drying and wetting processes follow transition (i.e. scanning curves) between the main wetting and the main drying branches of the SWCC, and there exist endless number of scanning curves for given soil depending on the drying-wetting history and initial water content.

In this study, the scanning curves between the virgin branches of the SWCC have been modelled by using geometric-based relations, which are devised by means of the observations on the graphical scheme. The proposed model is derived from geometry of various scanning curves observed in the literature. It is a power-type

interpolation between the existing θ, Ψ values and a "target point", which is the residual state while drying, or a water content value interpolated, based on the point of regime reversal, between the values that correspond to zero suction while wetting. It is assumed that the initial drying curve and main wetting curve bound all scanning curves so that transition always occurs between these two curves. In the following Fig. 3.3, the variables of the proposed relations are illustrated.

In the formulation of scanning curves, the unknown suction value for the volumetric water content at a time step is derived by considering the suction values corresponding to the same θ on the drying and wetting branches for both that and the preceding time step.

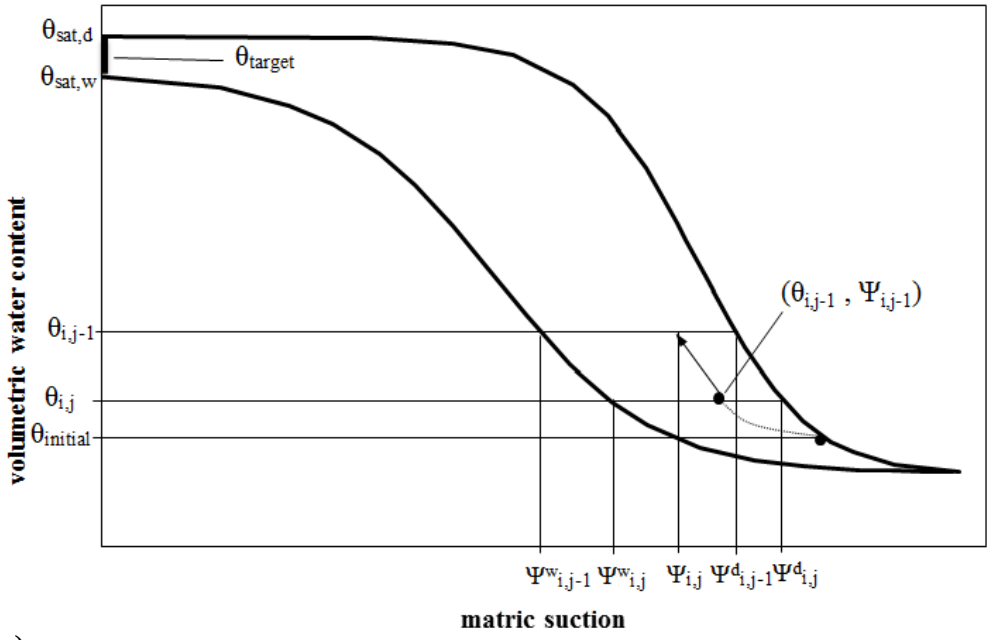

(a)

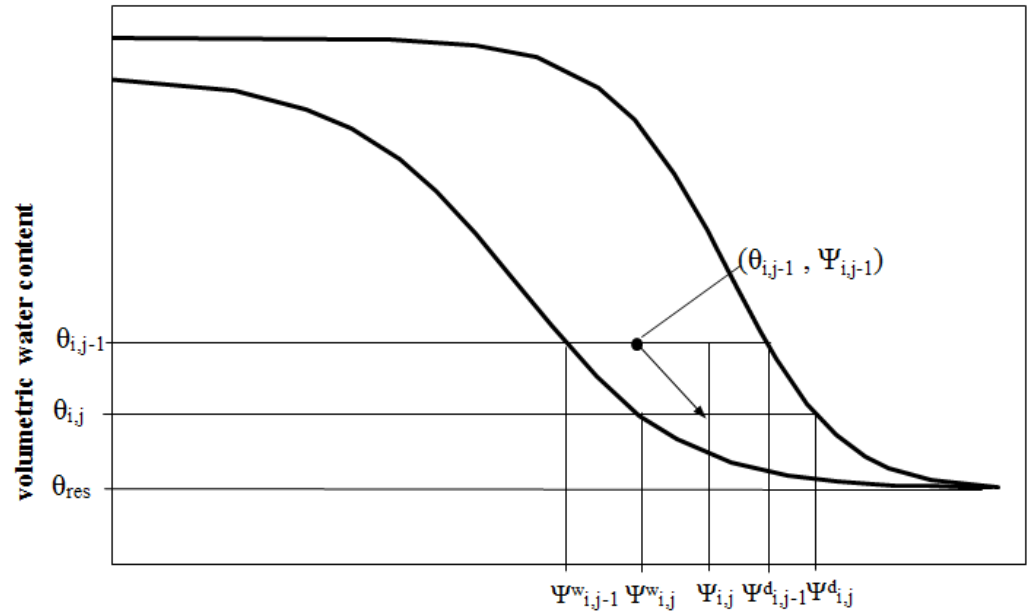

(b)

Figure 3. 3. The schematic illustration of the variables used in the derivation of (a) wetting scanning curve, and (b) drying scanning curve.

In the direction of wetting, the ultimate value (i.e. target point) of water content is its saturated value. The wetting "saturated" water content differs from the drying saturated water content due to air entrapment. The amount of trapped air depends on the minimal degree of saturation, or the highest matric suction, that the soil had experienced before wetting (Chen et al., 2014). In this study, the different values of θ_{sat} were defined in the following Eq. 3.10 by linear interpolation.

$$\theta_{target} = \theta_{sat,w} + \frac{\theta_{sat,d} - \theta_{sat,w}}{\theta_{sat,d} - \theta_{res}} \left(\theta_{initial} - \theta_{res} \right) \qquad (3.10)$$

where, θ_{target} is wetting saturated water content depending on the initial suction at the begining of wetting, $\theta_{sat,w}$ is the wetting saturated water content of the main wetting curve, $\theta_{sat,d}$ is the drying saturated water content of the initial drying curve, θ_{res} is the residual water content and $\theta_{initial}$ is the initial value of water content at the begining of wetting. According to this equation, the saturated value of main wetting

curve is reached in case of a soil starting from the residual water content, if wetting proceeds continuously.

The equation of scanning curve in the wetting direction for ith slice element is given in the Eq. 3.11.

$$\log(\psi_{i,j}) = \log\left(\psi_{i,j}^{w}\right) + \frac{\log\left(\frac{\psi_{i,j-1}}{\psi_{i,j-1}^{w}}\right)}{\log\left(\frac{\psi_{i,j-1}^{d}}{\psi_{i,j-1}^{w}}\right)}\left(\frac{\theta_{target}^{i} - \theta_{i,j}}{\theta_{target}^{i} - \theta_{i,j-1}}\right)^{K} \log\left(\frac{\psi_{i,j}^{d}}{\psi_{i,j}^{w}}\right) \qquad (3.11)$$

where, $\log(\psi_{i,j})$ is the logarithm of unknown suction value at the jth time step, $\log\left(\psi_{i,j}^{w}\right)$ is the logarithm of the corresponding value of suction on the main wetting curve at the $\theta_{i,j}$ and jth time step, $\psi_{i,j-1}$ is the value of suction at the (j-1)th time step, $\psi_{i,j-1}^{w}$ is the corresponding value of suction on the main wetting curve at the $\theta_{i,j-1}$ and (j-1)th time step, $\psi_{i,j-1}^{d}$ is the corresponding value of suction on the initial drying curve at the $\theta_{i,j-1}$ and (j-1)th time step, θ_{target}^{i} is the ultimate wetting saturated water content for ith slice element, $\theta_{i,j}$ is the water content at jth time step, $\theta_{i,j-1}$ is the water content at the (j-1)th time step, $\psi_{i,j}^{d}$ is the corresponding value of suction on the initial drying curve at the $\theta_{i,j}$ and jth time step, $\psi_{i,j}^{w}$ is the corresponding value of suction on the main wetting curve at the $\theta_{i,j}$ and jth time step and K is the power-type parameter, which controls the flatness of the scanning curve. It should be noted that the initial drying and main wetting curves can be interpolation between experimental data points or in the form of retention curve equations (such as Van Genuchten, 1980).

The equation of scanning curve in the drying direction is similarly given in the Eq. 3.12.

$$\log(\psi_{i,j}) = \log\left(\psi_{i,j}^{d}\right) - \frac{\log\left(\frac{\psi_{i,j-1}^{d}}{\psi_{i,j-1}}\right)}{\log\left(\frac{\psi_{i,j-1}^{d}}{\psi_{i,j-1}^{w}}\right)}\left(\frac{\theta_{i,j}-\theta_{res}}{\theta_{i,j-1}-\theta_{res}}\right)^{K}\log\left(\frac{\psi_{i,j}^{d}}{\psi_{i,j}^{w}}\right) \qquad (3.12)$$

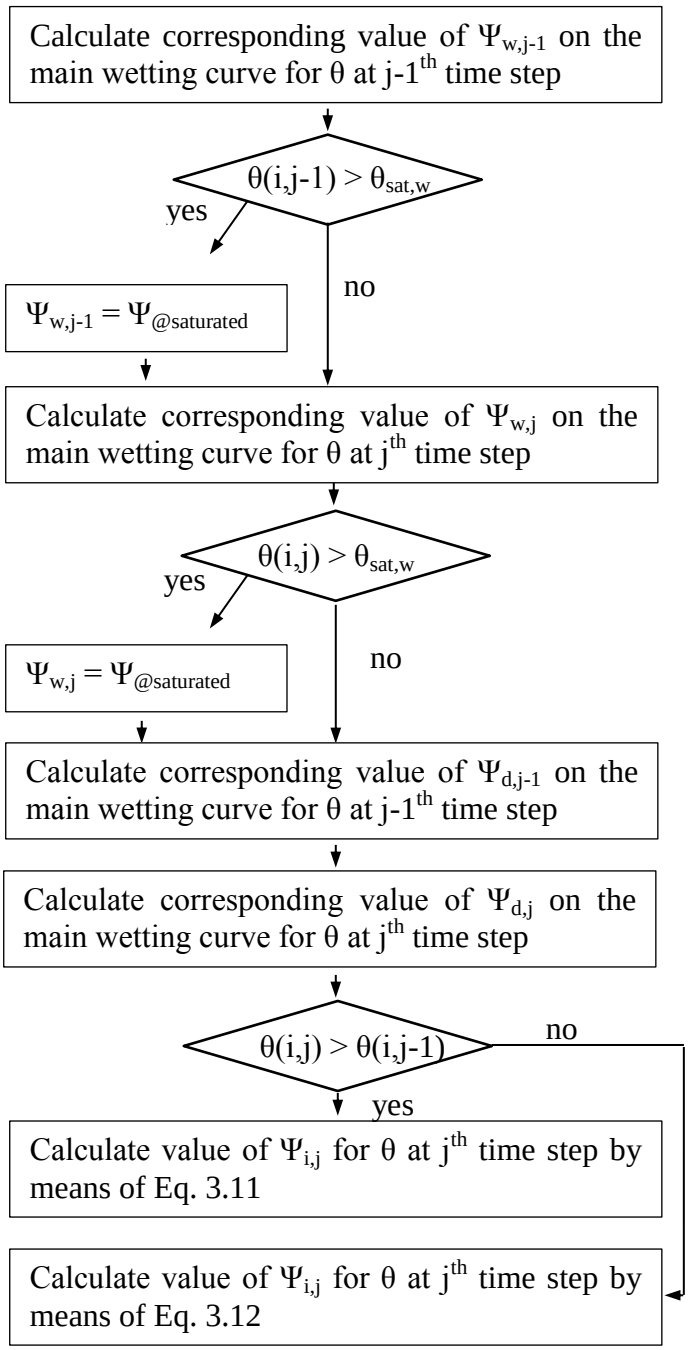

Figure 3. 4. Hysteresis algorithm.

It should be noted that the proposed relations can be used in incremental form to predict suction in different frameworks (e.g. elastoplastic models) and other physical problems.

3.4.1. Validation of Proposed Hysteresis Model

The various experimental data reported in the literature were used to verify the proposed equations. In the experimental data reported by Lins et al. (2007) and Sakai and Toride (2007), a single hysteresis loop was obtained for sand type soil (Fig 3.5 and Fig. 3.6). Viena et al. (1994) also reported the experimental data of scanning soil water characteristic curve (Fig. 3.7). Talsma (1970) reported data of two drying scanning curves originated from different initial suction values for same sand soil (Fig. 3.8) and Poulovassilis and Childs (1971) also reported similar experimental study in case of wetting (Fig. 3.9). The proposed relations are fitted to the experimental data by means of least square regression method. In the regression analysis, logarithm of suction values are set as independent variable.

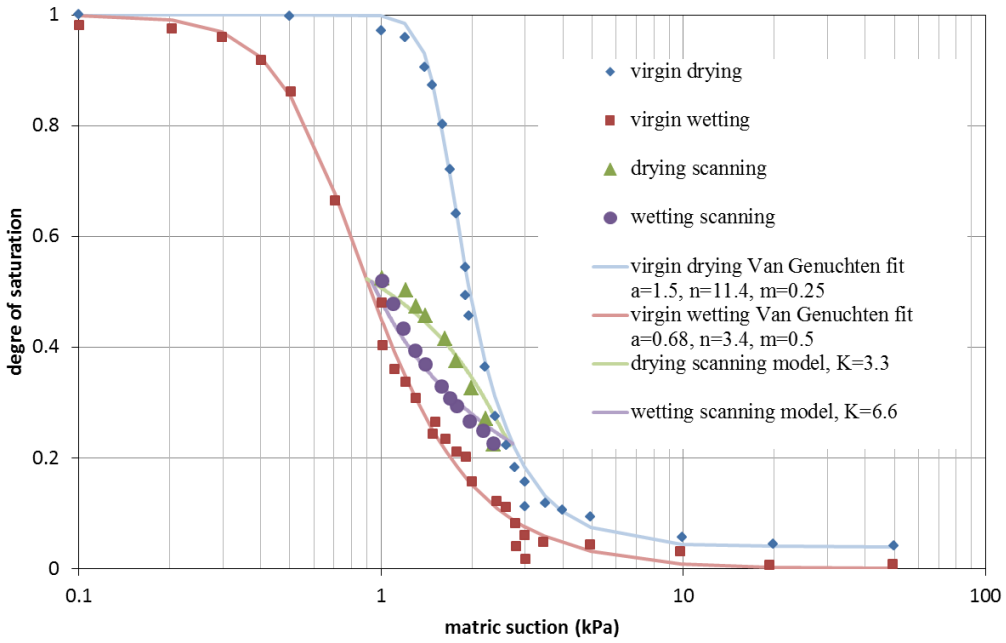

Figure 3. 5. The proposed hysteresis model for a hysteresis loop (experimental data from Lins et al., 2007), the R^2 values for drying and wetting scanning curves are 0.0.880 and 0.921, respectively.

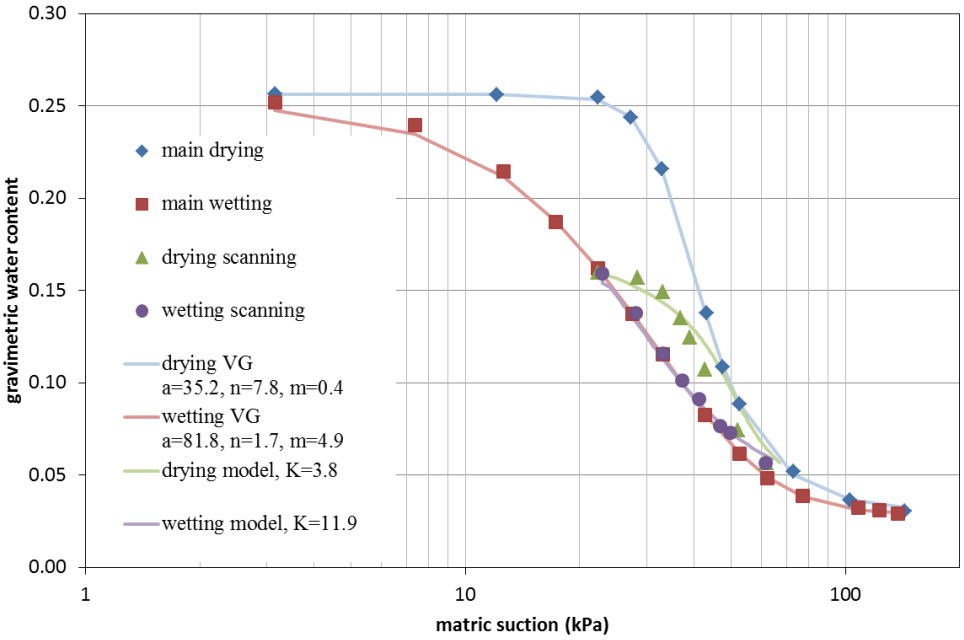

Figure 3. 6. The proposed hysteresis model for a hysteresis loop (experimental data from Viena et al., 1994), the R^2 values for drying and wetting scanning curves are 0.916 and 0.993, respectively.

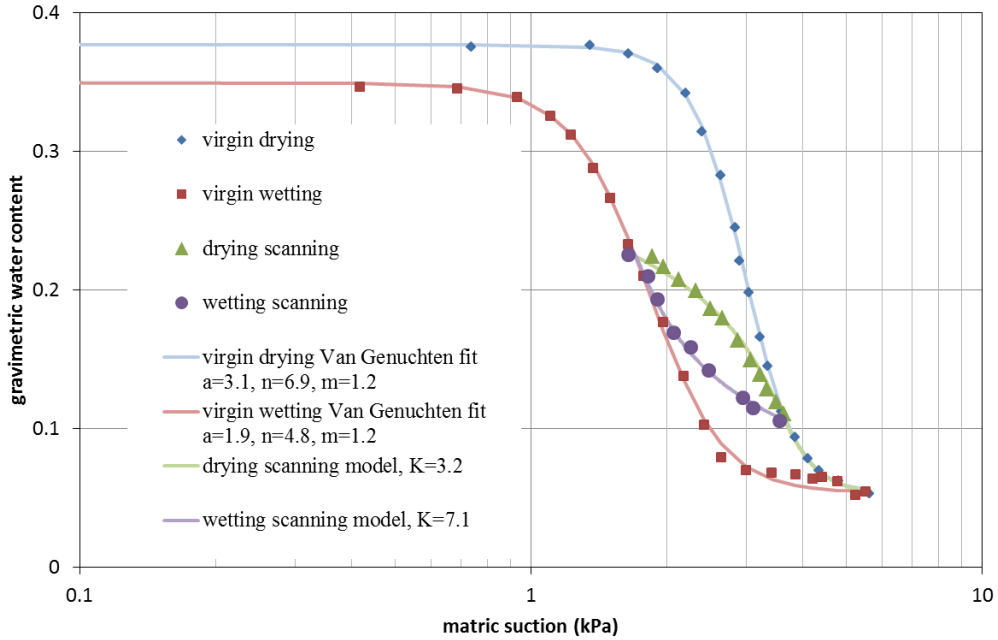

Figure 3. 7. The proposed hysteresis model for a hysteresis loop (experimental data from Sakai and Toride, 2007), the R^2 values for drying and wetting scanning curves are 0.981 and 0.991, respectively.

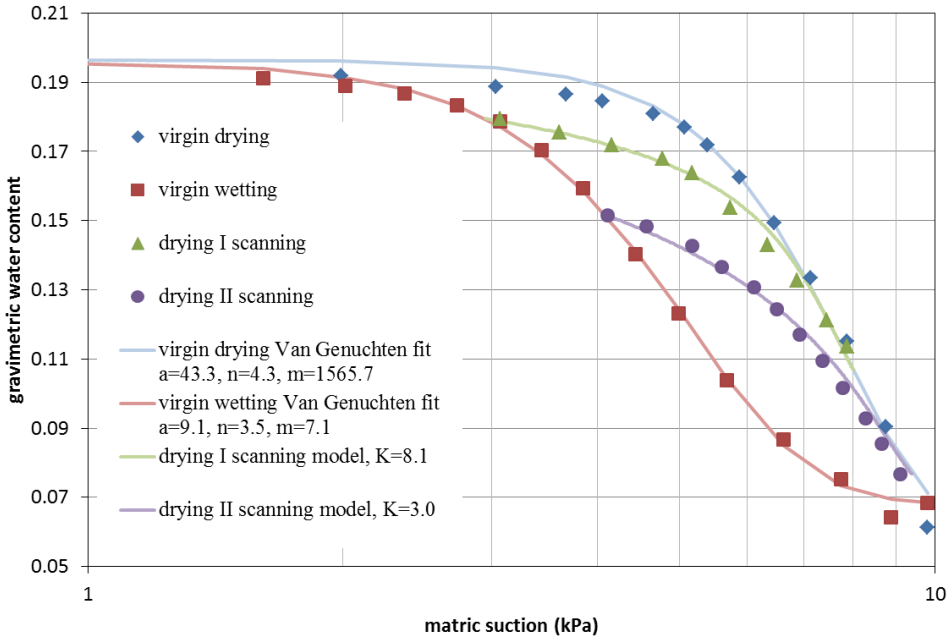

Figure 3. 8. The proposed hysteresis model for a hysteresis loop (experimental data from Talsma, 1970), the R^2 values for drying I and drying II scanning curves are 0.993 and 0.991, respectively.

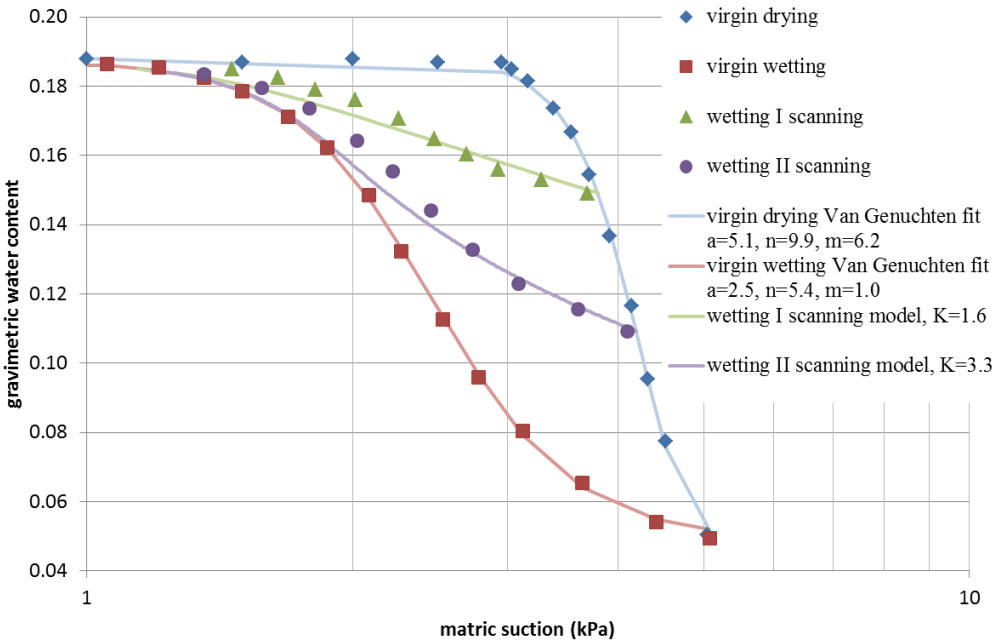

Figure 3. 9. The proposed hysteresis model for a hysteresis loop (experimental data from Poulovassilis and Childs, 1971), the R^2 value for wetting I and wetting II scanning curves are 0.919 and 0.976, respectively.

The experimental results collected in the literature are limited and the soils used in those experimental studies are generally sand. Obviously, more experimental data should be assembled in order to make an extensive interpretation.

There is only one material-depended parameter exists in the proposed relations, which is K. This power parameter in the relations appears to depend on various other properties, such as wetting-drying direction and type of material. However, variation of the power parameter only marginally changes the shape of the generated scanning curves, which means the model can be simplified by assuming a constant average value for this parameter (for example, K=3 yielded consistent results with the experimental ones).

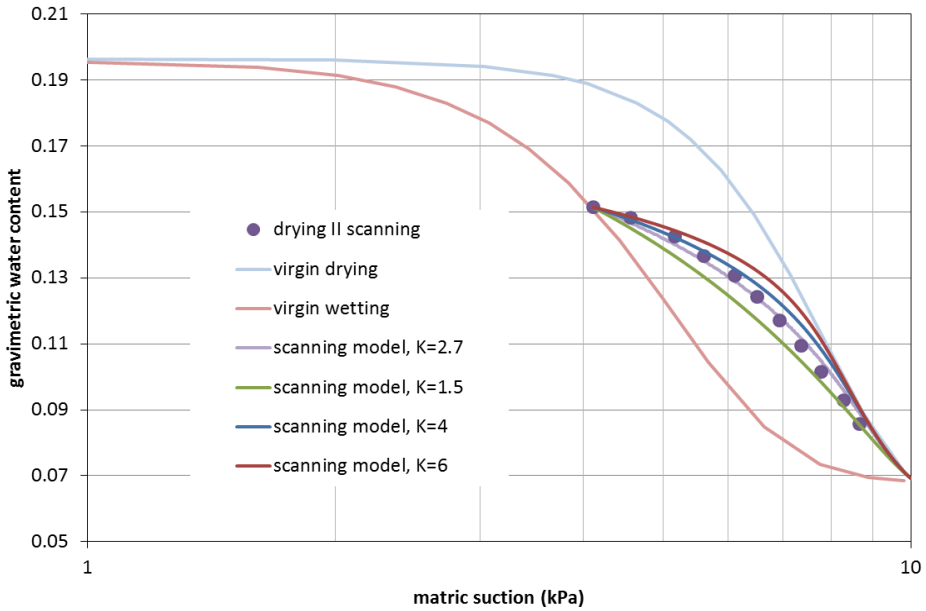

Figure 3. 10. Sensitivity of scanning curves for parameter K (experimental data from Talsma, 1970), the R^2 values for K=1.5, K=2.7, K=4 and K=6 are 0.954, 0.989, 0.958 and 0.938, respectively.

Table 3. 1. List of K values fitted to experimental results

K, drying	K, wetting	reference
3.3	6.6	Lins et al., 2007
3.8	11.9	Viena et al., 2004
3.2	7.1	Sakai and Toride, 2007
8.1 – 3.0	-	Talsma, 1970
-	1.6 – 3.3	Poulovassilis and Childs, 1971

3.5. Numerical Issues

In this study, the numerical modelling of water transport in the unsaturated soil has been generated in a mass-conservative form. However, possible numerical errors can emerge in case of slice elements near to saturation or at the boundaries of the computation domain and violate the conservation of mass principle.

3.5.1. Excess or Deficient Water Distribution Algorithm

A water distribution algorithm, which ensures the spatial variation of the water content within the infinite slope is always physically possible at all locations by bounding the values of water content between residual water content and saturated water content, is generated in order to handle numerical problems. The idea is once a slice element is detected to be overfilled due to excess water mass transport into it, then excess portion is distributed to neighboring slice elements. In case of drying, reverse of the procedure is used for the slice elements that have less water content than the residual value. The distribution is carried out in terms of volumetric water content, flux values that cause the overfilling are not changed in the water distribution algorithm. Nevertheless, the effect of flux values are corrected and the flux can be recalculated based on the redistributed water content values if needed. Fig. 3.10 and Fig. 3.11 illustrate the flow charts of water distribution algorithms.

The detection of overfill is carried out by checking the volumetric water contents of each slice element at the next time step , which are determined by means of the already calculated flux values at the current time step, against the θ_{target} of each slice. Once the overfilled slices are detected, their spatial indices, i and the amount of excees water that causes overfilling for each slice element are stored. The water distribution always commences from the the bottommost problematic slice element. The excess amount of water for that slice element is transferred to its upper neighbor and the θ of overfilled slice element is adjusted as equal to its θ_{target}. In this case, two alternatives are possible i) the volume of distributed water fills the upper slice and cause another overfill or, ii) the volume of distributed water is less than the empty volume of upper slice and not causes overfill, that is, the distribution is completed. In

the first case the amount of distributed water is decreased to the difference of the amount of distributed water and the amount of empty volume of the upper slice element. The volumetric water content value of the upper slice is again adjusted as equal to its target saturated volumetric water content. Then, remaining excess water is distributed to the next upper slice element by means of the same procedure until all of the excess water diminishes. If the upper slice element also has overfill problem of its own, the excess water for this slice is added to the volume of the water to be distributed. When the uppermost slice is reached and there is still excess water that should be distributed, the remaining excess water is recorded as the surface run-off.
In case of drying, the same algorithm is inverted: the distribution commences from the uppermost problematic slice element and the deficiency (instead of overfill) of water volume, which means that the volumetric water content of a slice element is less than the residual value, is provided from underlying slice element. The detailed procedure, which mirrors that of the overfill volumes, is as follows:

The water volume deficieny is detected by checking for the volumetric water content values less than the residual value. The spatial index numbers of the detected slices are stored. The distribution commences from the uppermost problematic slice element. The deficient volume of water for this slice element is supplied from the underlying slice element. If the transferred water volume causes deficiency in the underlying slice, the amount of water volume that can be transferred is taken and the deficient water volume is decreased by considering this transferred water volume. Then, the volumetric water content of the underlying slice element becomes equal to the residual value. In order to eliminate remaining deficiency, the slice elements underlying the corrected ones are investigated individually by means of the same procedure.
It should be noted that the water flow in the saturated zone can be included in the computations and it is possible to model the rising groundwater table within the infinite slope by means of the water distribution algorithm. The development of positive pore water pressure at the bottom of slope for the saturated zone can be taken into account by considering only the gravitational head, which is simply the summation of height of saturated slices above the concerned depth.

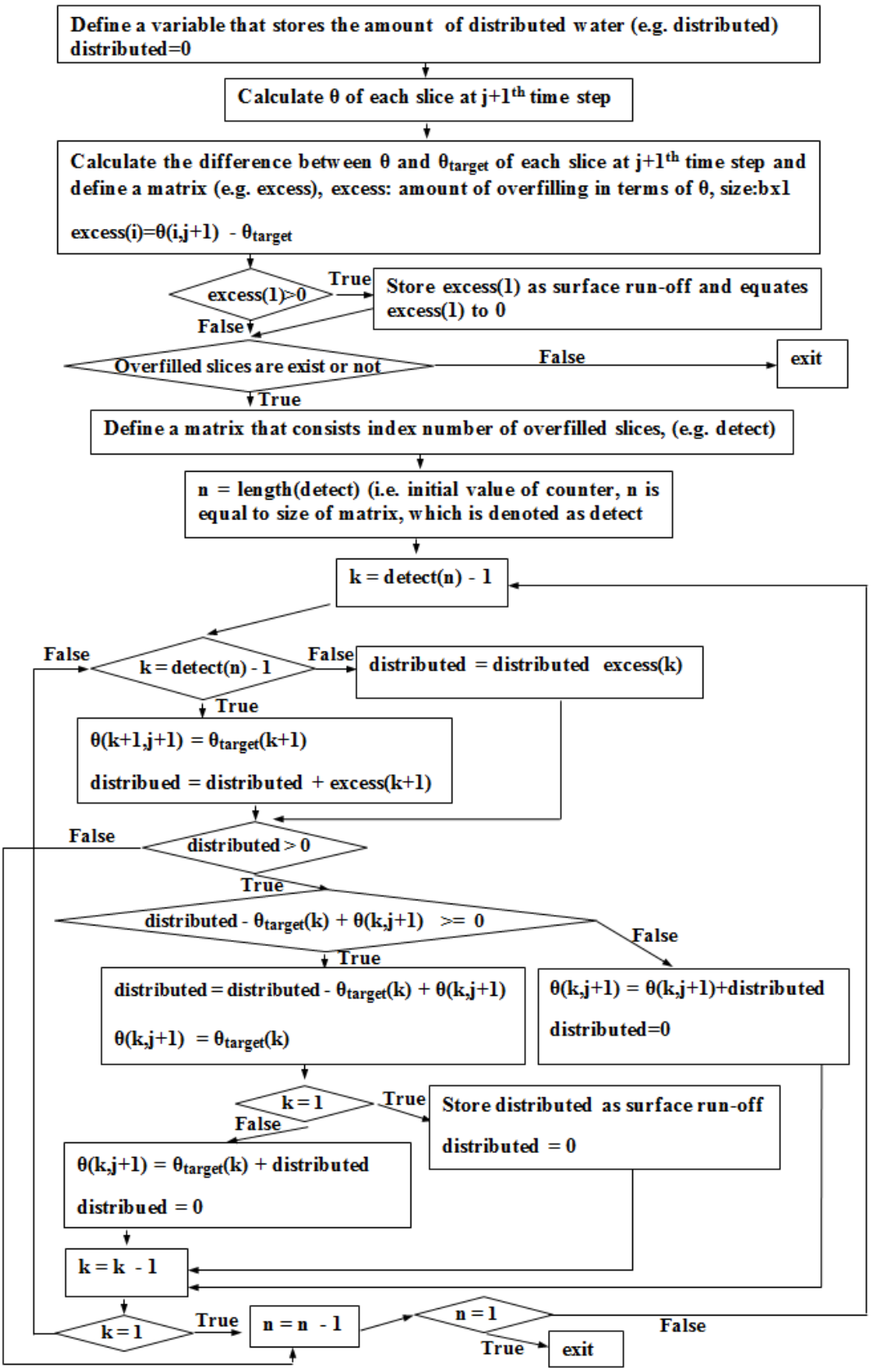

Figure 3. 11. Flowchart of excess water distribution algorithm for wetting.

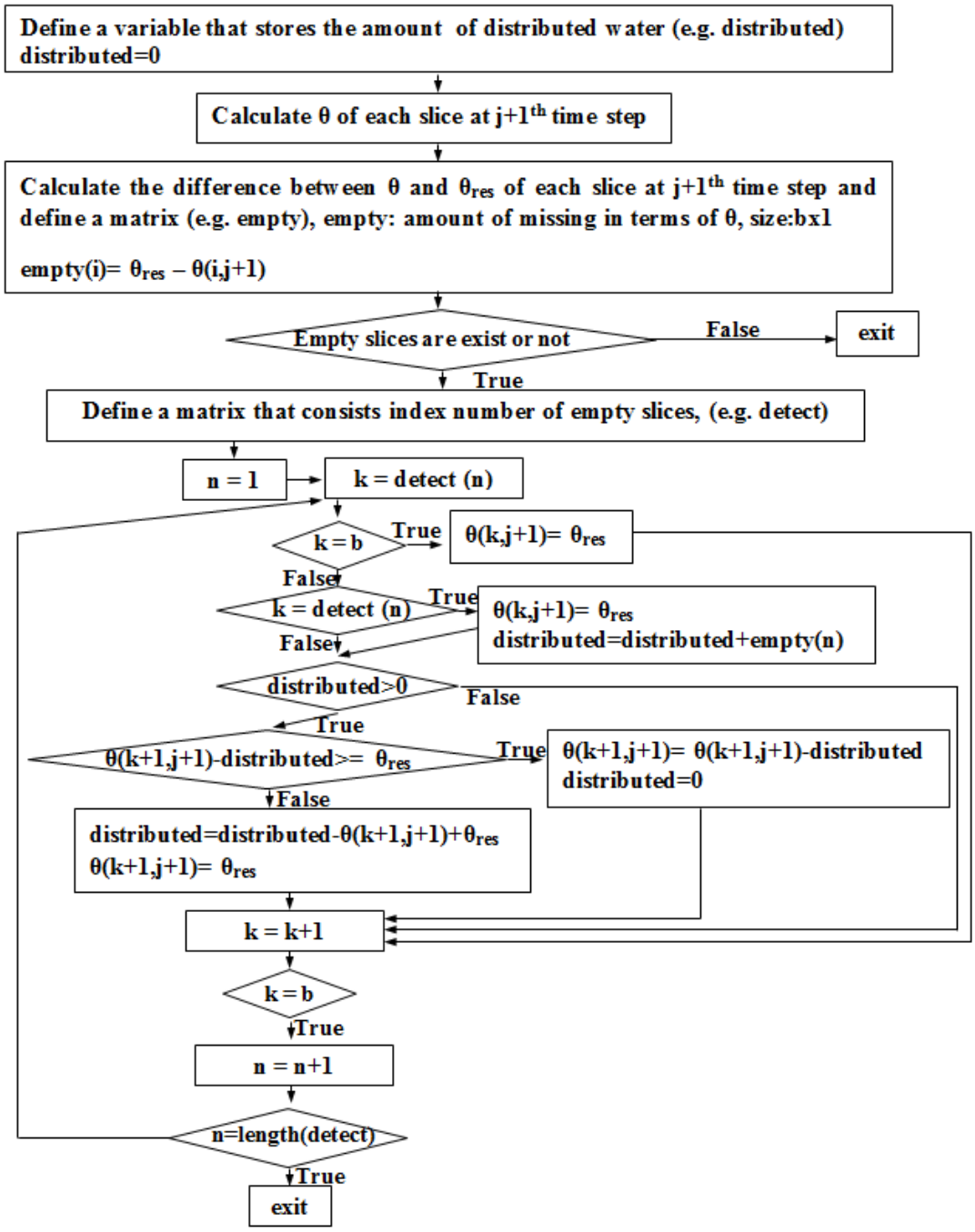

Figure 3. 12. Pseudocode of deficient water distribution algorithm for drying.

3.5.2. Predictor-Corrector Over Time Axis

The error-accumulation in the computations can cause erroneous results in the numerical modelling. To eliminate this problem, Heun's Method (Reference?) is employed. In this approach, the computations for the each time step are performed

twice. The first set of solution is called as predictor solution and these are used to estimate second set of solution, namely, corrector solution. The final or corrected set of solution is obtained by taking the average of predictor and corrector solution results. In the algorithm, the hydraulic conductivity values and the matric suction values are corrected according to the aformentioned procedure. Then, the flux and volumetric water content values are calculated by using corrected values of matric suction and hydraulic conductivity.

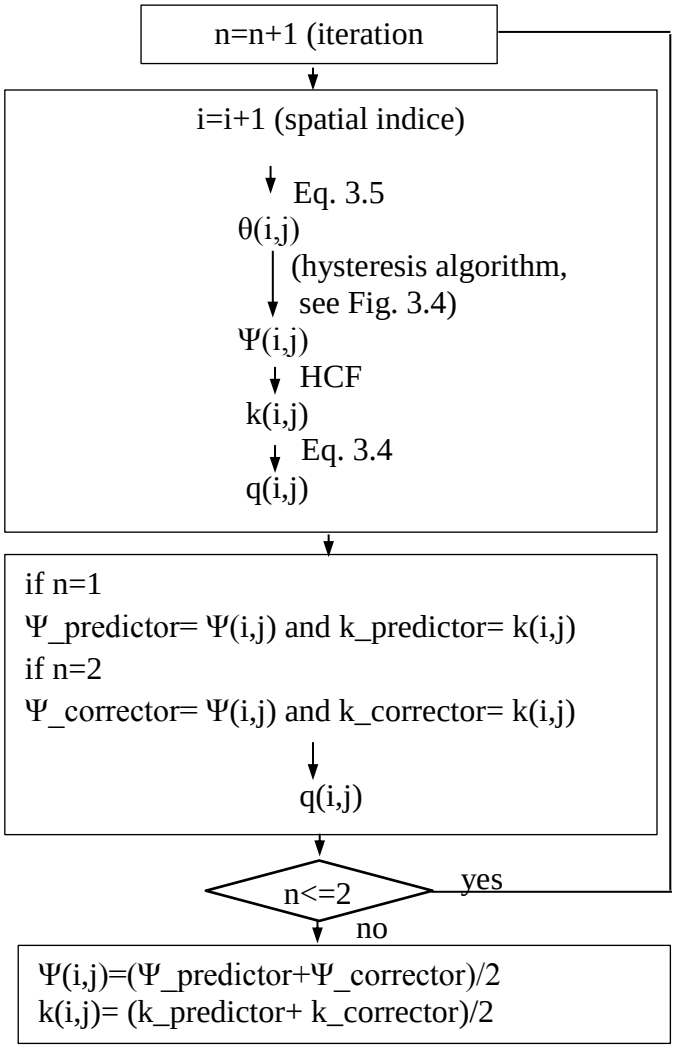

Figure 3. 13. Flowchart of predictor-corrector solution.

3.5.3. Effect of Slice Height and Time Step Size

The effect of slice height on the results was investigated by performing analyses with different slice height values. The slope geometry was divided into 10, 20, 50, 100 and 200 slices. It was determined that the slice height of 1 cm for slope height of 1 m is sufficient in the analyses. According to the results shown in Fig. 3.14, the slice height of 1 cm was deemed fine enough for 1 m thick soil layer. It should be noted that, this set of analyses was conducted at an earlier stage, when the hydraulic conductivity between successive slices was approximated by the artihmetic mean, as explained in section 3.2, and exhibits greater sensitivity to slice thickness. A numerically more advanced (i.e. higher order) method of calculating the equivalent hydraulic is devised to eliminate this problem (see section 5.3.1), for future uses of the algorithm.

There is an overlap between the results of the simulations with 1 second and 0.1 second. The time step size was choosen as 1 second in this study. It should be noted that to use too large time step size may cause numerical error in the calculations and the simulation results can not be obtained. Also, it is possible to suffer from oscillation problem, especially for the slices near to saturation. For both cases, smaller time size were used in the analyses.

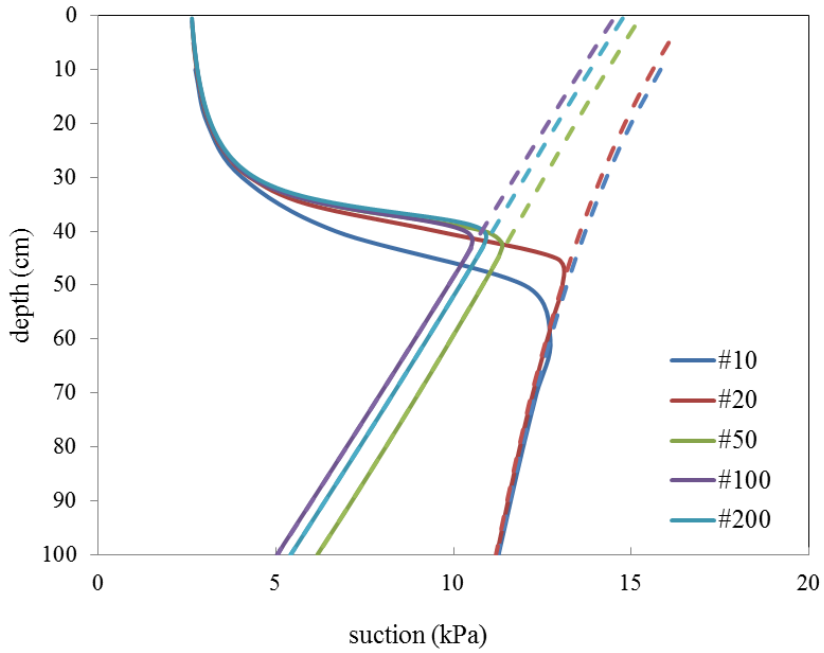

Figure 3. 14. The effect of slice height on the simulations.

3.6. Validation of Infiltration Algorithm with the Results of Infiltration Column Experiment

The numerical model for infiltration is validated by comparing the numerical simulations with experimental results. Ahmadi-adli, (2014) carried out an infiltration column test (ASTM D7664) in order to determine the hydraulic conductivity function of a sand and reported the infiltration column test results with detailed description of material properties (Fig. 3. 12 and Fig. 3.13).

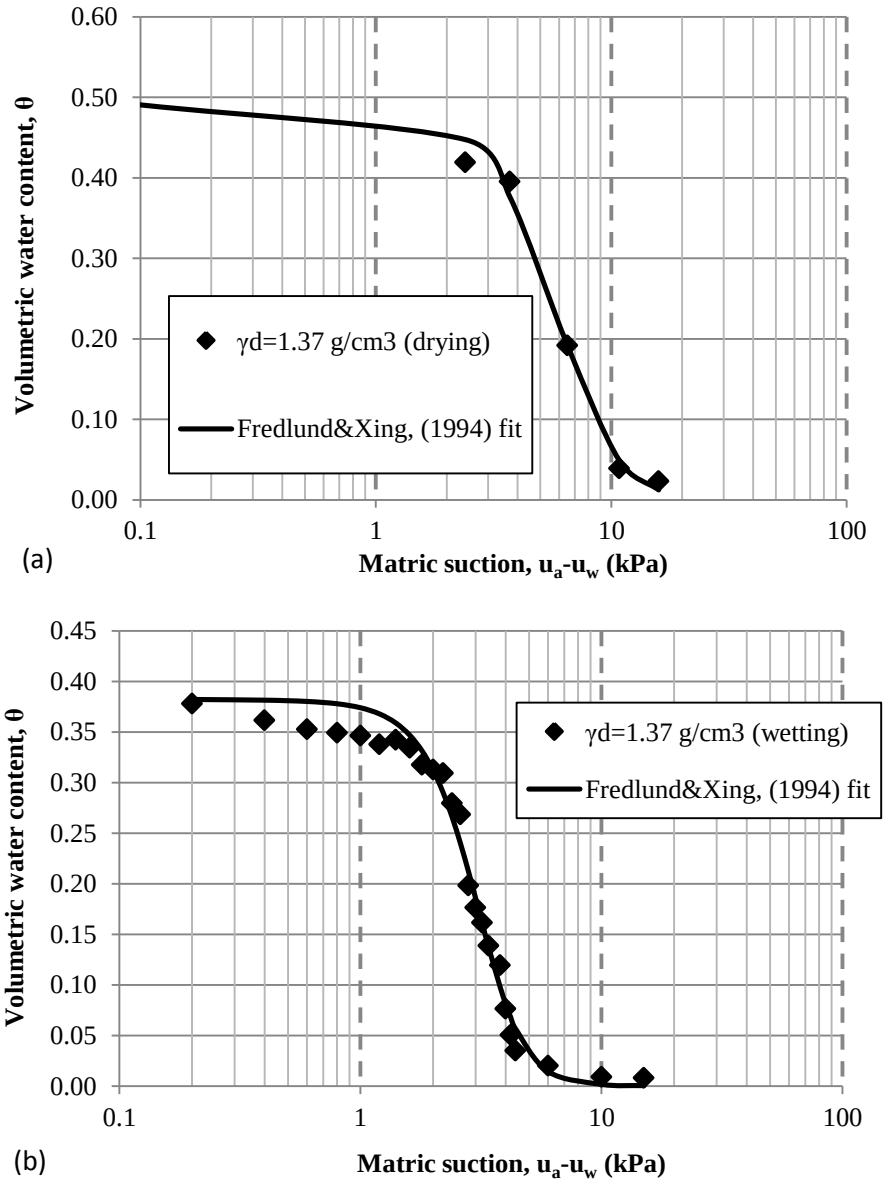

Figure 3. 15. The soil-water characteristic curve of the sand used in the infiltration column experiment, (a) drying SWCC, (b), wetting SWCC, (Ahmadi-adli, 2014).

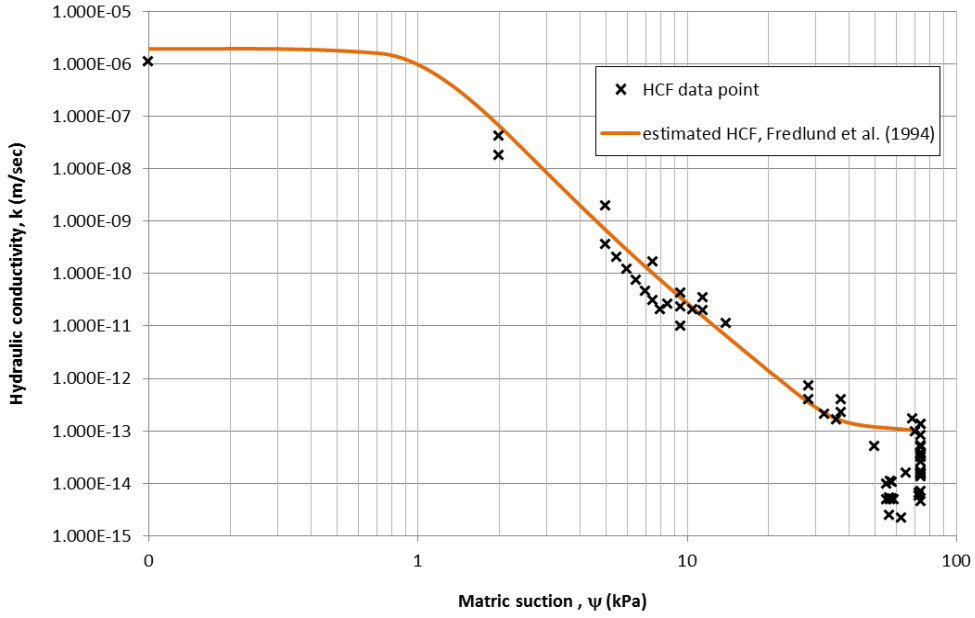

Figure 3. 16. The hydraulic conductivity function (wetting) of the sand used in infiltration column experiment, (Ahmadi-adli, 2014).

In his study, the matric suction values along the infiltration column had been measured from five different elevations by means of tensiometers. These recording stations had been called tns1, tns2, tns3, tns4 and tns5 from highest to lowest elevation. The distance between the stations were 25 cm.

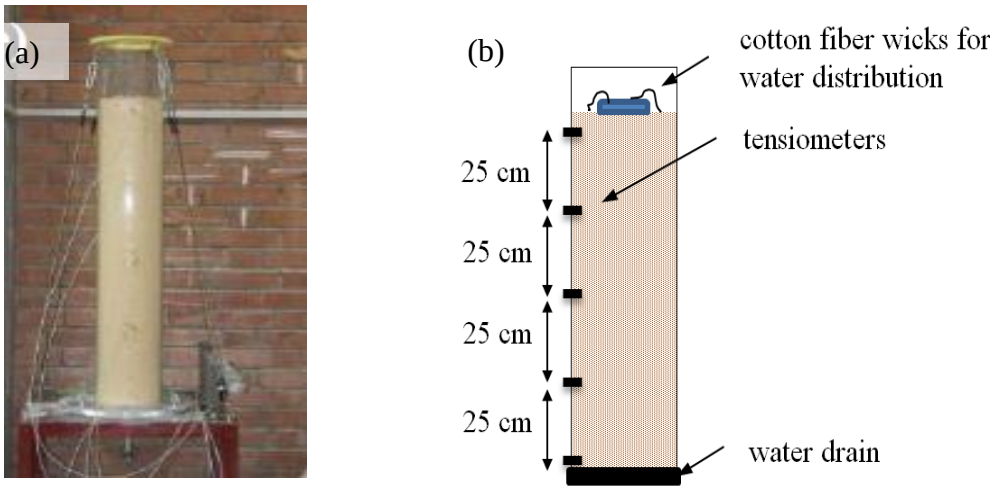

Figure 3. 17. The pictures of (a) infiltration column setup (b) sketch of setup (Ahmadi-adli, 2014).

The rate of propagation of wetting front and suction profile in the infiltration column test was analysed in the generated algorithm. The infiltration column experiment was

simulated by taking the base angle parameter as zero. The upper boundary condition was assigned as a flux value of 1.3 mm/hr that had been reported by Ahmadi-adli (2014). The bottom boundary was considered impervious. The slice element size and the time step size were choosen as 0.01 m and 10 sec., respectively. The results were found to be very sensitive to differences in initial water content at low values. Initial θ was assumed as 1.23e-5, and the initial Ψ was taken as 74 kPa that had been measured at the start of experiment by Ahmadi-adli (2014).

The matric suction values of slice elements which correspond to elevation of reading stations located on the infiltration column were determined in the simulation. The results of simulation, together with the experimental results are illustrated in Fig. 3.10.

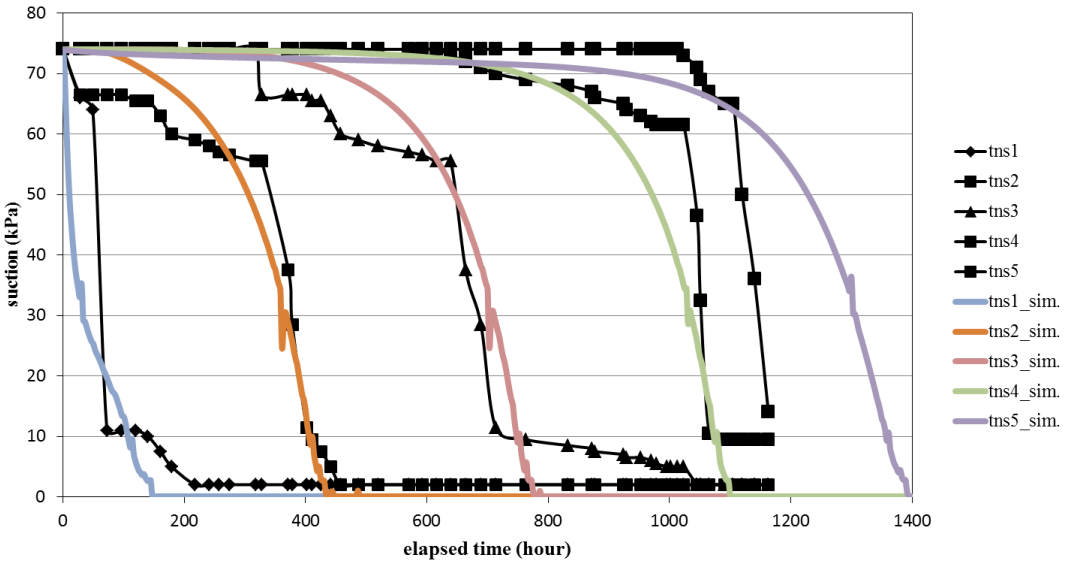

Figure 3. 18. The comparision of experimental results and the results of simulations. Curves with data points illustrate the experimental results and smooth curves illustrate simulation results.

The rate of wetting front propagation observed in the experiment is in agreement with the simulation results; however, there is a deviation for the last tensiometer readings. But simulation results have been considered consistent. A homogeneous soil profile was assumed in the simulation, therefore the time required for the propagation of wetting front through the reading stations that seperated in equal distances must be close to each other.

CHAPTER 4

RAINFALL-INDUCED LANDSLIDE ANALYSIS

After flow calculations, the second stage is to carry out the stability analysis for the infinite slope.

4.1. Geometry

The landslides triggered by infiltration of rain water are generally shallow and the failure planes are parallel to the slope surface; in such cases infinite slope model can be used (see Section 2.6).

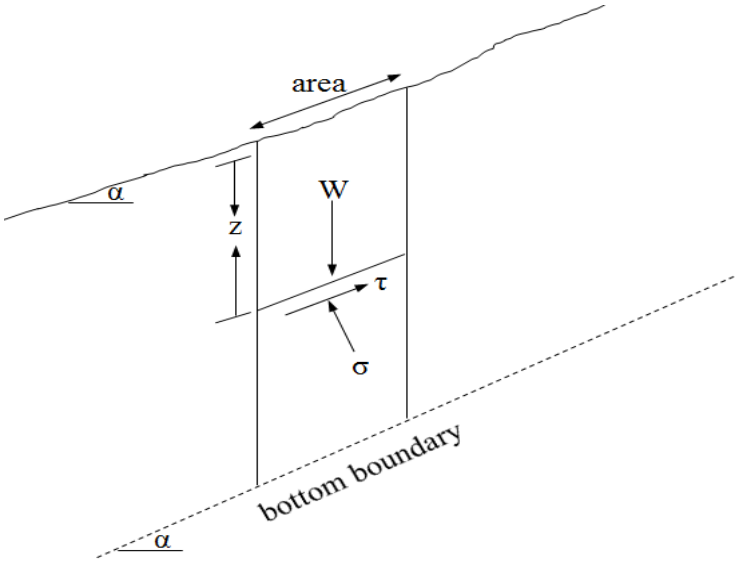

Figure 4. 1. Sketch of the geometry used in stability analyses.

Figure 4.1 shows the infinite slope model used in the stability analyses with the base angle (α), vertical force due to the weight of the soil column over the considered plane (W), the resistive force along the potential failure surface (τ) and the normal force that acts on the potential failure surface (σ). These parameters are defined in the following equations,

$$W = \gamma_{bulk} \times z \times \cos\alpha \times area \tag{4.1}$$

$$\sigma = W\cos\alpha \tag{4.2}$$

$$\tau = W\sin\alpha \tag{4.3}$$

where γ_{bulk} is the bulk unit weight of the soil, and z is the depth of the soil column.

4.2. Stability Model

In the stability analyses, limit equilibrium approach is applied to assess the factor of safety. Factor of safety is defined as the ratio of driving forces (D) and resisting forces (R).

Driving forces that cause instability in the infinite slope can be expressed in the following Eq. 4.4 by combining Eq. 4.1 and Eq. 4.3.

$$D = \sum_{n=1}^{i} \gamma_{i,j} \times \Delta z \times \cos\alpha \times \sin\alpha \times area \tag{4.4}$$

where $\sum_{n=1}^{i} \gamma_{i,j}$ is the cumulative value of bulk unit weight. In the Eq. 4.5, the bulk unit weight of each slice, $\gamma_{i,j}$ is given

$$\gamma_{i,j} = \gamma_{dry} + \theta_{i,j} \times g \tag{4.5}$$

where γ_{dry} and ρ_{dry} are the dry unit weight and the dry density, respectively. As a result, the increase in the soil weight due to increasing water content is taken into account in the calculations by using cumulative weight of the upper slices.

Resisting forces are determined by the shear strength of the soil. In the algorithm, the effect of matric suction is included by using the equation (2.16), as proposed by Vanapalli et al. (1996):

$$R = area \times \left(\left(c + \gamma_{bulk} \times \Delta z \times \left(\cos \alpha \right)^2 \times \tan \phi \right) + \left(\frac{\psi_{i,j} + \psi_{i+1,j}}{2} \times \tan \phi \times \chi \right) \right) \qquad (4.6)$$

where c and ϕ are the effective cohesion and the internal angle of friction, respectively. The parameter χ is equal to the $\left(\frac{\theta_{i,j} - \theta_r}{\theta_{sat} - \theta_r} \right)$ according to Vanapalli et al. (1996).

As a result, the factor of safety becomes,

$$FS(i, j) = \frac{R}{D} \qquad (4.7)$$

4.3. Hypothetical Soils

The effect of SWCC characteristics on the rainfall-induced landslides have been investigated by means the developed algorithm.

Ahmadi-adli (2014) generated realistic hypothetical soils by changing one of the characteristic parameters (air-entry pressure, AEV, saturated volumetric content, θ_s, de-saturation rate, DSR and residual volumetric water content, θ_r of a real sand soil (AEV=1.75 kPa, θ_s=0.44, DSR=0.06 and θ_r=0.135) and assuming other parameters remain constant. The detailed description for the theory about the generation of hypothetical soils could be found in his aforementioned study. Briefly, the soils of different air-entry values had been generated by multiplying suction values of original SWCC with corresponding constant numbers since AEV of a soil is related to its grain size. For the soils with different saturated volumetric water contents, SWCCs had been obtained by increasing/decreasing θ values proportionally. The soils with different DSR values had been generated by multiplying the DSR of original soil with corresponding constant numbers. The soils with different residual volumetric water content values had been generated by decreasing and increasing the

volumetric water content values at the tail of SWCC. HCFs of hypothetical soils had been estimated by using method proposed by Fredlund et al. (1994).

It is also possible to see the capability of the infiltration algorithm by using these various type of soils since each soil may lead different hydraulic mechanism that results in numerical problems in the computations; for example, the soils that have steep hydraulic functions may cause numerical instability resulting in oscillation of values. The SWCCs and HCFs of hypothetical soils are shown in Fig. 4.3 – 4.9.

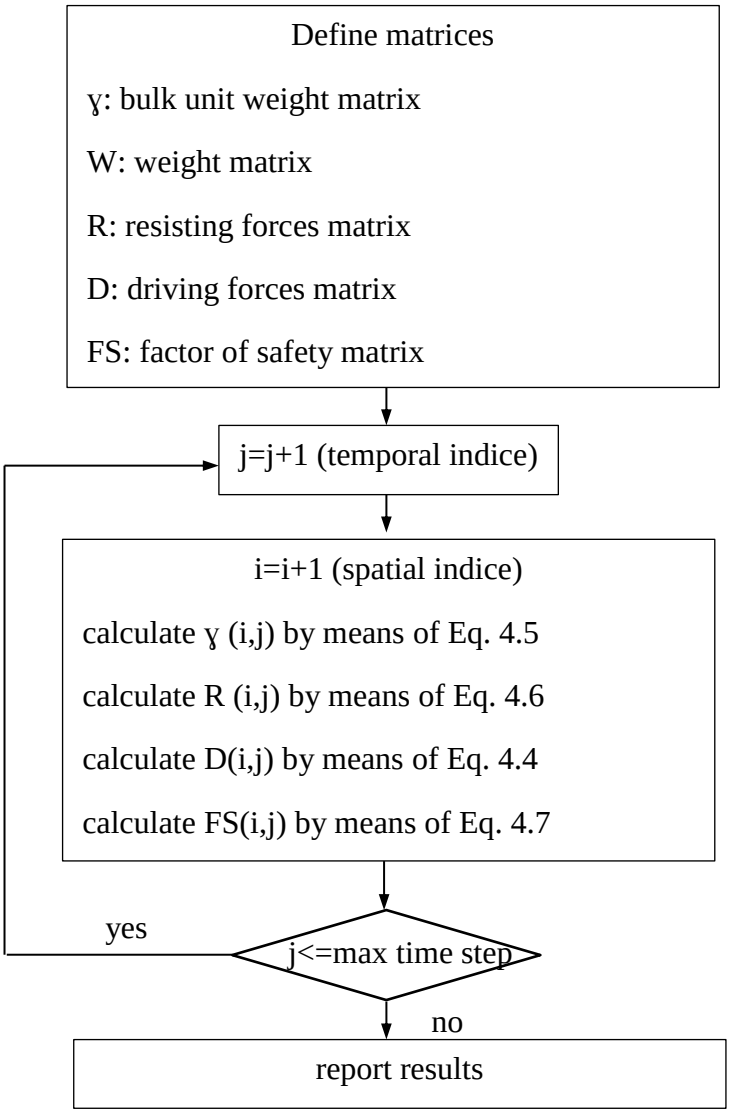

Figure 4. 2. Flow chart of stability calculations.

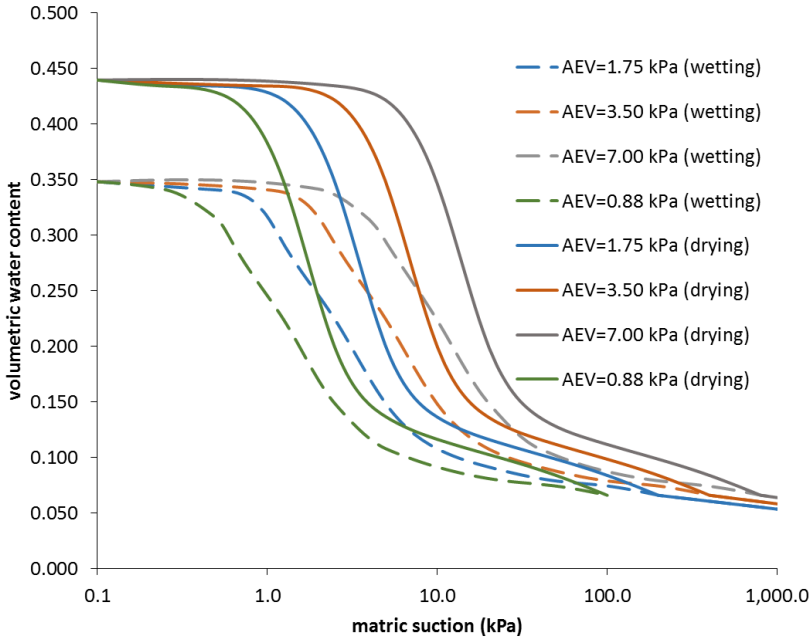

Figure 4. 3. SWCCs of hypothetical soils with different AEV (Ahmadi-Adli, 2014).

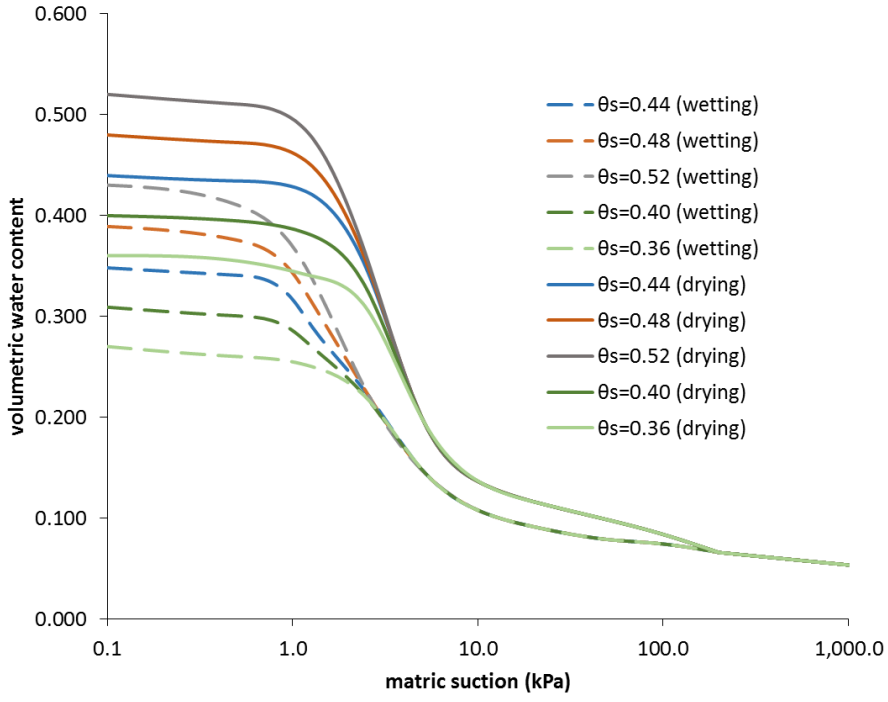

Figure 4. 4. SWCCs of hypothetical soils with different θ_s (Ahmadi-Adli, 2014).

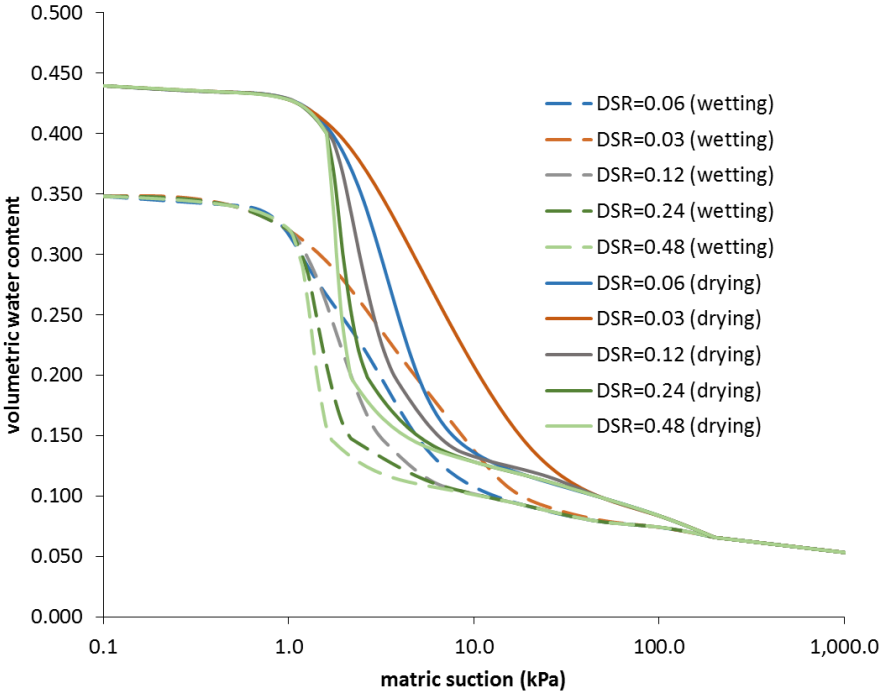

Figure 4. 5. SWCCs of hypothetical soils with different DSR (Ahmadi-Adli, 2014).

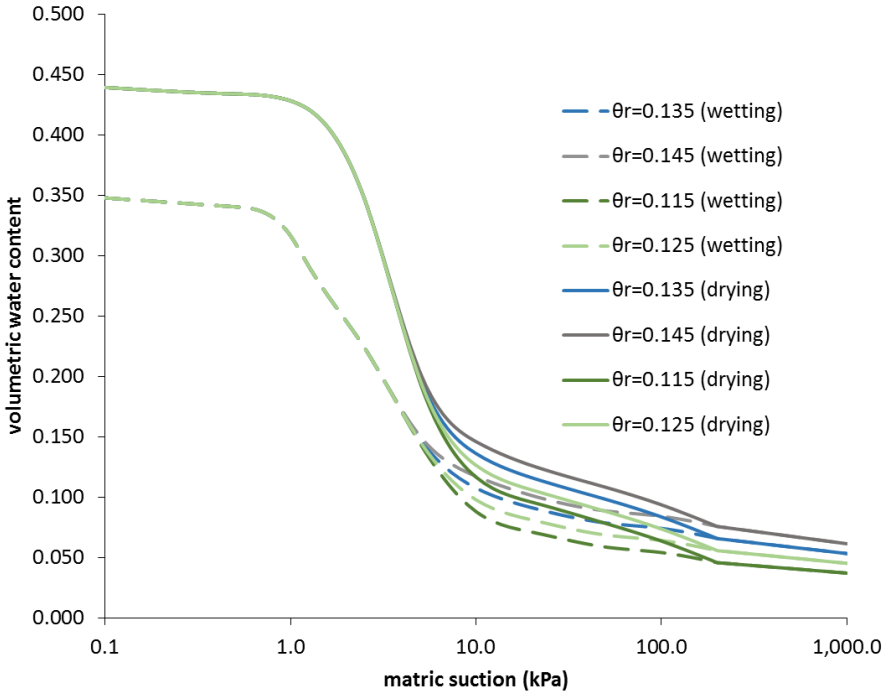

Figure 4. 6. SWCCs of hypothetical soils with different θ_r (Ahmadi-Adli, 2014).

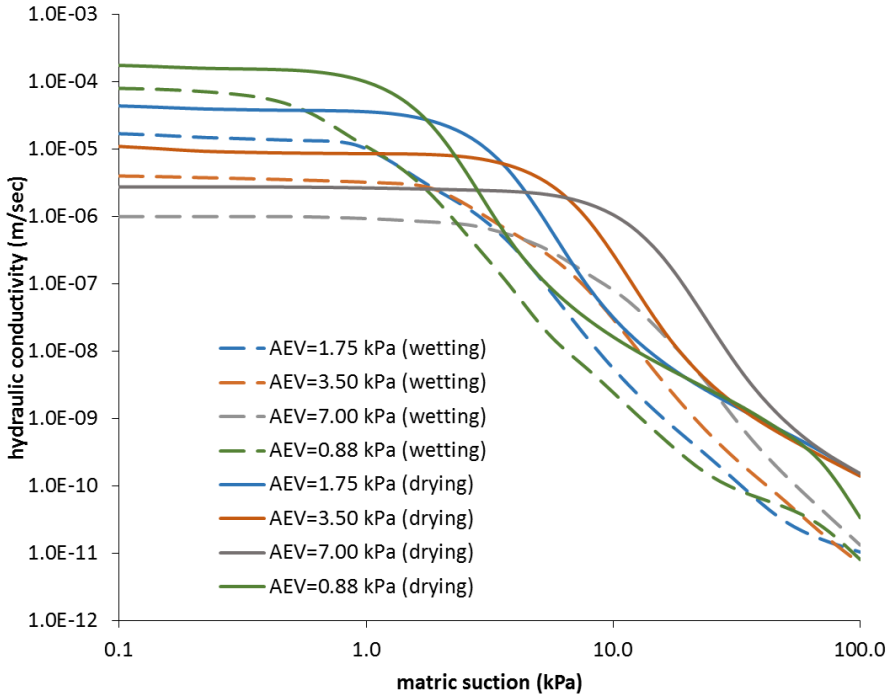

Figure 4. 7. HCFs of hypothetical soils with different AEV (Ahmadi-Adli, 2014).

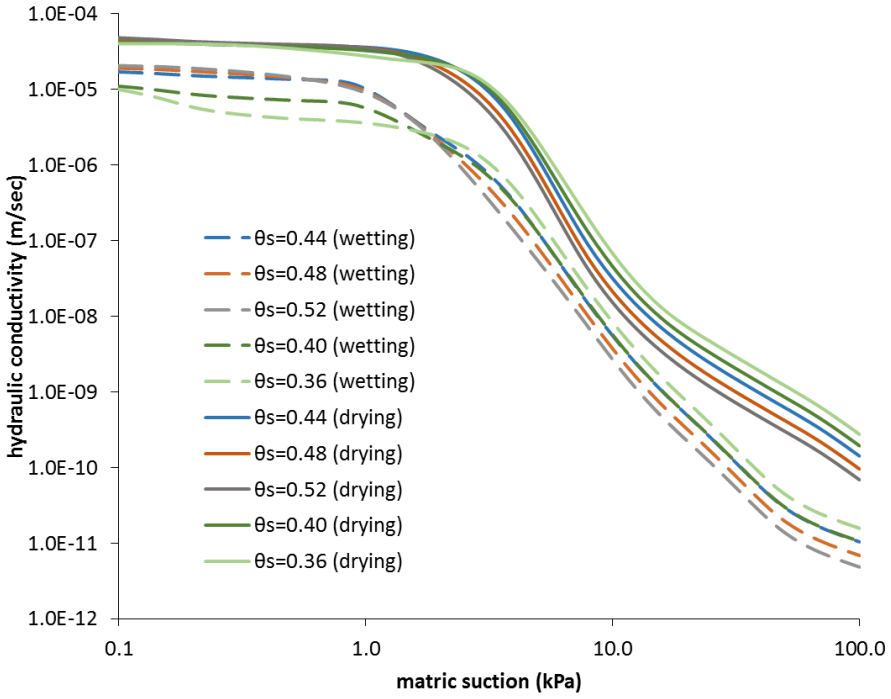

Figure 4. 8. HCFs of hypothetical soils with different θ_s (Ahmadi-Adli, 2014).

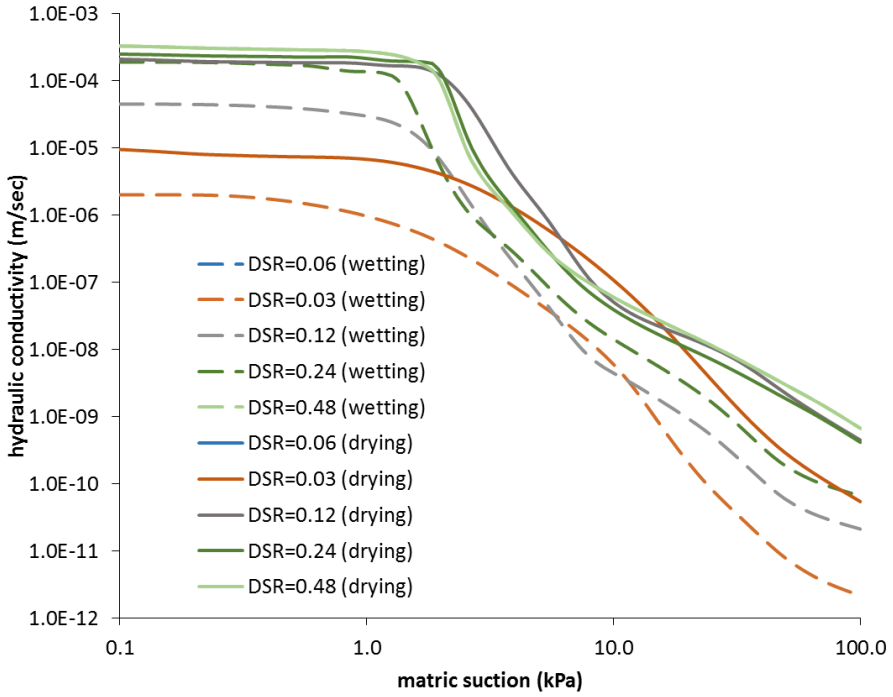

Figure 4. 9. HCFs of hypothetical soils with different DSR (Ahmadi-Adli, 2014).

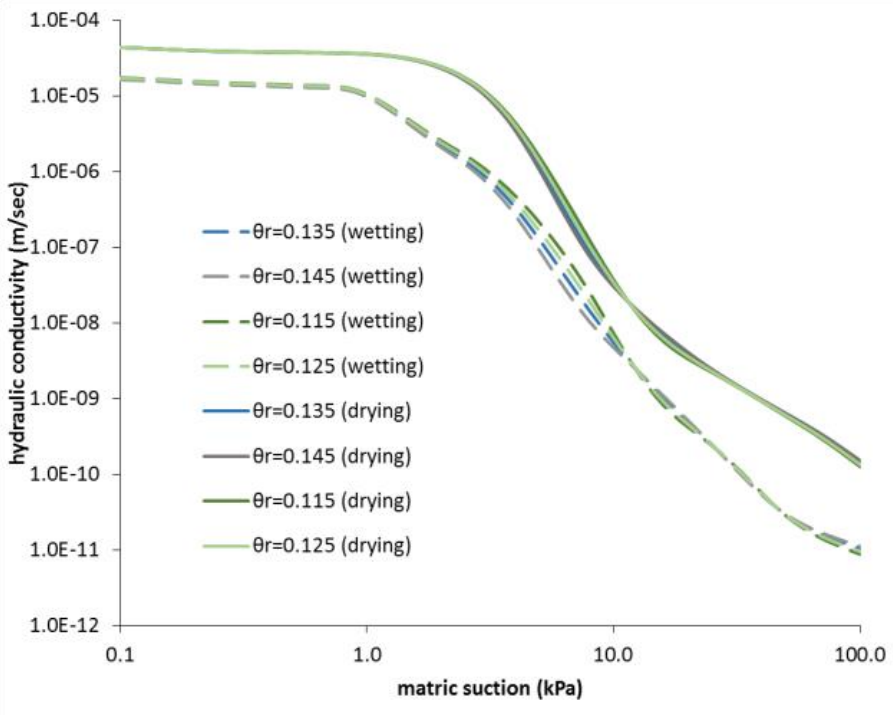

Figure 4. 10. HCFs of hypothetical soils with different θ_r (Ahmadi-Adli, 2014).

4.4. Parametric Study

The generated algorithm was used to simulate the infiltration of rain water and to analyse the stability of the unsaturated infinite slopes that consist of various hypothetical soils.

In all simulations, 1 m height infinite slope was considered. The bottom boundary was assumed impervious. The analyses were carried out at constant rainfall intensities of 1 mm/hr, 5 mm/hr, 10 mm/hr, 20 mm/hr, 40mm/hr and 80 mm/hr. For each type of soil, initial conditions were determined by carrying out an equalization analysis. During equalization stage, infiltration algorithm was run by assigning zero flux to the uppermost boundary. The water flow due to gravity ceased when the steady state condition is reached. The initial condition for the equalization stage was arranged by assigning volumetric water content value of 0.1 for all slice elements. The only exception was that initial volumetric water content value was taken as 0.08 in the analyses of hypothetical soils that have varying residual volumetric water content values. Evaporation is not allowed during equalization stage. Then, the suction and volumetric water content profile of the slope at the end of equalization was assigned as initial condition in the rainfalling stage. The hydraulic conductivity function was considered in the volumetric water content-based relationship instead of the matric suction-based since the hysteresis phenomenon is not observed in case of volumetric water content-based hydraulic conductivity values.

The base angle of the slope, internal friction angle and effective cohesion were taken as 46 degree, 37 degree and 0 kPa, respectively.

4.4.1. Results of Simulations

In this section, the results of the parametric analyses have been illustrated in the following figures. These figures include suction and volumetric water content profiles at the time of failure for varying rainfall intensities and rainfall intensity and duration thresholds of each hypothetical soil.

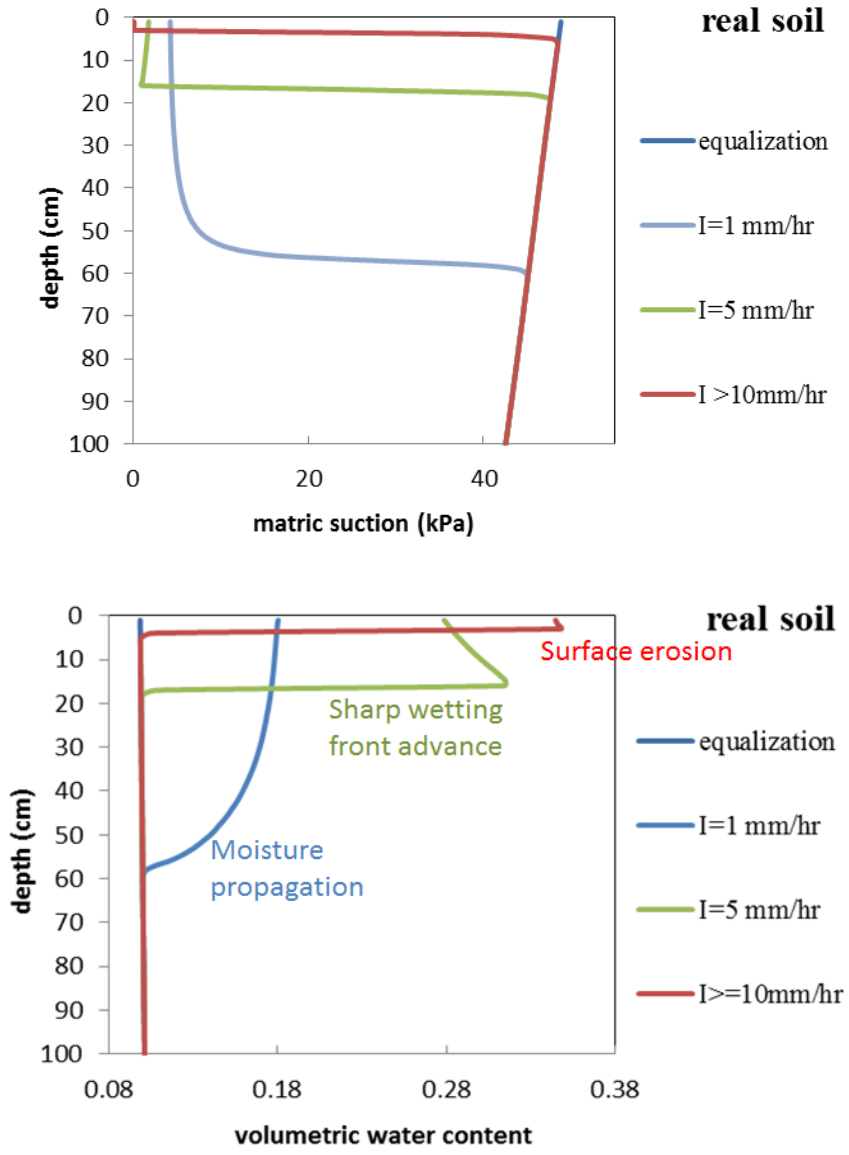

Figure 4. 11. The matric suction and volumetric water content profiles at the time of failure for hypothetical soils that have different air-entry values.

In Fig. 4.11 the matric suction and water content profiles of the simulation for the real soil is illustrated. All other results can be found in the appendix. The water content profiles of all soils show three different type of wetting front shape responsible for failure. The low intensity rainfalls yield moisture propagation (M denotes moisture propagation). For example, 1 mm/hr rainfall intensity causes moisture propagation at the time of failure for real soil. As rainfall intensity increases, sharp wetting fronts are observed (W denotes sharp wetting front) (e.g. 5

mm/hr rainfall intensity for real soil). Although decreasing water content after the passage of the wetting front in the sharp wetting front mode might appear unrealistic, this type of wetting fronts are reported in experimental studies in the literature (Shiozawa and Fujimaki 2004, DiCarlo 2004 and DiCarlo 2007). However, at the later stage of this study, it was realized that the possible reason of unrealistic wetting front propagation might be caused by the sensitivity of the results to the element size (i.e. slice height) (see Section 5.3.1). Higher rainfall intensities (10, 20, 40 and 80 mm/hr) yield failure at the surface. This type of failure due to quick wetting front propagation is considered as surface erosion (E denotes surface erosion).

Table 4. 1. Results of analyses for real soil.

AEV=1.75					
I (mm/hr)	f. depth(cm)	f. time(min)	Ψ_failure (kPa)	θ_failure	f. type
1	46	1568.5	6.30	0.149	M
5	15	274.7	1.10	0.315	W
10	2	48.7	0.17	0.346	E
20	2	44.2	0.16	0.346	E
40	2	42.2	0.16	0.346	E
80	2	41.2	0.15	0.347	E

Where, I is the rainfall intensity (mm/hr), f.depth is the failure depth (cm), f. time is the time of failure (minute), Ψ_failure is the value of matric suction for given failure depth at the time of failure, θ_failure is the value of volumetric water content for given failure depth at the time of failure and f.type is type of failure.

The rainfall intensity – duration tresholds are illustrated in the following Fig. 4.12 – 4. 15. All data points are classified according to wetting front shape. In these figures, red color data point denotes E type wetting front, green color data point denotes W type wetting front and blue color data point denotes M type wetting front.

The results of parametric study reveal the following conclusions,

- The amount of rainfall intensity does not change the failure mechanism within the slope after a certain upper limit since some of rainfall water does not infiltrate into the soil and generate surface-run off. This can be seen both from overlapped suction (or volumetric water content) profiles for higher

rainfall intensities and from the straight part of rainfall intensity-duration plots corresponding to high rainfall intensities.

- High rainfall intensities usually cause extremely shallow failures (a few centimeters) since upper parts of the slope become saturated quickly and failure occurs prior to propagation of wetting front into the deep layers of the slope. This can perhaps be labeled as “erosion” rather than “landslide”. The decrease in the matric suction reduces the contribution to the soil strength and triggers failure. Low intensity rainfalls infiltrate into deep layers without reducing matric suction of upper layers too much and not cause shallow failures. But the effect of driving forces becomes more significant due to increasing soil mass over the potential slip surface. In this case, relatively small decrease in matric suction together with increasing effect of soil weight trigger failure in the slope.
- For the soils that have higher air-entry pressure, failure is postponed (see Fig 4.12).
- The soils that have steep soil water characteristic function (higher DSR values) show changeable failure mechanisms. For these soils, small changes in volumetric water content result in sudden changes in the matric suction and infiltration can cause failure at any depth depending on the rainfall intensity. On the contrary, the soils that have smooth soil water characteristic function (lower DSR values) do not show sudden changes in matric suction and the failure occurs in similar mechanism (see Fig. B1- B9).
- The soils that have lower saturated volumetric water content values or higher dry density remain stable shorter period of time compared to soils that have higher saturated volumetric water content values. This result might cause misconception since it is expected that increase in dry density also increases the friction angle; however, in this study this effect is not considered (see Fig 4.14).
- The failure time is higher for the soils that have higher residuel volumetric water content values since the initial value of matric suction becomes higher for the same volumetric water content value (see Fig 4.15).

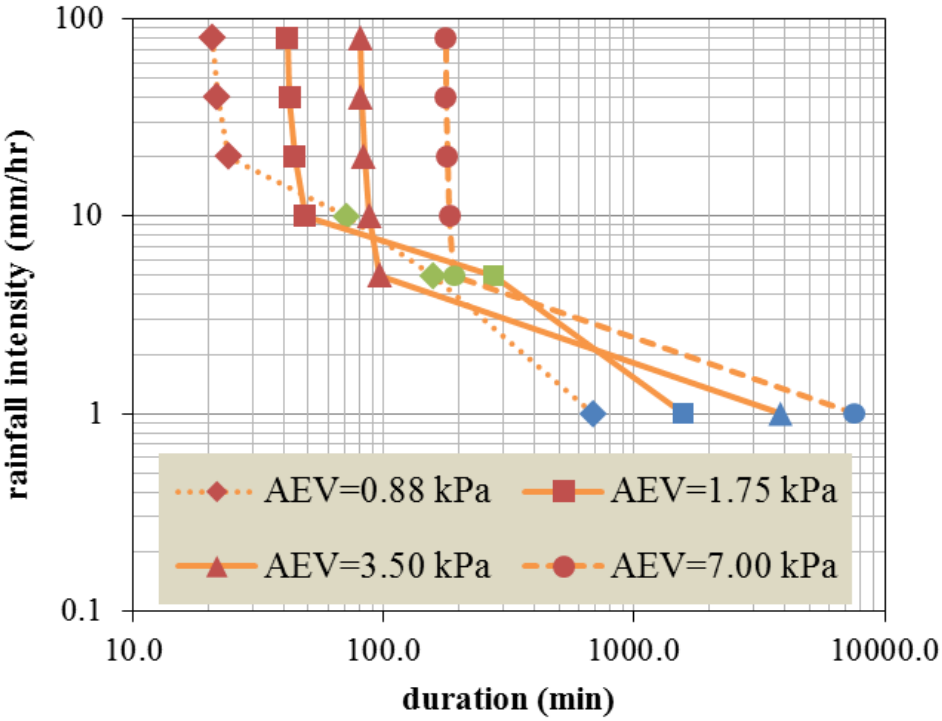

Figure 4. 12. I-D thresholds for soils that have different AEV.

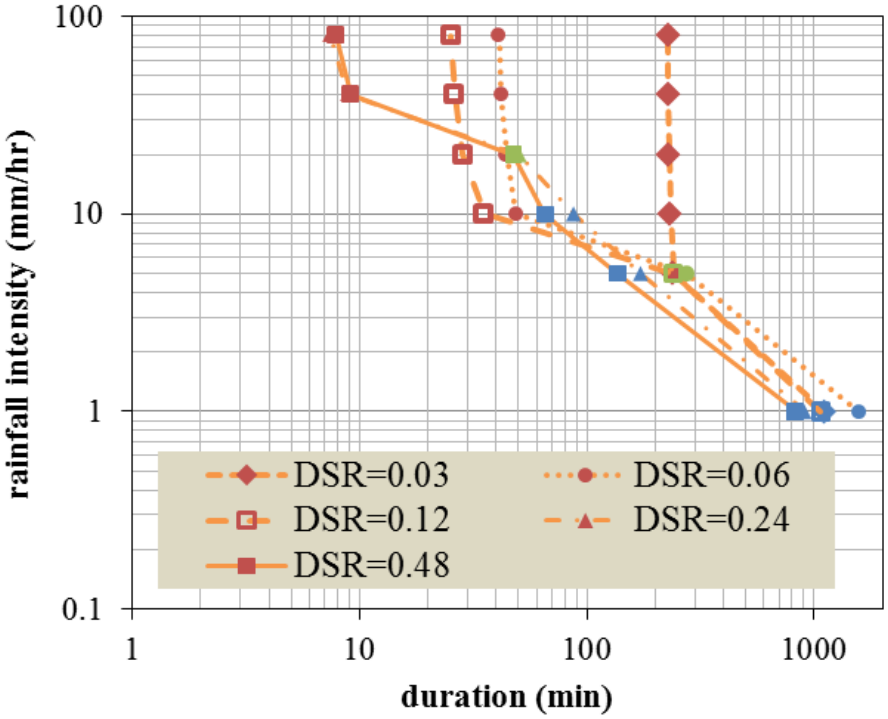

Figure 4. 13. I-D thresholds for soils that have different DSR.

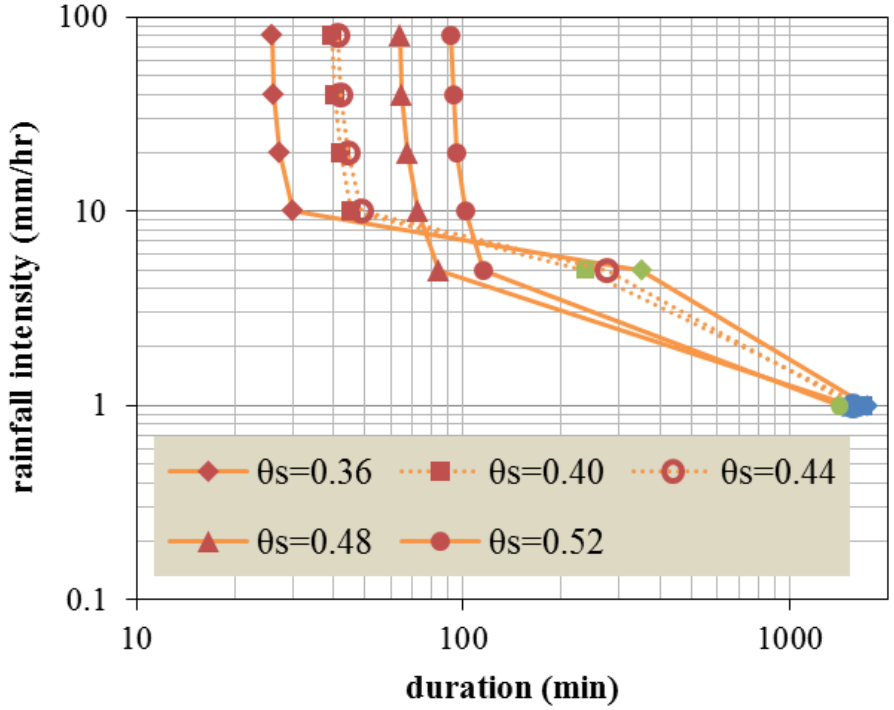

Figure 4. 14. I-D thresholds for soils that have different θ_s.

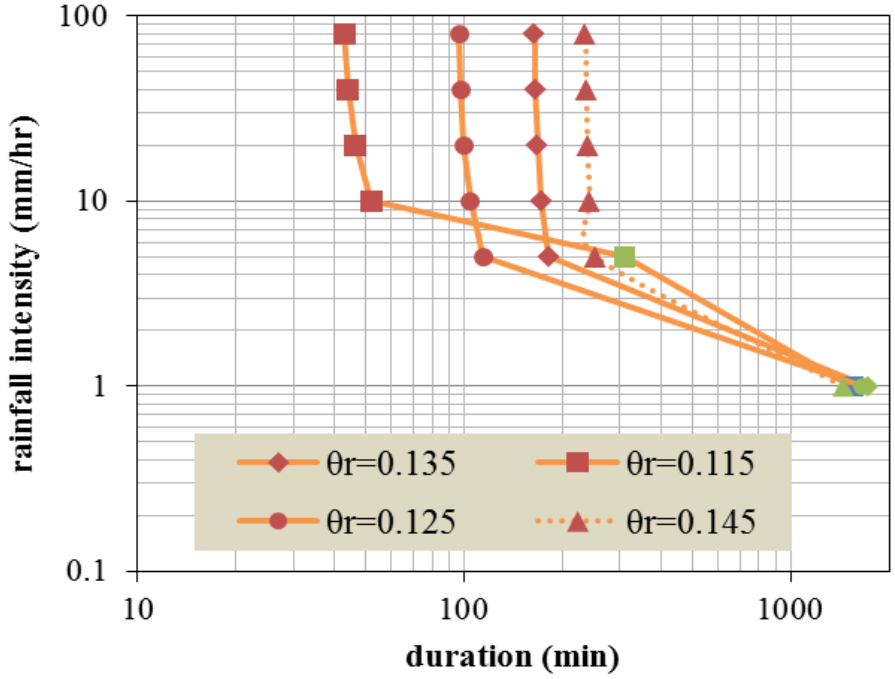

Figure 4. 15. I-D thresholds for soils that have different θ_r.

4.4.2. Effect of Base Angle and Initial Water Content

The effect of base angle on the I-D thresholds were investigated by assigning different base angle values (38°, 39°, 40°, 42°, 46° and 50°) in the simulations. The real soil (AEV = 1.75 kPa, DSR = 0.06, θ_s = 0.44 and θ_r = 0.135) was used and initial value of volumetric water content was taken as 0.10 in all analyses.

As it can be seen in Fig. 4.16, the variation of base angle causes shifting of I-D thresholds along the time axis. The failure mechanism of slope also changes from E (surface erosion) to W (sharp wetting front propagation) as the base angle decreases. It should be noted that I-D thresholds for base angle of 50° and base angle of 46° almost overlap; therefore, further increase of base angle did not change the I-D threshold.

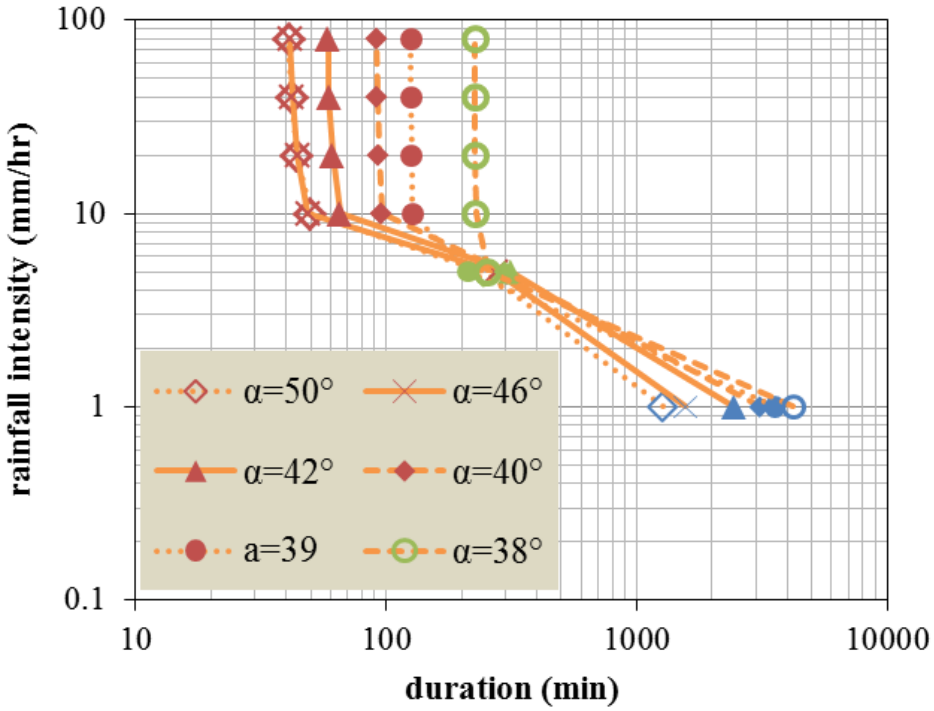

Figure 4. 16. Effect of base angle on the I-D thresholds.

The effect of initial volumetric water content on the I-D thresholds were also investigated. The real soil (AEV = 1.75 kPa, DSR = 0.06, θ_s = 0.44 and θ_r = 0.135)

was used and value of base angle was taken as 40° in all analyses. As the initial value of volumetric water content increases, failure occurs at deeper parts of the slope.

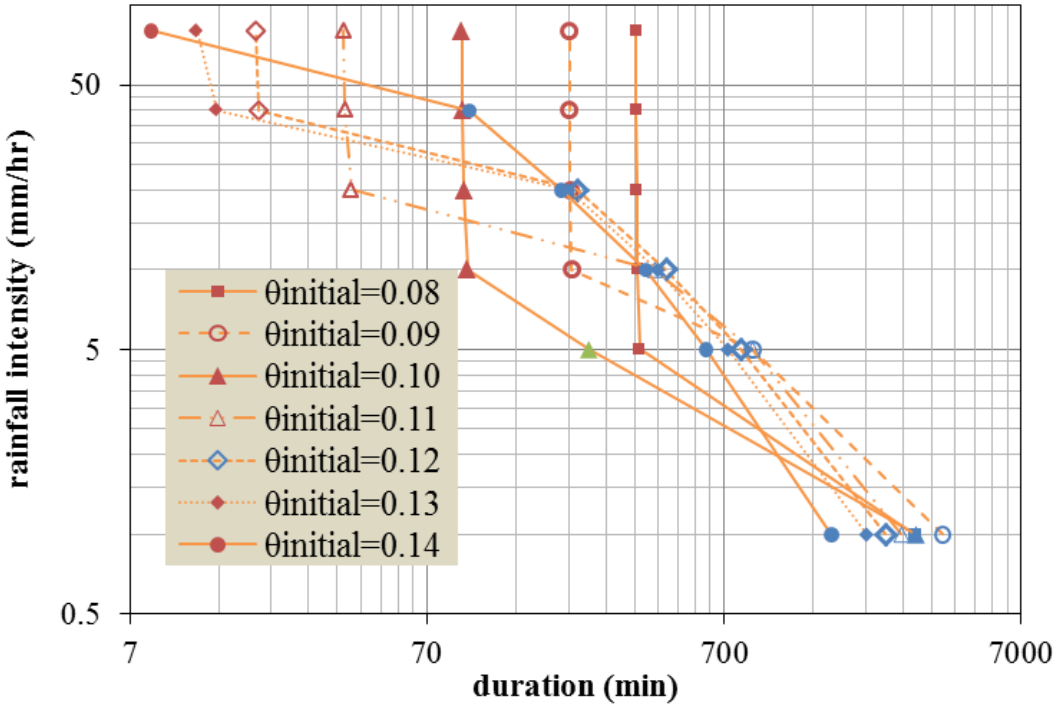

Figure 4. 17. Effect of initial volumetric water content value on the I-D thresholds.

CHAPTER 5

CONCLUSION

5.1. Achievements

In this study, a numerical algorithm was developed to estimate the water pressure profile within the unsaturated soil slope and to perform stability analyses.

One dimensional seepage problem was considered to carry out hydraulic calculations. The numerical modelling of seepage problem was achieved by implementing Darcy's law and principle of mass conservation in the formulations. The prediction capability of the developed model was improved by using different numerical techniques (i.e. predictor-corrector based solutions, novel water distribution algorithm). The experimental results reported by Ahmadi-adli (2014) were used to verify the numerical model by simulating his infiltration column test in the developed algorithm and consistent results were obtained.

The important novelty in this study is the proposed hysteresis model that can be used to trace transition curves between the main branches of the soil water characteristic function. This model can be used in incremental form to predict suction in different frameworks (e.g. constitutive models) and other physical problems. The scanning curve model fits the general shape of retention curves found in the literature.

5.2. Conclusions

The proposed equations for hysteresis modelling were used to trace experimentally determined scanning curves. It was deemed that the scanning curves show variations

depending on the wetting/drying direction and material type. But, an average value of power-type parameter (*K*) can be used for those equations since this parameter marginally changes the shape of the scanning curve.

The one-dimensional flow algorithm was developed by making the reasonable assumptions to simplify natural mechanism. It was seen that this numerical model can be used to estimate soil water pressure(or water content) profile.

The parametric study reveals that there are many factors responsible for the stability of slopes. These factors can be classified into two different category; i) material-dependent factors such as gradation, uniformity, dry density, fines content, ii) external factors such as rainfall intensity, base angle, natural characteristics of real boundary conditions, rainfall history. There are numerious combinations of these factors that result in failure for a given slope. Therefore, failure is observed in different mechanisms.

The amount of rainfall intensity does not change the failure mechanism within the slope after a certain upper limit since some of rainfall water does not infiltrate into the soil and generate surface-run off. This can be seen both from overlapped suction (or volumetric water content) profiles for higher rainfall intensities and from the straight part of rainfall intensity-duration plots corresponding to high rainfall intensities.

High rainfall intensities usually cause extremely shallow failures (a few centimeters) since upper parts of the slope become saturated quickly and failure occurs prior to propagation of wetting front into the deep layers of the slope. The decrease in the matric suction reduces the contribution to the soil strength and triggers failure. Low intensity rainfalls infiltrate into deep layers without reducing matric suction of upper layers too much and not cause shallow failures. But the effect of driving forces becomes more significant due to increasing soil mass over the potential slip surface. In this case, relatively small decrease in matric suction together with increasing effect of soil weight trigger failure in the slope.

5.3. Future Works

- More experimental results can be found in the literature and can be used for the proposed hysteresis model. Therefore, the power-type parameter in the relations might be better interpreted.

- The ultimate aim in this research is to develop numerical algorithm that can be used in landslide prediction. The generated model in this study can be used in basin scale by seperating the wide area into elemental pieces. The algorithm then used to analyse the water pressure profile and stability for each elemental area. To do this, the algorithm might be inserted into a GIS-based framework.

- In this study, main effort has been spent on the modelling of hydraulic process. However, the results of stability analyses directly effect the accuracy of the prediction. Therefore, more works concerning the stability analyses will be required.

- The another issue is related to use the algorithm in elemental area to obtain results in the basin scale. For this purpose, a run-off model should also be developed in order to distribute the surface run-off between the elemental areas.

- Simulations can be forced to continue after surface erosion is initiated, by modifying the algorithm to progressively change the upper boundary. This might help modelling of surface erosion and perhaps even mudflow mechanism.

5.3.1. Equivalent Hydraulic Conductivity

The sensitivity of simulation results to the element size becomes important in case of determining equivalent hydraulic conductivity between successive slices in Eq. 3.4. At early parts of this study, arithmethic mean was prefered and the effect of element size on the results was investigated based on this assumption. The method was then changed by taking harmonic mean in the Eq. 3.4 and all simulation results that are presented in Chapter 4 were obtained by assuming harmonic mean for the equivalent value of conductivity in Eq. 3.4. At the final stage of this study, it was realized that the effect of element size on the simulations became more sensitive after changing the method in the Eq. 3.4. Therefore, it was decided that the method for determining

the equivalent value of hydraulic conductivity should be changed and following approach can be considered.

In the numerical modelling of seepage within the unsaturated soil slope (see Chapter 3), parameters of matric suction (ψ), volumetric water content (θ) and hydraulic conductivity (k) were considered. Once one of these parameters are calculated during calculations, it is assumed that this result is corresponding average value for each slice; for example, $\psi(i, j)$, $\theta(i, j)$ or $k(i, j)$ correspond to average value of each parameter at the mid-height of i^{th} slice at the j^{th} time step. Therefore, these calculated values become known value of the distribution function of ψ, θ and k at the mid-height of the slices within the slope. The parameter of flux (q) is calculated based on these parameters and $q(i, j)$ corresponds to value of flux from i^{th} slice to $i+1^{th}$ slice. However, an equivalent value of k should be determined in order to use in the Darcy's equation. An expression for equivalent value of k can be derived by considering the fact that the summation of infinitesimal headloss within each slice element is equal to total headloss within slope.

$$\Delta h = \int d\Delta h \tag{5.1}$$

where Δh is the total headloss within the slope and $d\Delta h$ is the headloss within a slice element. Darcy's equation can be used to obtained following relationship,

$$k_{eqv} = \frac{\Delta z}{\int \frac{dz}{k}} \tag{5.2}$$

where k_{eqv} is the equivalent hydraulic conductivity, Δz spatial integration of infinitesimal height element dz.

The important point in Eq. 5.2 is spatial integration of k values are required in order to obtain k_{eqv}.

In order to accurately calculate the flux, equivalent value of the k might be determined by using known values of k at the mid-points of two neighboring slices and a third value of k to numerically integrate the spatial distribution function of k

along the slices. The Simpson's rule can be implemented by using three known values of *k*. The third point for k can be obtained by considering following method.

Assuming a third degree polynomial can describe the variation of θ within a slice and its neighnors (similar to a cubic spline), the unknown value of θ at the border just between two successive slice elements can be estimated by using two known values of θ at the mid-heights of slice elements and implementing centered finite difference approximation. Since the curvature of the equation is constant, the second derivative of the second order equation becomes a constant value; therefore it is possible to write following linear relationship,

$$\theta''_{border}(i,j) = \frac{\theta''(i,j) + \theta''(i+1,j)}{2} \tag{5.3}$$

where $\theta''_{border}(i,j)$ is the value of second derivative of the variation function of the θ at the border between the i^{th} and $i+1^{th}$ slices, $\theta''(i,j)$ is the value of second derivative of the variation function of the θ at the mid-height of the i^{th} slice and $\theta''(i+1,j)$ is the value of second derivative of the variation function of the θ at the mid-height of the $i+1^{th}$ slice.

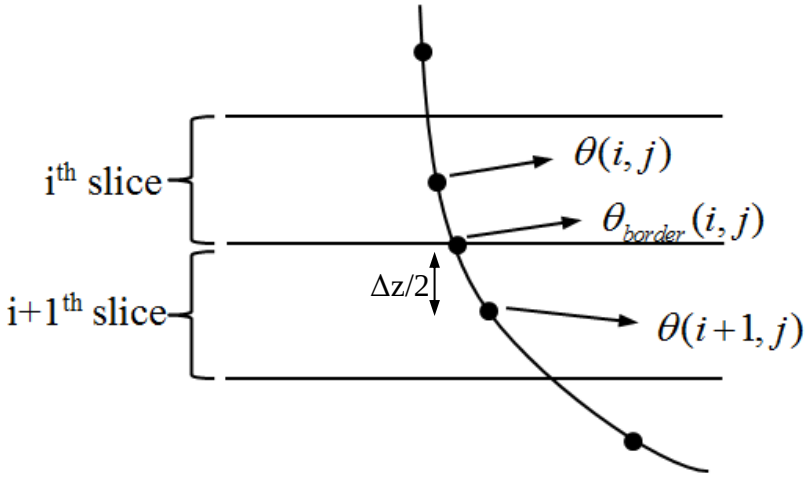

Figure 5. 1. Schematic illustration of proposed method.

The second derivatives in the Eq. 5.3 can be extended by implementing centered finite difference approximation and following relation is obtained,

$$\frac{\theta(i,j)-2\,\theta_{border}(i,j)+\theta(i+1,j)}{\frac{\Delta z^2}{4}}=\frac{\theta(i-1,j)-2\theta(i,j)+\theta(i+1,j)}{2\Delta z^2}$$
$$+\frac{\theta(i,j)-2\theta(i+1,j)+\theta(i+2,j)}{2\Delta z^2} \qquad (5.4)$$

And the value of $\theta_{border}(i,j)$ can be obtained in the following Eq. 5.5,

$$\theta_{border}(i,j)=\frac{-\theta(i-1,j)+9\theta(i,j)+9\theta(i+1,j)-\theta(i+2,j)}{16} \qquad (5.5)$$

$\theta_{border}(i,j)$ can be used to calculate the *k* value at the border between successive slice elements by means of HCF and this value of *k* can be denoted by k_b.

The equivalent hydraulic conductivity can be espressed in the following Eq. 5.6 by using Simpson's Rule.

$$k_{eqv}=\frac{\Delta z}{\int\frac{dz}{k}}=\frac{\Delta z}{\left(\frac{1}{k(i,j)}+\frac{4}{k_b(i,j)}+\frac{1}{k(i+1,j)}\right)\frac{\Delta z/2}{3}} \qquad (5.6)$$

In the following Fig. 5.2, the equivalent hydraulic conductivity approach and harmonic mean approach is compared by performing same simulation (rainfall intensity 5mm/hr and real soil was used). The convergence of equivalent hydraulic conductivity can be observed since there is an overlap for the results of 100 slices and 200 slices. The interesting issue is the unrealistic wetting front propagation disappears in case of equivalent hydraulic conductivity approach.

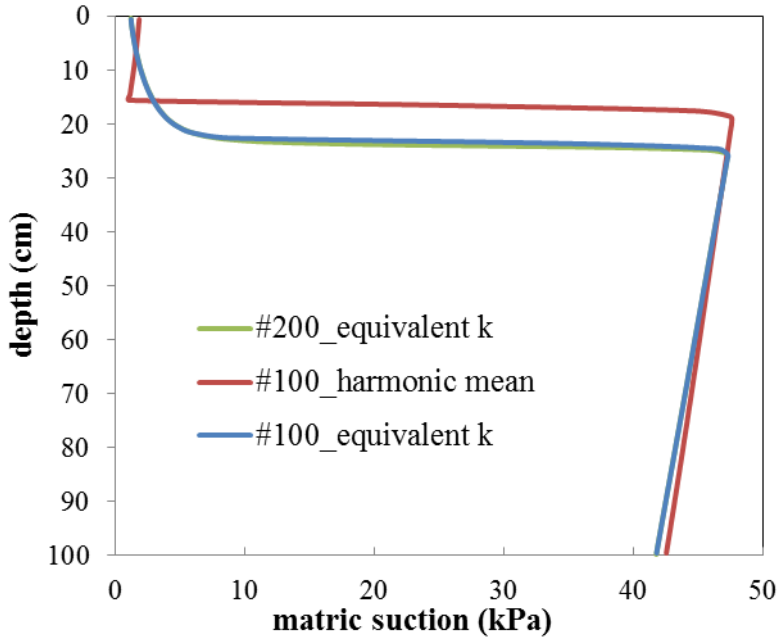

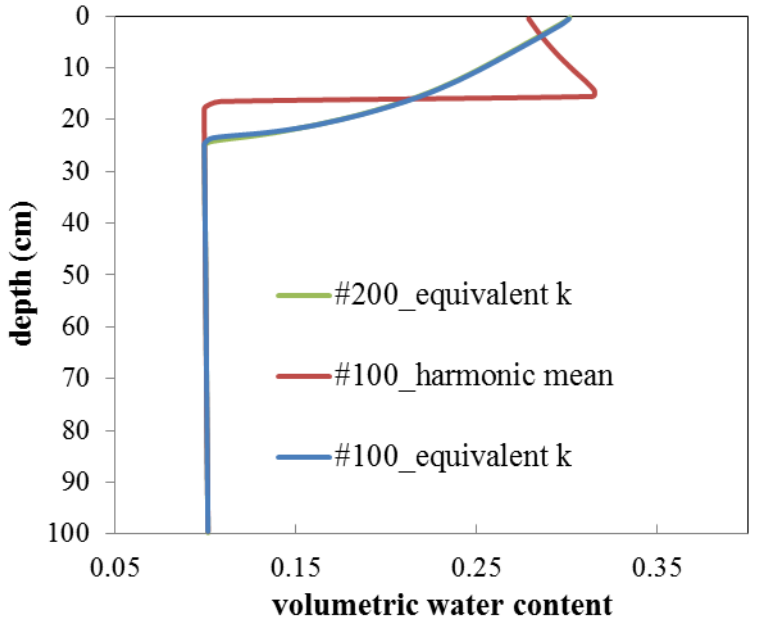

Figure 5. 2. Comparison of equivalent hydraulic conductivity approach and harmonic mean approach.

REFERENCES

Ahmadi-adli, M. (2014)."Shallow Landslides Triggered by Rainfall in Unsaturated Soils" Doctor of philosophy dissertation in civil engineering, Middle East Technical University.

Aitchson, G. D. (1965). Moisture Equilibria and Moisture Changes in Soils beneath Covered Areas, Butterworths.

Arya, L. M. and Paris, J. F. (1981). "Physicoempirical model to predict the SMC from particle size distribution and bulk density data", Soil Science Society of America Journal, Vol.45, pp.1023-1030.

ASTM D6836-02(2008)e2, Standard Test Methods for Determination of the Soil Water Chararcteristic Curve for Desorption Using a Hanging Column, Pressure Extractor, Chilled Mirror Hygrometer, and/or Centrifuge, ASTM International, West Conshohocken, PA, 2008

ASTM D7664, Standart test methods for measurement of hydraulic conductivity of unsaturated soils.

Averjanov, S.F. (1950). "About permeability of subsurface soils in case of complete saturation",English Collection,7,19-21.

Beese, F., and Van Der Ploeg, R.R. (1976)."Influence of hysteresis on moisture flow in an undisturbed soil monolith". Soil Sci. Am. J. 40:480-483.

Bishop, A. W. (1959). "The principle of effective stress", Teknisk Ukeblad, Vol.106, No.39, pp.859-863.

Bishop, A. W. and Donald, I. B. (1961). "The experimental study of partly saturated soil in the triaxial apparatus", 5th International Conference on Soil Mechanics and Foundation Engineering, Paris, Vol.1, pp.13-21.

Brooks, R., Corey, A. (1964) "Hydraulic Properties of Porous Media", Hydrology Paper, 3, Colorado State University, CO, US.

Bruce, R., and Klute, A. (1956)."The measurement of soil moisture diffusivity". Soil Science Society of America Proceedings, 20, 458-462.

Burdine, N.T.(1953). "Relative permeability calculation from size distribution data" Transactions, American Institue of Miningi Metallurgical and Petroleum Engineers, 198, 71-78.

Chen, P., Wei, C., and Ma, T. (2014)," Analytical model of soil-water characteristics considering the effect of air entrapment." Int. J. Geomech., 15(6), 0414102.

Childs, E.C., and Collis-George, N. (1950). "The permeability of porous materials", Royal Society, London, Series A, 210, 392-405.

Chiu, T. F., Shackelford, C. D. (1998)."Unsaturated hydraulic conducitivity of compacted sand-kaolin mixtures". J. Gecotech. Geoenviron. Eng., ASCE, Vol. 124, No. 2, pp. 160-170.

Cho, S.E., and Lee, S.R. (2002)."Evaluation of surficial stability for homogeneous slopes considering rainfall characteristics". J. Geptech. Geoenviron. Eng, 128(9):756-763.

Corey, A.T. (1957)."Measurement of water and air permeability in unsaturated soil", Proceedings Soil Science Society of America, 21(1), 7-10.

Daniel, D. (1983). "Permeability tests for unsaturated soils" Geotech. Test. J., Vol. 6, No.2, pp. 81-86.

DiCarlo, D.A. (2004). "Experimental measurements of saturation overshoot on infiltration" Water Resour. Res., 40, W04215, doi:10.1029/2003WR002670.

DiCArlo, D.A. (2007). "Capillary pressure overshoot as a funnction of imbibition flux and initial water content" Water Resour. Res., 43, W0842, doi:10.1029/2006WR005550.

Ersoy, Ş.E. (2013). Disasters Report 2013:"World and Turkey".

Fredlund, D. And Xing, A. (1994)."Equations for the soil-water characteristic curve", Canadian Geotechnical Journal, 31(4), 521-532.

Fredlund, D. G. and Morgenstern, N. R. (1977). “Stress state variables for unsaturated soils”, Journal of Geotechnical Division, ASCE, Vol.103, No GT5, pp.447-466.

Fredlund, D.G. and Rahardjo, H. (1993). Soil mechanics for unsaturated soils, John Wiley and Sons Inc. New York.

Fredlund, D.G., Rahardjo, H., and Fredlund, M.D. (2012). Unsaturated soil mechanics in engineering practice. New York: John Wiley and Sons Inc.

Fredlund, D.G., Xing, A., and Huang, S.Y. (1994). "Predicting the permeability function for unsaturated soils using the soil water characteristic curve, Canadian Geotechnical Journal, Vol. 31, No. 4, 533-546.

Hamilton, J. M., Daniel, D. E., and Olson, R. E. (1981). "Measurement of hydraulic conductivity of partially saturated soils". Permeability and Groundwater Contaminant Transport, ASTM STP 746 T. F. Zimmie and C. O. Riggs, Eds., ASTM, pp. 182-196.

Hammervold, W.L., Knutsen, Ø., Iversen, J.E., and Skjæveland, S.M. (1998)."Capillary pressure scanning curves by the micropore membrane technique". Journal of Petroleum Science and Engineering 20, 253-258.

Hillel, Daniel (2003). Introduction to Environmental Soil Physics. Academic Press, Elsevier Science, USA.

Huvaj, N., Toker, N.K., Egeli, I., Ahmadi-adli, M., and Sahin, Y. (2013)." Mechanism and modelling of rainfall triggered shallow landslides. Ankara:TUBITAK.

Ildır, B. (1995)."Türkiye'de heyelanların dağılımı ve afetler yasası ile ilgili uygulamalar". Proceedings of the 2nd national landslide symposium, Turkey, Sakarya University, pp 1-9.

Iverson, R.M. (2000)."Landslide triggering by rain infiltration". Water Resour. Res., 36(7):1897-1910.

Jean-Louis Briaud (2013). Geotechnical Engineering: Saturated and Unsaturated Soils, John Wiley and Sons Inc., Hoboken, New Jersey.

Karube, D., Kato, S., Hamada, K. and Honda, M. (1996). "The Relationship between the mechanical behavior and the state of pore water in soil", Journal of JSCE, Vol.535, pp.83-92.

Kong, L. W. and Tan, L. R. (2000), "A simple method of determining the soil-water characteristic curve indirectly", Proceedings of Asian Conference on Unsaturated Soils, Singapore, pp.341-345.

Lepore, C., Arnone, E., Noto, L.V., Sivandran, G., and Bras, R.L. (2013)."Physically based modelling of rainfall-triggered landslides: a case study in the Luquillo forest, Puerto Rico". Hydrol. Earth Syst. Sci., 17,3371-3387.

Li, W.C., Lee, L.M., Cai, H., Li, H.J., Dai, F.C., and Wang, M.L. (2013)."Combined roles of saturated permeability and rainfall characteristics on surficial failure of homogeneous soil slope". Eng. Geol., 153:105-113.

Li, X.S. (2005)."Modelling of hysteresis response for arbitrary wetting/drying paths". Computers and Geotechnics, Vol.32, No.2, pp. 133-137.

Likos, W. J., and Lu, N. (2004). "Hysteresis of capillary stress in unsaturated granular soil." J. Eng. Mech., 130(6), 646-655.

Likos, W.J., and Yao, J. (2014)."Effects of constraints on van Genuchten parameters for modelling soil-water characteristic curves", J. Geotech. Geoenviron. Eng.,140(12):06014013.

Likos, W.J., Lu, N., Godt, J.W. (2013)."Hysteresis and uncertainty in soil water-retention curve parameters", J. Geotech. Geoenviron. Eng., 140(4):04013050.

Lins, Y., Zou, Y., and Schanz, T. (2007)."Physical modelling of SWCC for granular materials". Theoretical and numerical unsaturated soil mechanics, Weimar, Germany, p.61-74.

Lu, N.,and Likos, W.J. (2006)."Suction stress characteristic curve for unsaturated soil", J. Geotech. Geoenviron. Eng., 132(2), 131-142.

Lu, N.,Godt, J.W., and Wu, D. (2010)."A closed-form for effective stress in variably saturated soil", Water Resources Research.

Lu,N. And Likos,W.J. (2004). Unsaturated Soil Mechanics, John Wiley and Sons Inc. Hoboken, New Jersey.

Meerdink, J., Benson, C., and Khire, M. (1996)."Unsaturated hydraulic conductivity of two compacted barrier soils" J. Gecotech. Geoenviron. Eng., ASCE, Vol. 122, No. 7, pp. 565-576.

Miller, G.A., Khoury, C.N., Muraleetharan, K.K., Liu, C., and Kibbey, T.C.G. (2008)."Effects of soil skeleton deformations on hysteretic soil water characteristic curves: Experiments and simulations". Water Res. Res. 44, W00C06.

Mualem, Y. (1978). "Hydraulic conductivity of unsaturated porous media: Generalized macroscopic approach", Water Resources Research, 14(2), 325-334.

Nelson, J.D. And Miller, D.J. (1992). Expansive Soils, Problems and Practice in Foundation and Pavement Engineering, John Wiley and Sons Inc., New York.

Ng, C.W.W. and Chen, R. (2005). "Advanced suction control techniques for testing unsaturated soils (in Chinese)". Keynote lecture, 2nd Nat. Conf. On Unsat. Soils, Hangzhou, China, Zhejiang University Press, 144-167.

Okalp, K., and Akgün, H. (2016)."National level landslide susceptibility assessment of Turkey utilizing public domain dataset". Environ Earth Sci. 75:847.

Öberg, A. L. and Sällfors, G. (1995). “A rational approach to the determination of the shear strength parameters of unsaturated soils”, Proceedings of First International conference on Unsaturated Soils, Paris, Vol.1, pp.151-158.

Pedroso, D.M., and Williams, D.J. (2010)."A novel approach for modelling soil-water characteristic curves with hysteresis". Computers and Geotechnics, Vol. 37, No. 3, pp. 374-380.

Petrucci, R. H. (1989). General Chemistry: Principles and Modern Applications, Macmillan Publishing Co., New York

Pham, Q.H. (2001)."An engineering model of hysteresis for soil-water characteristic curves". MSc thesis, University of Saskatchewan, Canada.

Poulovassilis, A., and Childs, E.C. (1971)."The hysteresis of pore water: The non-indepence of domains". Journal of Soil Science, 112(5):301-312.

Reichanbach, P., Cardinali, M., De Vita, P., and Guzzetti, F. (1998). "Regional hydrological thresholds for landslides and floods in the Tiber River Basin (central Italy)". Env. Geol., 35(2&3), 146-159.

Reis, S., and Yomralıoğlu, T. (2005)."Provincal disaster risk management using GIS". Turkish chamber of survey and cadastre engineers, 10th Scientific and technical meeting on Turkish mapping, 28 March-1 April 2005, Ankara.

Richards, L. A. (1931). "Capillary conduction of liquids through porous medium", Journal of Physics, 318-333.

Richards, L.A., and Weeks, L. (1953)"Capillary conductivity values from moisture yield and tension measurements on soil columns", Soil Science Society of America Proceedings, 55, 206-209.

Sakai,M., and Toride, N. (2007). "Soil water hydraulic functions for sandy soil and an aggregated soil". J. Jpn. Soc. Soil Ohys., 107, 63-77.

Sattari, A. S., Toker, N.K. (2016). "Obtaining soil-water characteristic curves by numerical modelling of drainage in particulate media", Computers and Geotechnics, 74, 196-210.

Shiozawa, S., and Fujimaki, H. (2004). "Unexpected water content profiles under flux-limited one-dimensional downward infiltration in initially dry granular media" Water Resour. Res., 40, W07404, doi:10.1029/2003WR002197.

Talsma, T. (1970). "Hysteresis in two sands and the independent domain model". Water Resources Research 6(3):964-970.

Terzaghi, K. (1943). Theoretical Soil Mechanics, John Wiley and Sons, Inc., New York.

Thomson, W., (1871). Philosophical Magazine, 42, 448.

Toker, N. K., Germaine, J. T., Sjoblom, K. J. and Culligan, P. J. (2004). “A new technique for rapid measurement of continuous SMC curves”, Geotechnique, Vol.54, No.3, pp.179-186.

Toker, N.K. (2007). "Modelling the relation between suction, effective stress and shear strength in partially saturated granular media" Ph.D. Thesis, Massachusetts Institute of Technology.

Topp, G.C. (1971)."Soil water hysteresis in silt loam and clay loam soils". Water Res. Res. 7, 914-920.

Tsai, T.L. (2008). "Influences of soil water characteristic curve on rainfall-induced shallow landslides". Environ. Geol., 53(7):153-1569.

Tsai, T.L., and Yang, J.C. (2006)."Modelling of rainfall-triggered shallow landslide". Environ. Geol., 50(4):525-534.

U.S. Bureau of Reclamation, "Water Management Manual".

Van Genuchten, M.T. (1980). "A closed-form equation for predicting the hydraulic conductivity of unsaturated soils", Soil Sci. Soc. Am. J. 44, 892-898.

Vanapalli, S.K., Fredlund, D.G., Pufahl, D.E., and Clifton, A.W. (1996)."Model for the prediction of shear strength with respect to soil suction". Canadian Geotechnical Journal, 33(3), 379-392.

Vanapalli, S.K., Sillers, W.S., and Fredlund, M.D. (1998)."The meaning and relevance of residual state to unsaturated soils", Proc., 51st Canadian Geotechnical Conf., Canadian Geotechnical Society, Richmond, BC, Canada.

Viane, P., Vereecken, H., Diels, J., and Feyen, J. (1994)."A statistical analysis of six hysteresis models for the moisture retention characteristic". Soil Sci. 157, 345-355.

Watson, K.K., Reginato, R.J., Jackson, R.D. (1975)."Soil water hysteresis in a field soil". Soil Sci. Soc. America J. 157, 345-355.

White, J.A., and Singham, D.I. (2012)."Slope stability assessment using stochastic rainfall simulation". Procedia Comput. Sci., 9:699-706.

Wilson, E.M. (1990). Engineering Hydrology ,Macmillan Education Ltd. Houndmills, Basingstoke, Hampshire.

Zhan, T.L.T., Jia, G.W., Chen, Y.M., Fredlund, D.G., and Li, H. (2012)."An analytical solution for rainfall infiltration into an unsaturated infinite slope and its application to slope stability analysis". Int. J. Numer. Anal. Methods Geomech., 37(12)Ç1737-1760.

Zhang, G., Q., Y., Wang, Z., and Zhao, B. (2014)."Analysis of rainfall infiltration law in unsaturated soil slope", The Scientific World Journal, Vol:2014, 567250, 7 pages.

Znidarcic, D., Illangasekare, T. and Manna, M. (1991). “Laboratory testing and parameter estimation for two-phase flow problems”, Geotechnical Special Publication 27, ASCE, pp.1089-1099.

APPENDIX A

RESULTS OF SIMULATIONS WITH SOILS OF DIFFERENT AEV

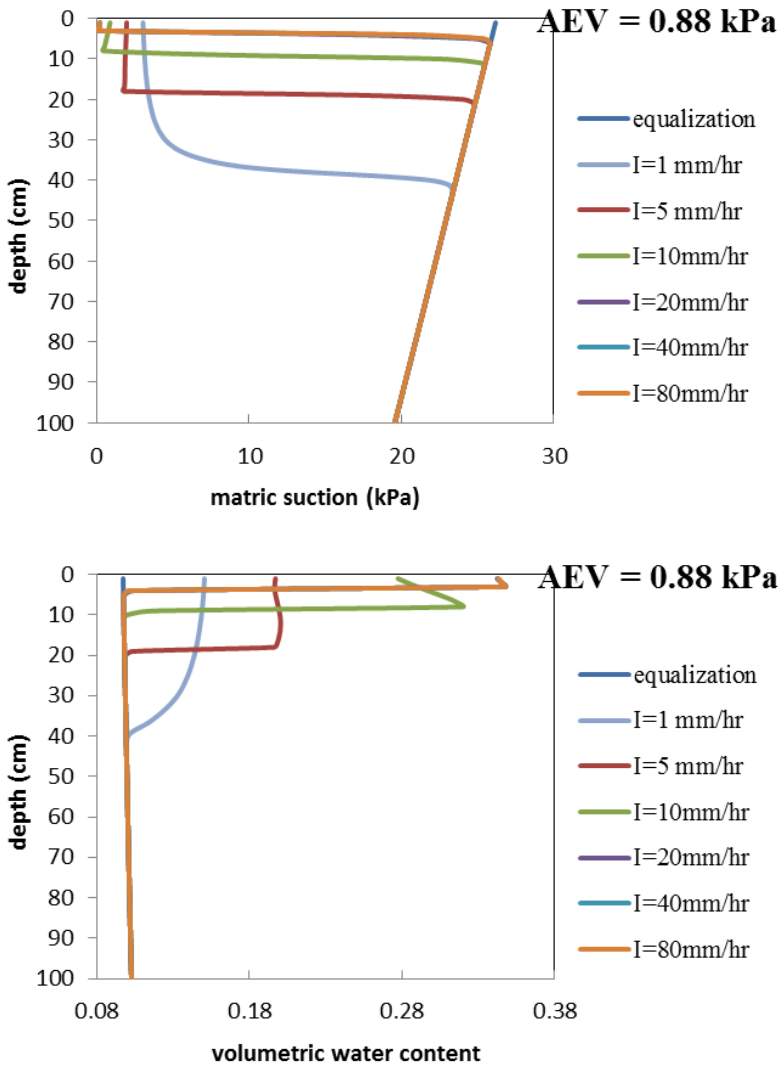

Figure A. 1. The matric suction and volumetric water content profiles at the time of failure for hypothetical soils that its AEV is 0.88 kPa.

Table A. 1. Results of analyses for AEV=0.88 kPa

AEV=0.88					
I (mm/hr)	f. depth(cm)	f. time(min)	Ψ_failure (kPa)	θ_failure	f. type
1	29	684.6	4.30	0.135	M
5	17	157.3	1.83	0.198	W
10	7	70.9	0.52	0.317	W
20	2	24.0	0.17	0.345	E
40	2	21.8	0.17	0.345	E
80	2	20.8	0.17	0.346	E

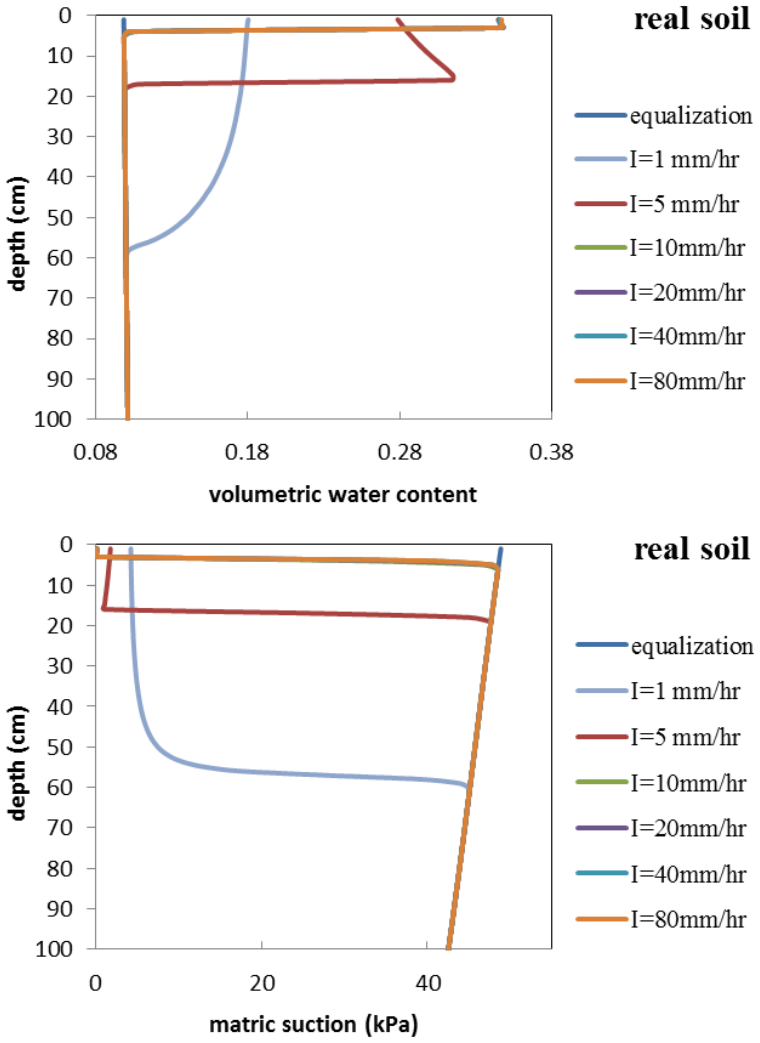

Figure A. 2. The matric suction and volumetric water content profiles at the time of failure for hypothetical soils that its AEV is 1.75 kPa.

Table A. 2. Results of analyses for AEV=1.75 kPa.

AEV=1.75					
I (mm/hr)	f. depth(cm)	f. time(min)	Ψ_failure (kPa)	θ_failure	f. type
1	46	1568.5	6.30	0.149	M
5	15	274.7	1.10	0.315	W
10	2	48.7	0.17	0.346	E
20	2	44.2	0.16	0.346	E
40	2	42.2	0.16	0.346	E
80	2	41.2	0.15	0.347	E

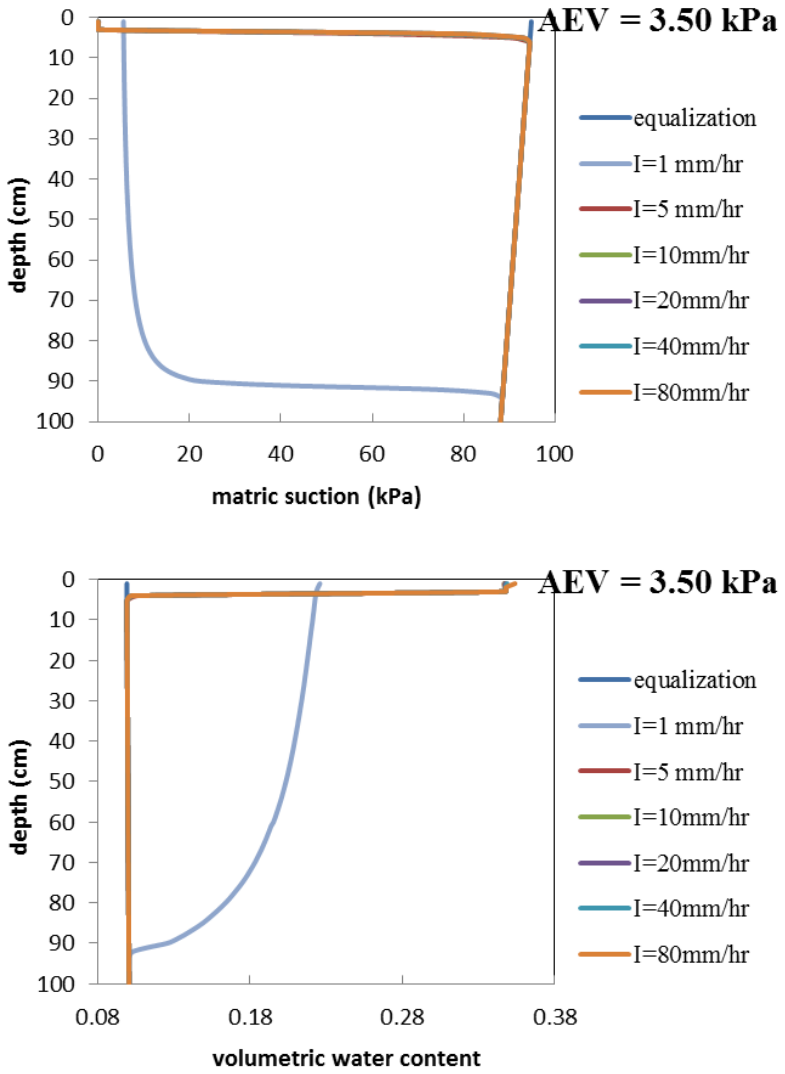

Figure A. 3. The matric suction and volumetric water content profiles at the time of failure for hypothetical soils that its AEV is 3.50 kPa.

Table A. 3. Results of analyses for AEV=3.50 kPa.

AEV=3.50					
I (mm/hr)	f. depth(cm)	f. time(min)	Ψ_failure (kPa)	θ_failure	f. type
1	77	3827.1	9.47	0.171	M
5	2	96.8	0.17	0.347	E
10	2	87.7	0.15	0.348	E
20	2	83.5	0.15	0.348	E
40	2	81.7	0.14	0.348	E
80	2	80.8	0.14	0.348	E

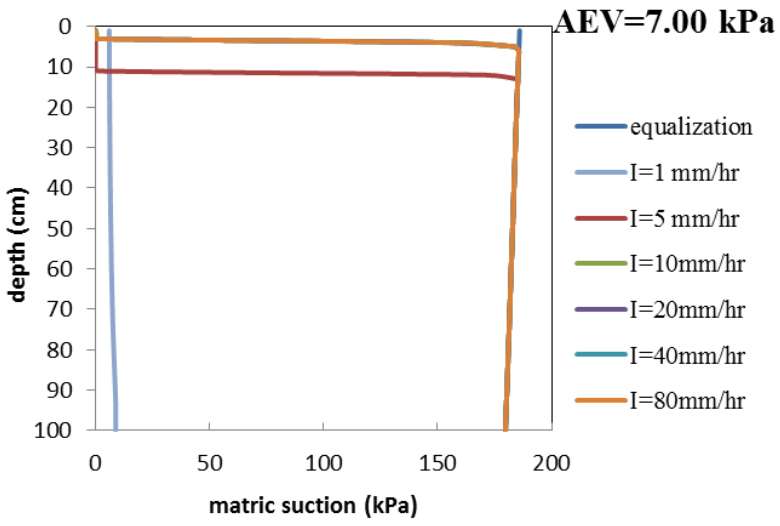

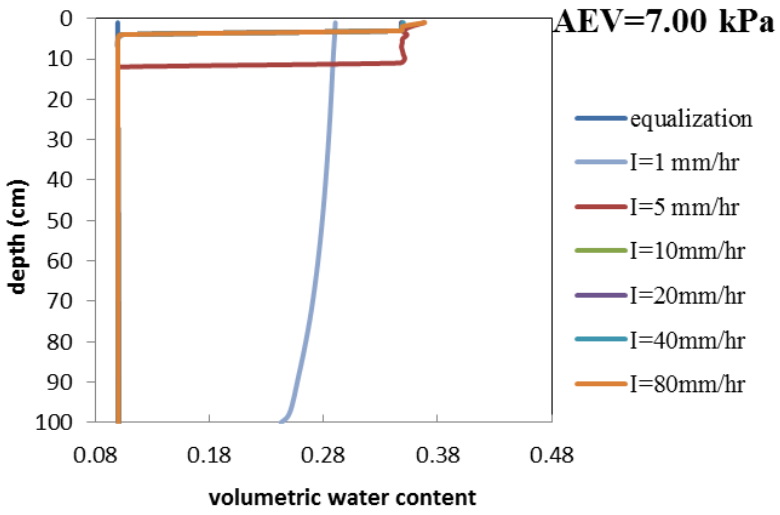

Figure A. 4. The matric suction and volumetric water content profiles at the time of failure for hypothetical soils that its AEV is 7.00 kPa.

Table A. 4. Results of analyses for AEV=7.00 kPa.

AEV=7.00					
I (mm/hr)	f. depth(cm)	f. time(min)	Ψ_failure (kPa)	θ_failure	f. type
1	99	7578.5	8.94	0.247	M
5	2	191.1	1.67	0.344	W
10	2	182.8	0.65	0.348	E
20	2	178.9	0.12	0.348	E
40	2	177.1	0.18	0.348	E
80	2	176.4	0.15	0.349	E

APPENDIX B

RESULTS OF SIMULATIONS WITH SOILS OF DIFFERENT DSR

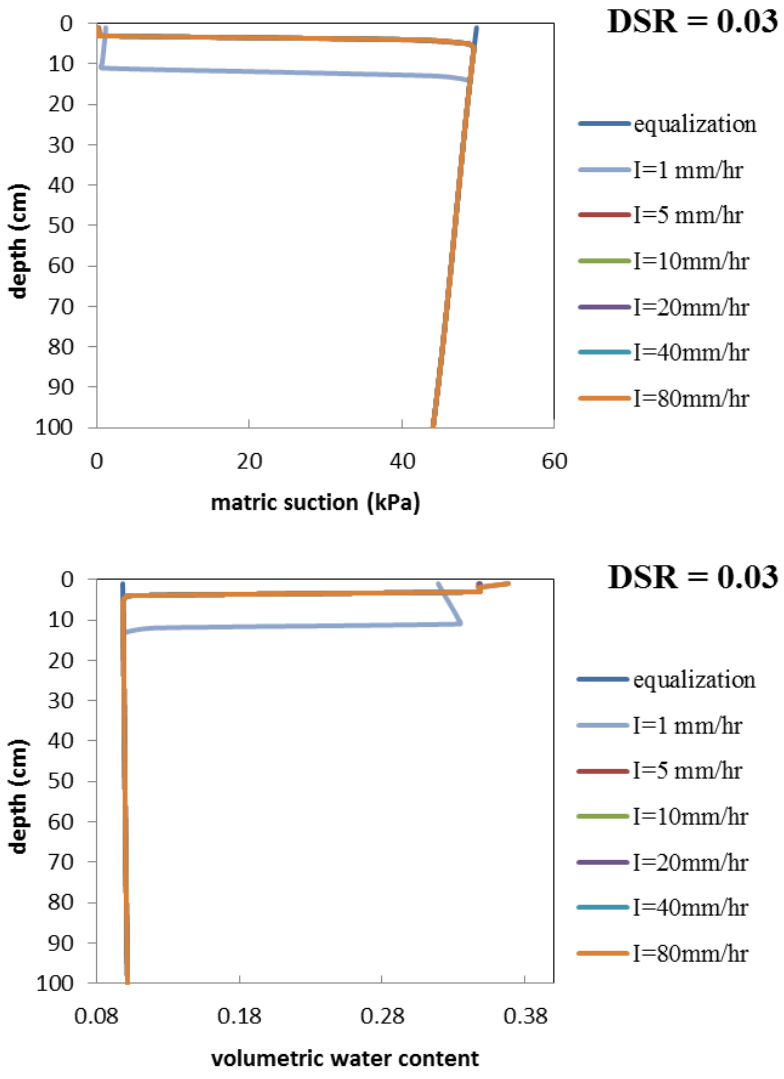

Figure B. 1. The matric suction and volumetric water content profiles at the time of failure for hypothetical soils that its DSR is 0.03.

Table B. 1. Results of analyses for DSR=0.03.

DSR=0.03					
I (mm/hr)	f. depth(cm)	f. time(min)	Ψ_failure (kPa)	θ_failure	f. type
1	10	1105.2	0.71	0.334	W
5	2	241.1	0.33	0.348	E
10	2	232.8	0.35	0.348	E
20	2	229.3	0.28	0.348	E
40	2	228.0	0.14	0.348	E
80	2	227.8	0.31	0.348	E

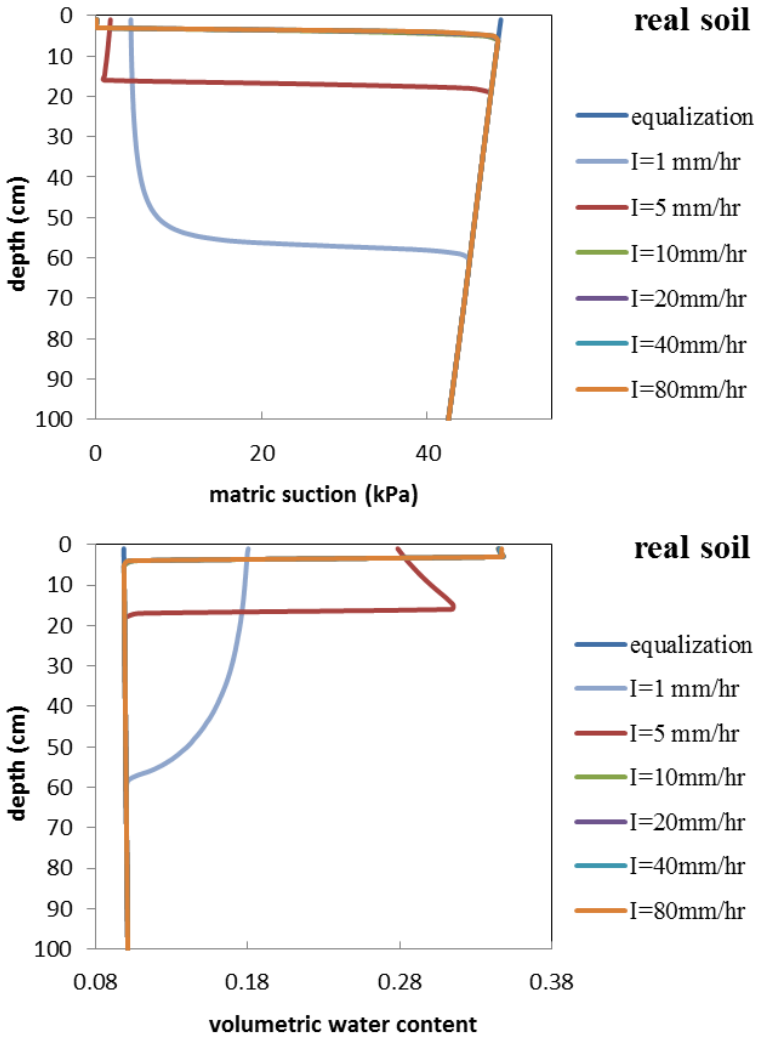

Figure B. 2. The matric suction and volumetric water content profiles at the time of failure for hypothetical soils that its DSR is 0.06.

Table B. 2.Results of analyses for DSR=0.06.

DSR=0.06					
I (mm/hr)	f. depth(cm)	f. time(min)	Ψ_failure (kPa)	θ_failure	f. type
1	46	1568.5	6.30	0.149	M
5	15	274.7	1.10	0.315	W
10	2	48.7	0.17	0.346	E
20	2	44.2	0.16	0.346	E
40	2	42.2	0.16	0.346	E
80	2	41.2	0.15	0.347	E

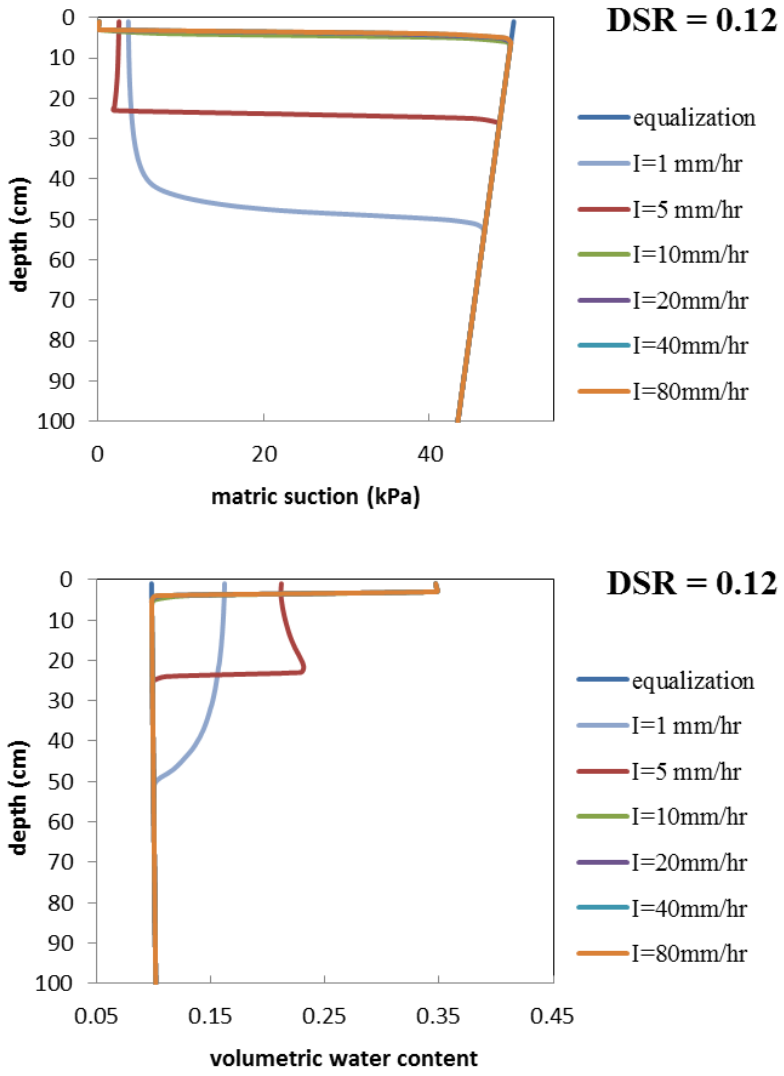

Figure B. 3. The matric suction and volumetric water content profiles at the time of failure for hypothetical soils that its DSR is 0.12.

Table B. 3. Results of analyses for DSR=0.12.

DSR=0.12					
I (mm/hr)	f. depth(cm)	f. time(min)	Ψ_failure (kPa)	θ_failure	f. type
1	37	1067.6	5.20	0.144	M
5	22	240.5	2.07	0.231	W
10	2	35.4	0.17	0.348	E
20	2	28.5	0.17	0.348	E
40	2	26.3	0.17	0.348	E
80	2	25.3	0.18	0.348	E

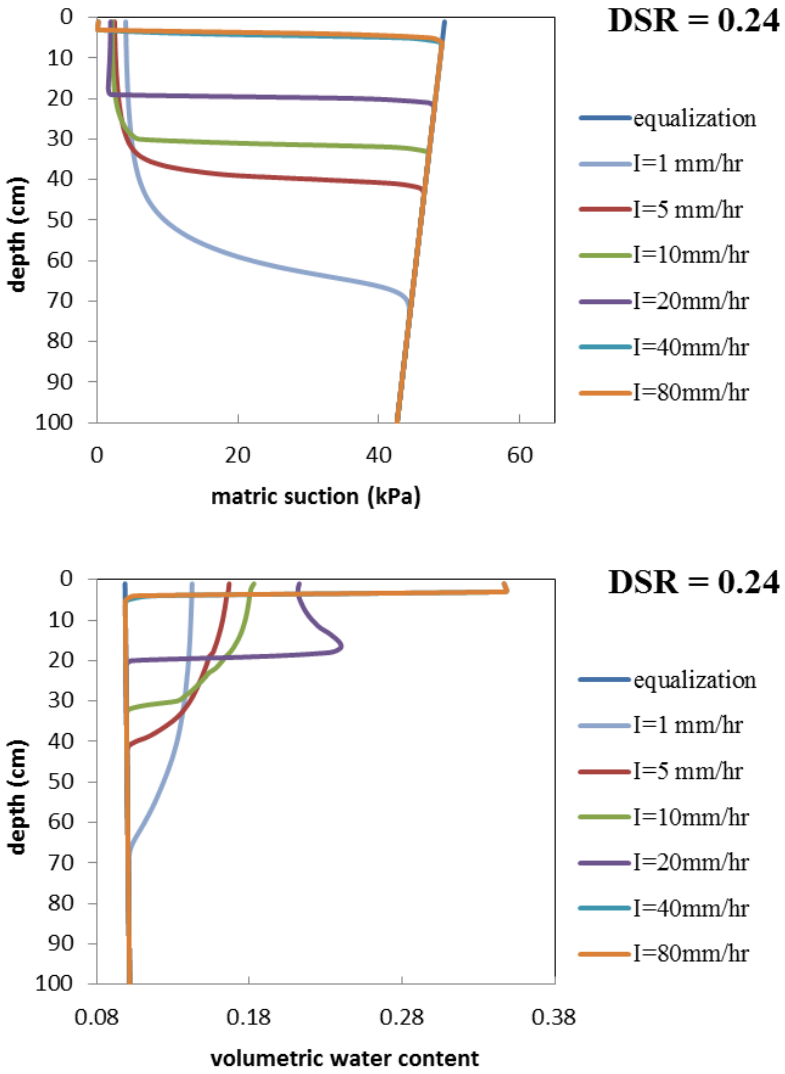

Figure B. 4. The matric suction and volumetric water content profiles at the time of failure for hypothetical soils that its DSR is 0.24.

Table B. 4. Results of analyses for DSR=0.24.

DSR=0.24					
I (mm/hr)	f. depth(cm)	f. time(min)	Ψ_failure (kPa)	θ_failure	f. type
1	40	903.3	6.04	0.133	M
5	28	172.1	3.91	0.144	M
10	23	87.3	3.04	0.154	M
20	18	50.3	1.66	0.233	W
40	18	8.9	0.16	0.348	E
80	2	7.5	0.16	0.348	E

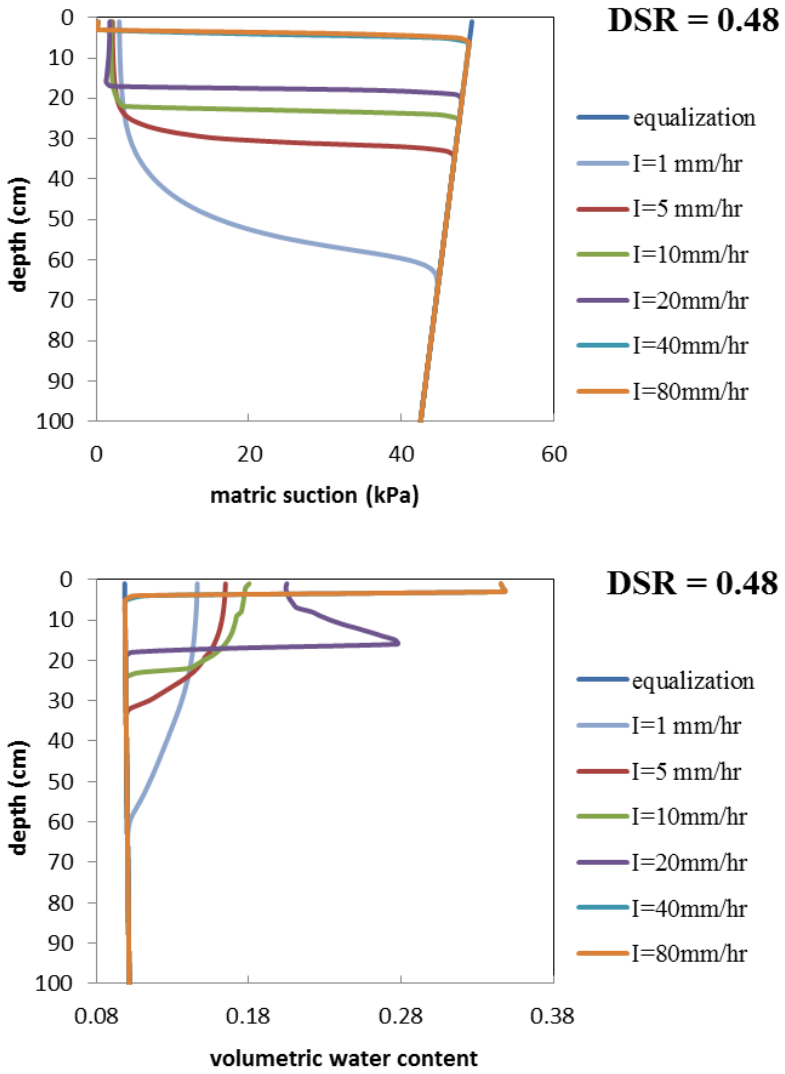

Figure B. 5. The matric suction and volumetric water content profiles at the time of failure for hypothetical soils that its DSR is 0.48.

Table B. 5. Results of analyses for DSR=0.48.

DSR=0.48					
I (mm/hr)	f. depth(cm)	f. time(min)	Ψ_failure (kPa)	θ_failure	f. type
1	30	824.8	4.40	0.136	M
5	21	136.6	2.84	0.148	M
10	19	65.6	2.46	0.155	M
20	16	47.4	1.29	0.278	W
40	2	9.1	0.17	0.347	E
80	2	7.9	0.17	0.347	E

APPENDIX C

RESULTS OF SIMULATIONS WITH SOILS OF DIFFERENT θ_S

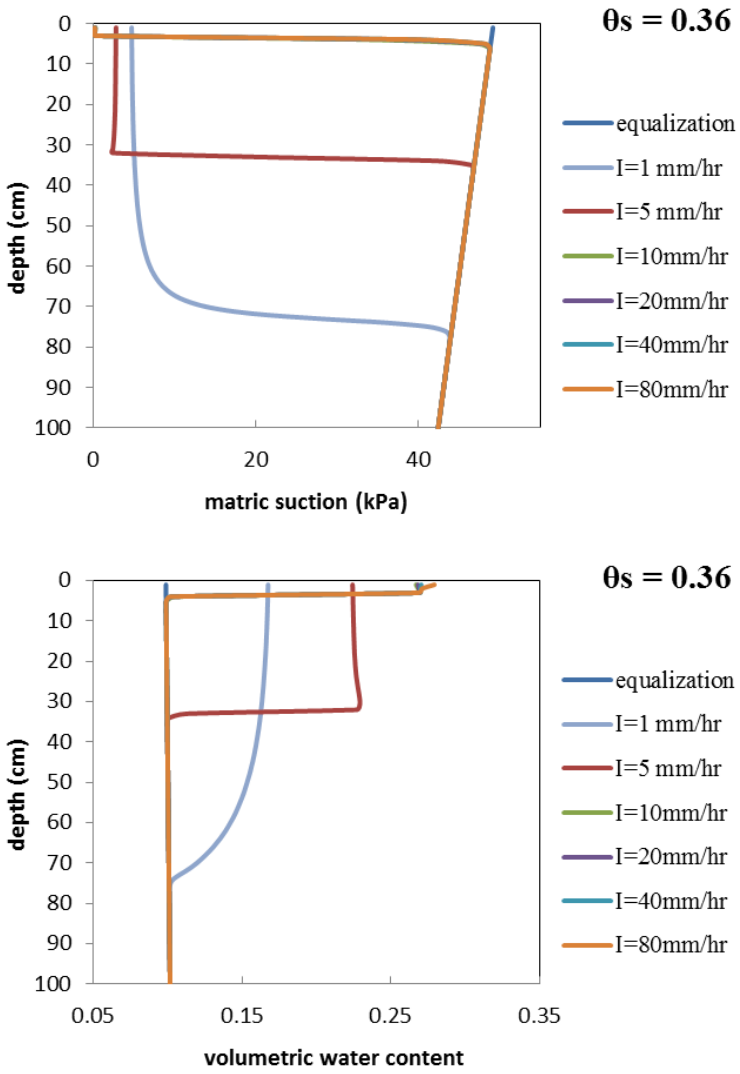

Figure C. 1. The matric suction and volumetric water content profiles at the time of failure for hypothetical soils that its θ_s is 0.36.

Table C. 1. Results of analyses for θ_s=0.36.

θs=0.36					
I (mm/hr)	f. depth(cm)	f. time(min)	Ψ_failure (kPa)	θ_failure	f. type
1	58	1730.4	6.5	0.145	M
5	31	351.9	2.4	0.229	W
10	2	30.1	0.2	0.268	E
20	2	27.5	0.2	0.269	E
40	2	26.4	0.1	0.270	E
80	2	26.0	0.1	0.271	E

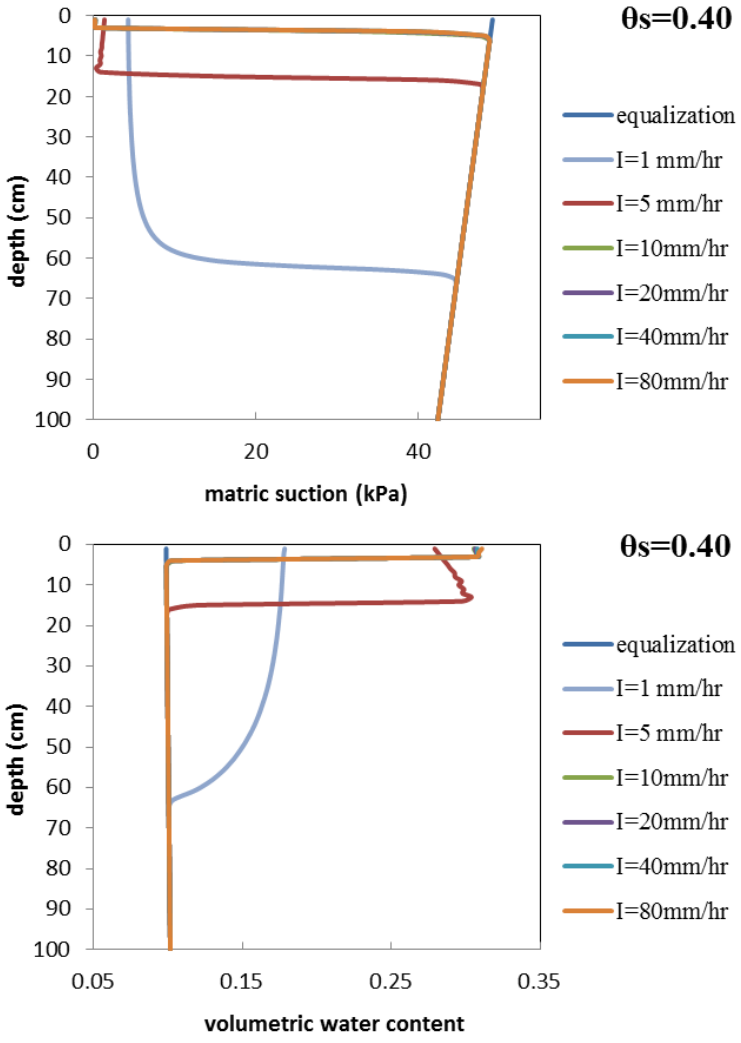

Figure C. 2. The matric suction and volumetric water content profiles at the time of failure for hypothetical soils that its θ_s is 0.40.

Table C. 2. Results of analyses for θ_s=0.40.

θs=0.40					
I (mm/hr)	f. depth(cm)	f. time(min)	Ψ_failure (kPa)	θ_failure	f. type
1	50	1684.4	6.1	0.150	M
5	13	236.5	0.3	0.304	W
10	2	45.4	0.2	0.307	E
20	2	41.9	0.2	0.307	E
40	2	40.4	0.2	0.308	E
80	2	39.8	0.1	0.309	E

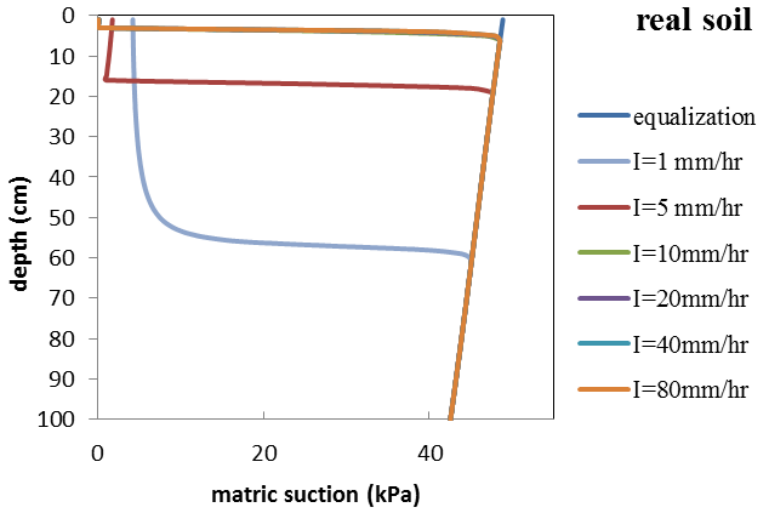

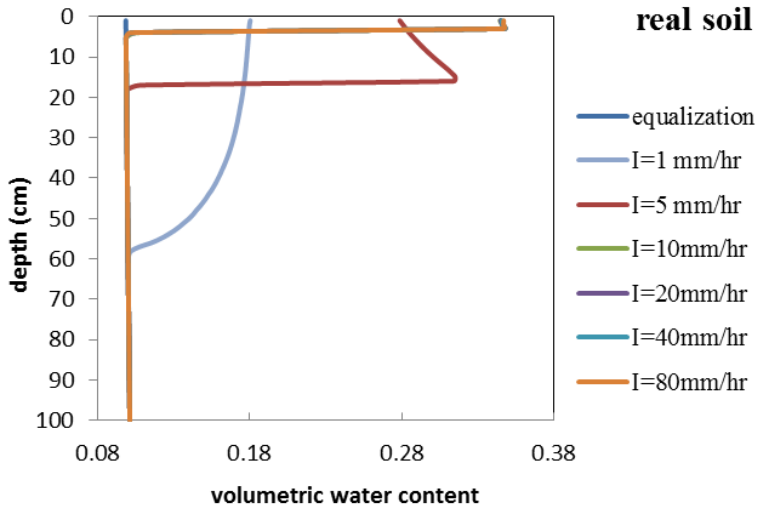

Figure C. 3. The matric suction and volumetric water content profiles at the time of failure for hypothetical soils that its θ_s is 0.44.

Table C. 3. Results of analyses for θ_s=0.44.

θs=0.44					
I (mm/hr)	f. depth(cm)	f. time(min)	Ψ_failure (kPa)	θ_failure	f. type
1	46	1568.5	6.3	0.149	M
5	15	274.7	1.1	0.315	W
10	2	48.7	0.2	0.346	E
20	2	44.2	0.2	0.346	E
40	2	42.2	0.2	0.346	E
80	2	41.2	0.2	0.347	E

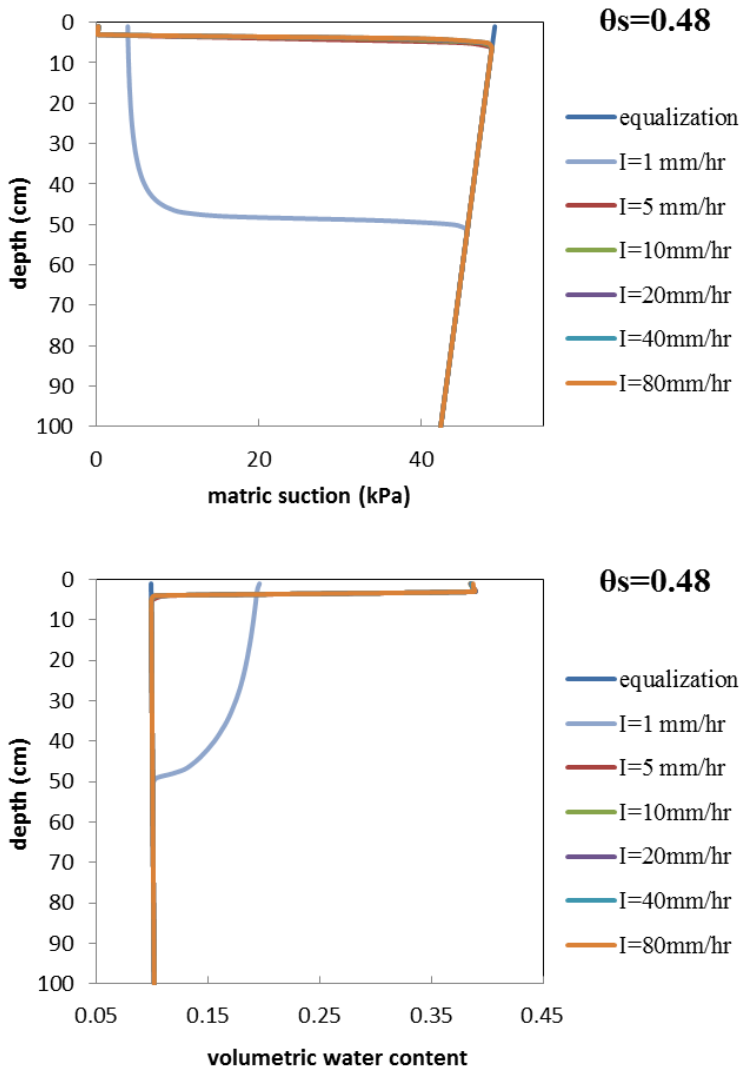

Figure C. 4. The matric suction and volumetric water content profiles at the time of failure for hypothetical soils that its θ_s is 0.48.

Table C. 4. Results of analyses for θ_s=0.48.

θs=0.48					
I (mm/hr)	f. depth(cm)	f. time(min)	Ψ_failure (kPa)	θ_failure	f. type
1	40	1551.3	5.9	0.155	M
5	2	84.5	0.2	0.387	E
10	2	72.8	0.2	0.387	E
20	2	67.5	0.2	0.387	E
40	2	65.1	0.2	0.387	E
80	2	64.0	0.2	0.387	E

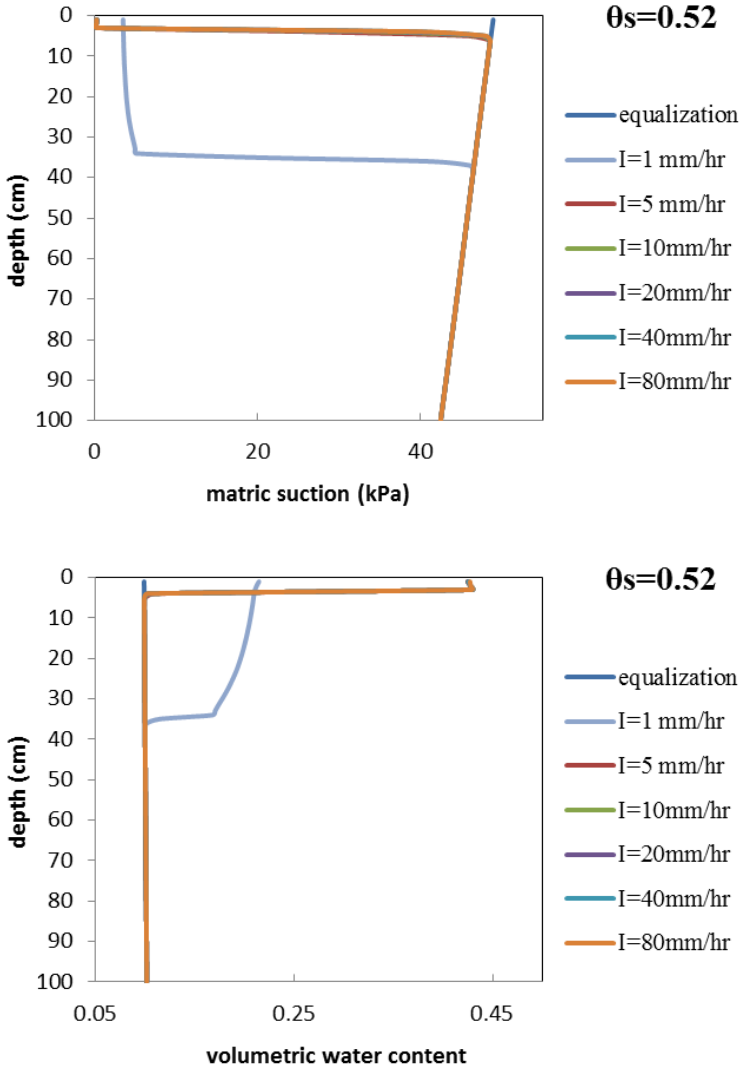

Figure C. 5. The matric suction and volumetric water content profiles at the time of failure for hypothetical soils that its θ_s is 0.52.

Table C. 5. Results of analyses for θ_s=0.52.

θs=0.52					
I (mm/hr)	f. depth(cm)	f. time(min)	Ψ_failure (kPa)	θ_failure	f. type
1	33	1425.5	4.9	0.170	M
5	2	115.2	0.2	0.427	E
10	2	102.1	0.2	0.427	E
20	2	96.0	0.2	0.427	E
40	2	93.2	0.2	0.427	E
80	2	92.0	0.2	0.428	E

APPENDIX D

RESULTS OF SIMULATIONS WITH SOILS OF DIFFERENT θ_R

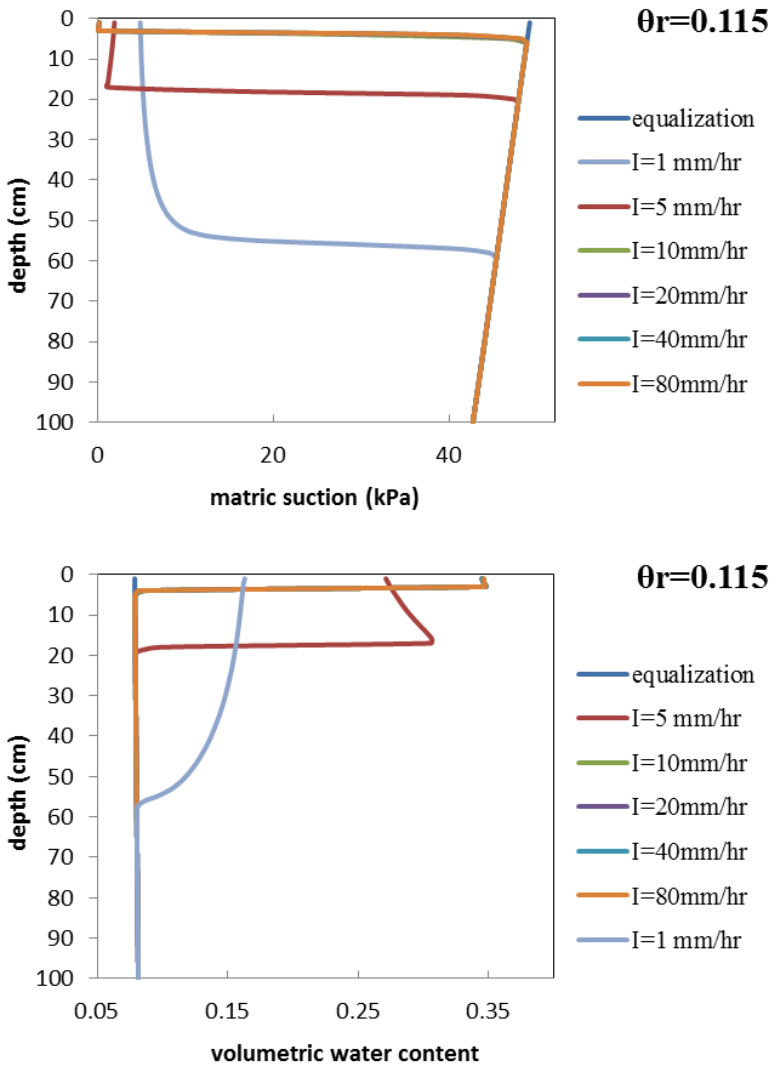

Figure D. 1. The matric suction and volumetric water content profiles at the time of failure for hypothetical soils that its θ_r is 0.115.

Table D. 1. Results of analyses for θ_r = 0.115.

θr=0.115					
I (mm/hr)	f. depth(cm)	f. time(min)	Ψ_failure (kPa)	θ_failure	f. type
1	48	1542.0	2.06	0.123	M
5	16	309.6	0.17	0.306	W
10	2	51.8	0.17	0.346	E
20	2	46.5	0.17	0.346	E
40	2	44.1	0.16	0.346	E
80	2	43.0	0.18	0.346	E

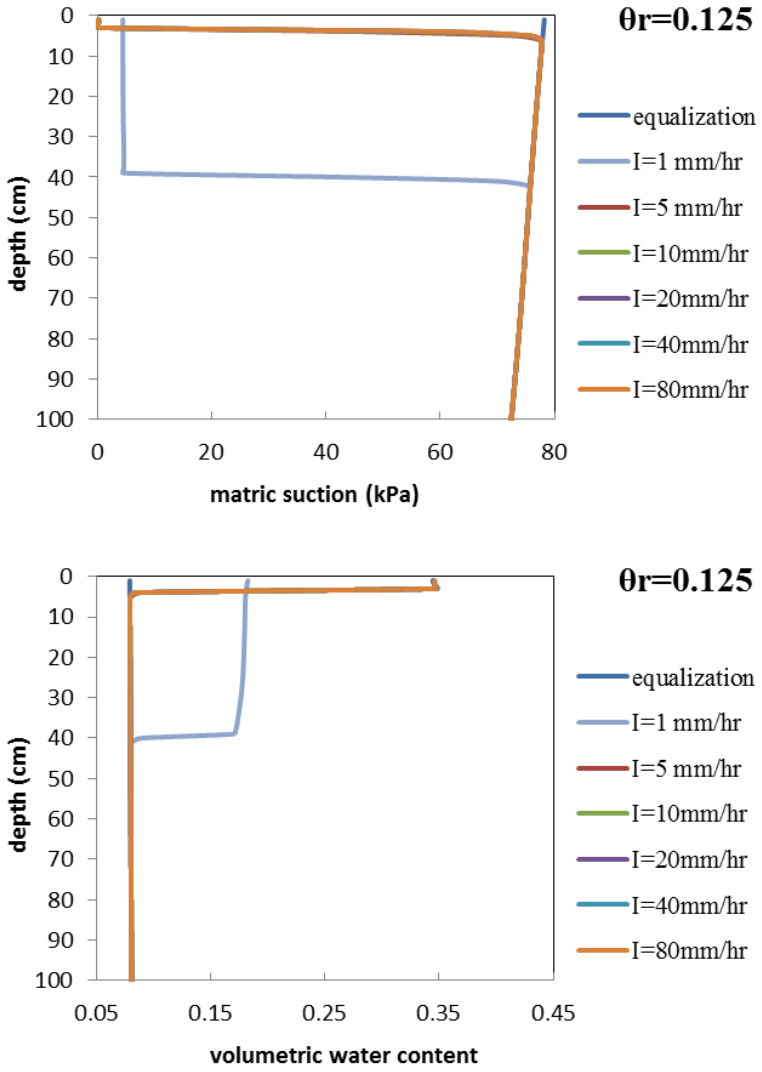

Figure D. 2. The matric suction and volumetric water content profiles at the time of failure for hypothetical soils that its θ_r is 0.125.

Table D. 2. Results of analyses for θ_r = 0.125.

θr=0.125					
I (mm/hr)	f. depth(cm)	f. time(min)	Ψ_failure (kPa)	θ_failure	f. type
1	38	1664.3	4.59	0.172	W
5	2	114.5	0.17	0.346	E
10	2	104.5	0.17	0.346	E
20	2	99.8	0.17	0.346	E
40	2	97.6	0.17	0.346	E
80	2	96.5	0.16	0.346	E

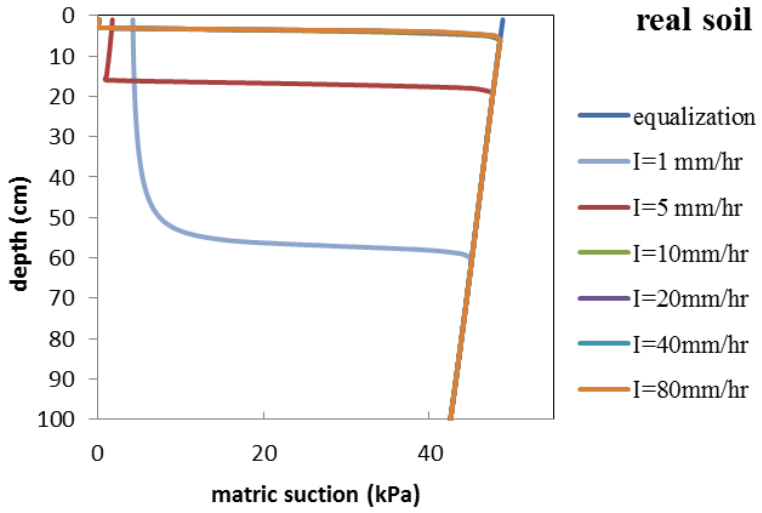

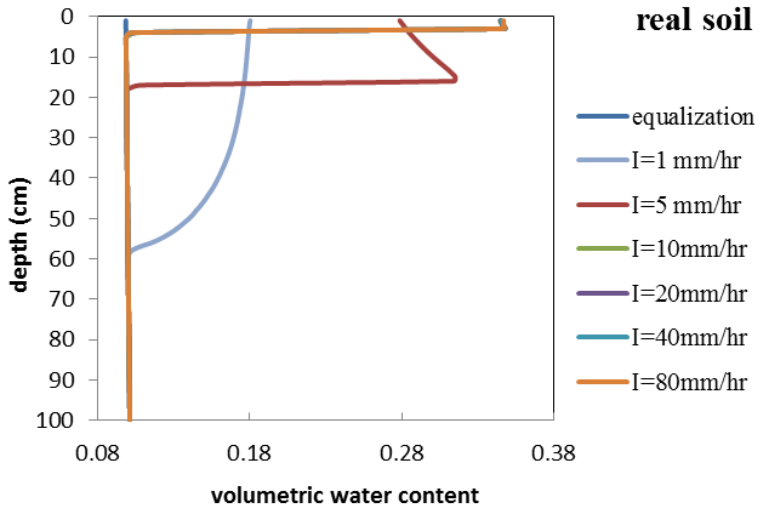

Figure D. 3. The matric suction and volumetric water content profiles at the time of failure for hypothetical soils that its θ_r is 0.135.

Table D. 3. Results of analyses for θ_r=0.135.

I (mm/hr)	f. depth(cm)	f. time(min)	Ψ_failure (kPa)	θ_failure	f. type
1	24	1720.7	2.06	0.254	W
5	2	181.5	0.17	0.346	E
10	2	172.1	0.17	0.346	E
20	2	167.7	0.17	0.346	E
40	2	165.6	0.16	0.346	E
80	2	164.7	0.18	0.346	E

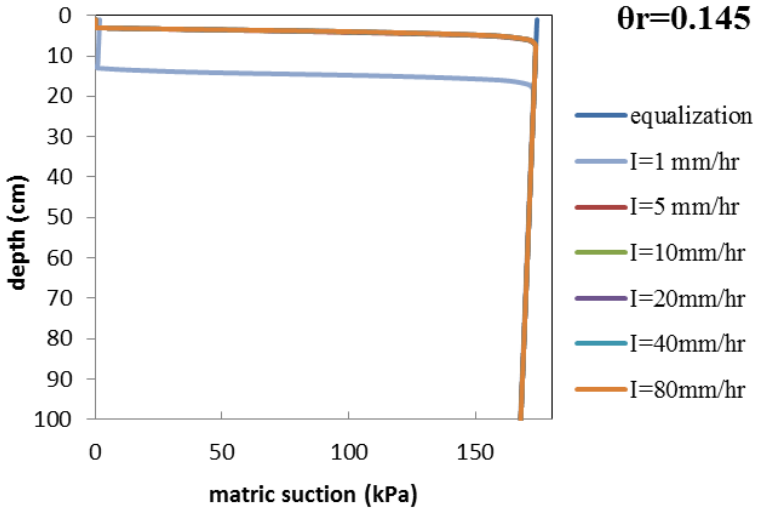

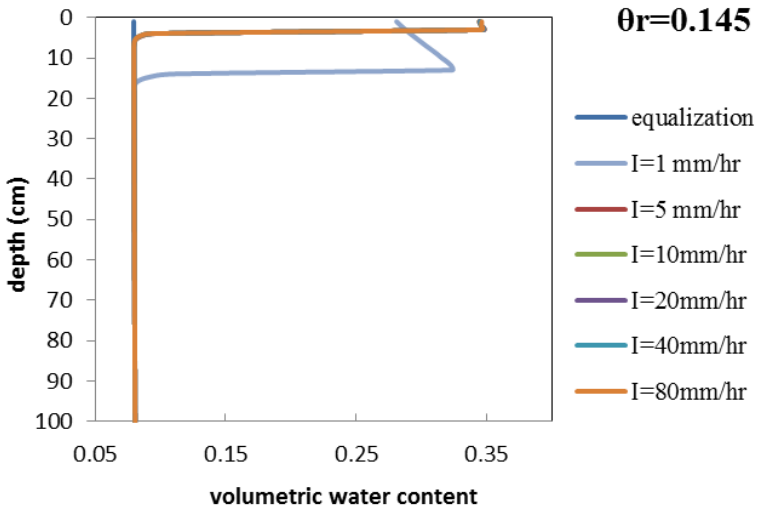

Figure D. 4. The matric suction and volumetric water content profiles at the time of failure for hypothetical soils that its θ_r is 0.145.

Table D. 4. Results of analyses for θ_r=0.145.

θr=0.145					
I (mm/hr)	f. depth(cm)	f. time(min)	Ψ_failure (kPa)	θ_failure	f. type
1	14	1448.4	0.99	0.323	W
5	2	251.8	0.17	0.346	E
10	2	242.8	0.17	0.346	E
20	2	238.7	0.16	0.346	E
40	2	236.7	0.17	0.346	E
80	2	235.8	0.17	0.346	E

APPENDIX E

RESULTS OF SIMULATIONS WITH DIFFERENT BASE ANGLES AND INITIAL VOLUMETRIC WATER CONTENTS

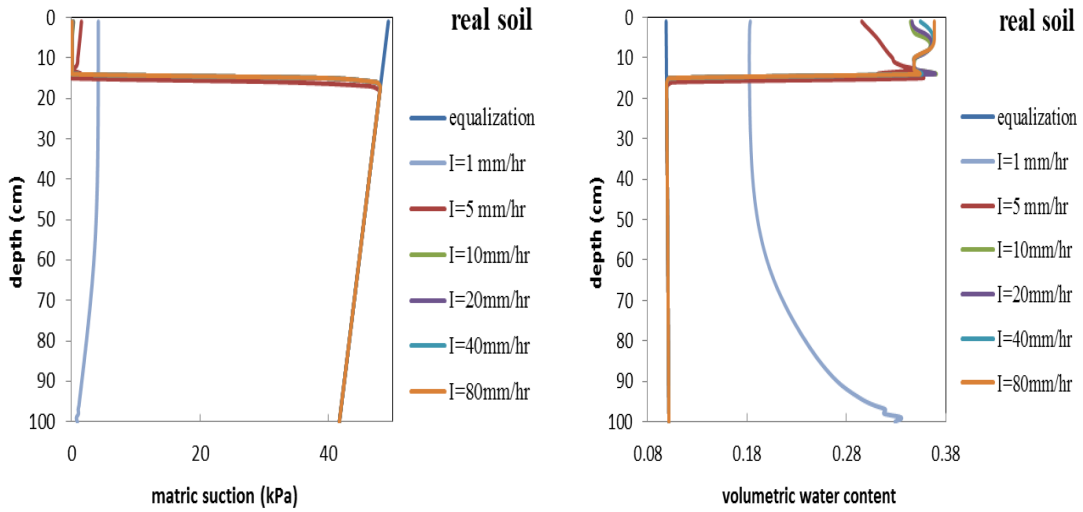

Figure E. 1. The matric suction and volumetric water content profiles at the time of failure for base angle of 38°.

Table E. 1. Results of analyses for base angle of 38°.

base angle=38°					
I (mm/hr)	f. depth(cm)	f. time(min)	Ψ_failure (kPa)	θ_failure	f. type
1	99	4231.3	0.75	0.335	M
5	13	254.9	0.10	0.349	W
10	13	228.5	0.11	0.350	W
20	13	227.6	0.11	0.351	W
40	13	227.1	0.12	0.349	W
80	13	226.9	0.12	0.348	W

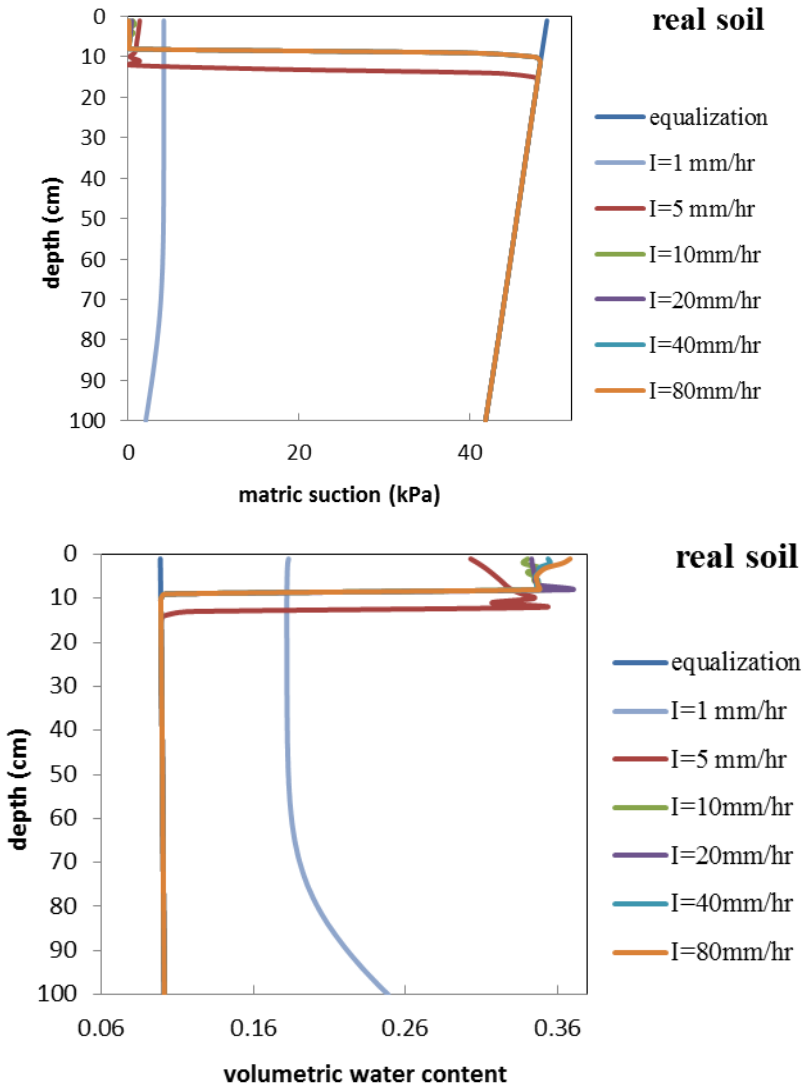

Figure E. 2. The matric suction and volumetric water content profiles at the time of failure for base angle of 39°.

Table E. 2. Results of analyses for base angle of 39°.

base angle=39°					
I (mm/hr)	f. depth(cm)	f. time(min)	Ψ_failure (kPa)	θ_failure	f. type
1	99	3579.0	2.13	0.246	M
5	10	211.9	0.23	0.345	W
10	7	127.8	0.12	0.349	E
20	7	126.7	0.13	0.348	E
40	7	125.9	0.17	0.346	E
80	7	125.7	0.14	0.347	E

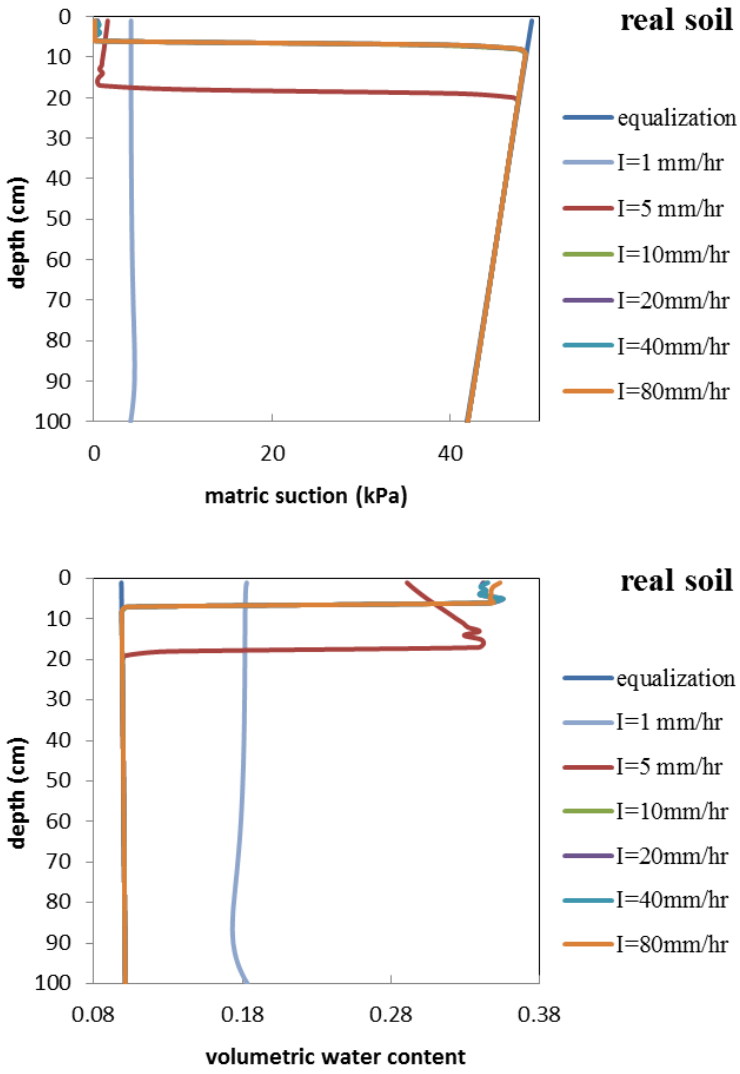

Figure E. 3. The matric suction and volumetric water content profiles at the time of failure for base angle of 40°.

Table E. 3. Results of analyses for base angle of 40°.

base angle=40°					
I (mm/hr)	f. depth(cm)	f. time(min)	Ψ_failure (kPa)	θ_failure	f. type
1	99	3101.3	4.20	0.182	M
5	13	245.7	0.19	0.345	W
10	5	96.0	0.12	0.349	E
20	5	93.4	0.11	0.355	E
40	5	92.3	0.10	0.355	E
80	5	92.0	0.17	0.346	E

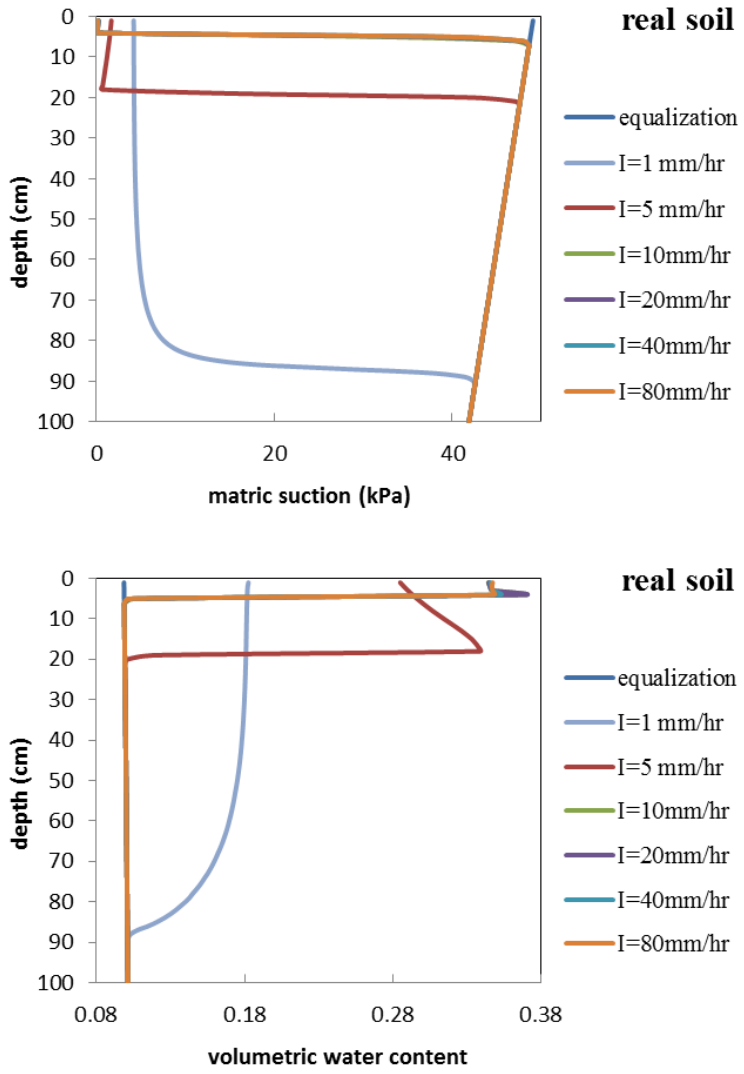

Figure E. 4. The matric suction and volumetric water content profiles at the time of failure for base angle of 42°.

Table E. 4. Results of analyses for base angle of 42°.

base angle=42°					
I (mm/hr)	f. depth(cm)	f. time(min)	Ψ_failure (kPa)	θ_failure	f. type
1	73	2438.5	5.79	0.155	M
5	17	313.4	0.71	0.347	W
10	3	65.6	0.13	0.347	E
20	3	61.4	0.14	0.347	E
40	3	59.3	0.14	0.347	E
80	3	58.5	0.14	0.347	E

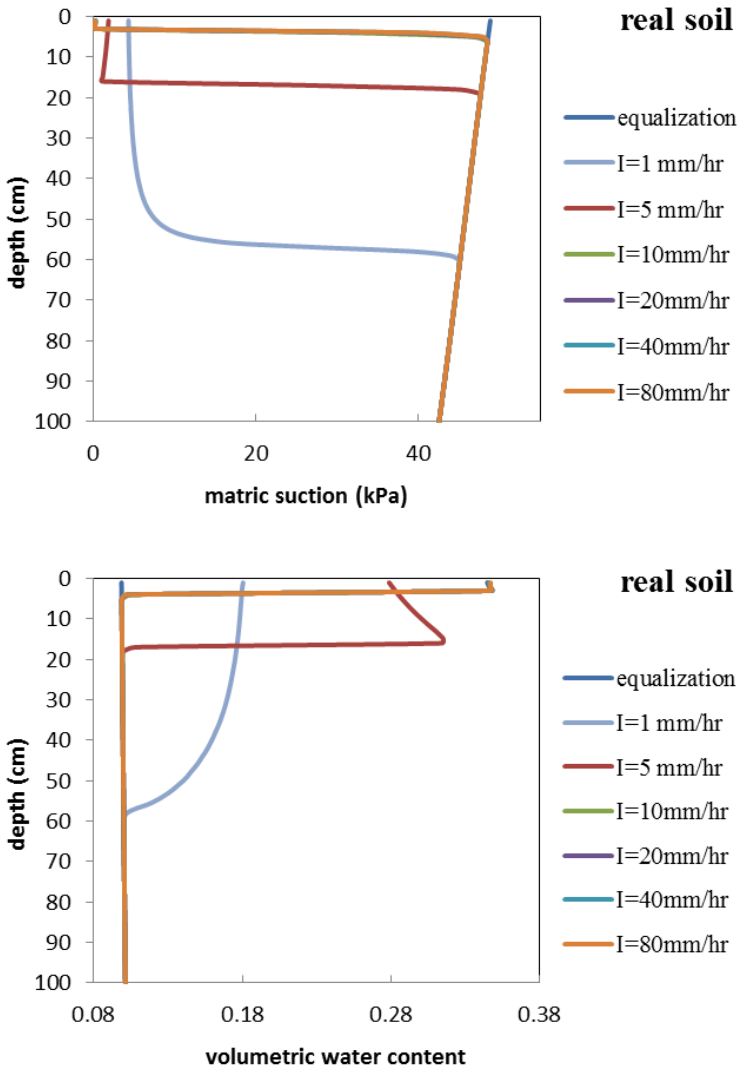

Figure E. 5. The matric suction and volumetric water content profiles at the time of failure for base angle of 46°.

Table E. 5. Results of analyses for base angle of 46°.

base angle=46°					
I (mm/hr)	f. depth(cm)	f. time(min)	Ψ_failure (kPa)	θ_failure	f. type
1	46	1568.5	6.30	0.149	M
5	15	274.7	1.10	0.315	W
10	2	48.7	0.17	0.346	E
20	2	44.2	0.16	0.346	E
40	2	42.2	0.16	0.346	E
80	2	41.2	0.15	0.347	E

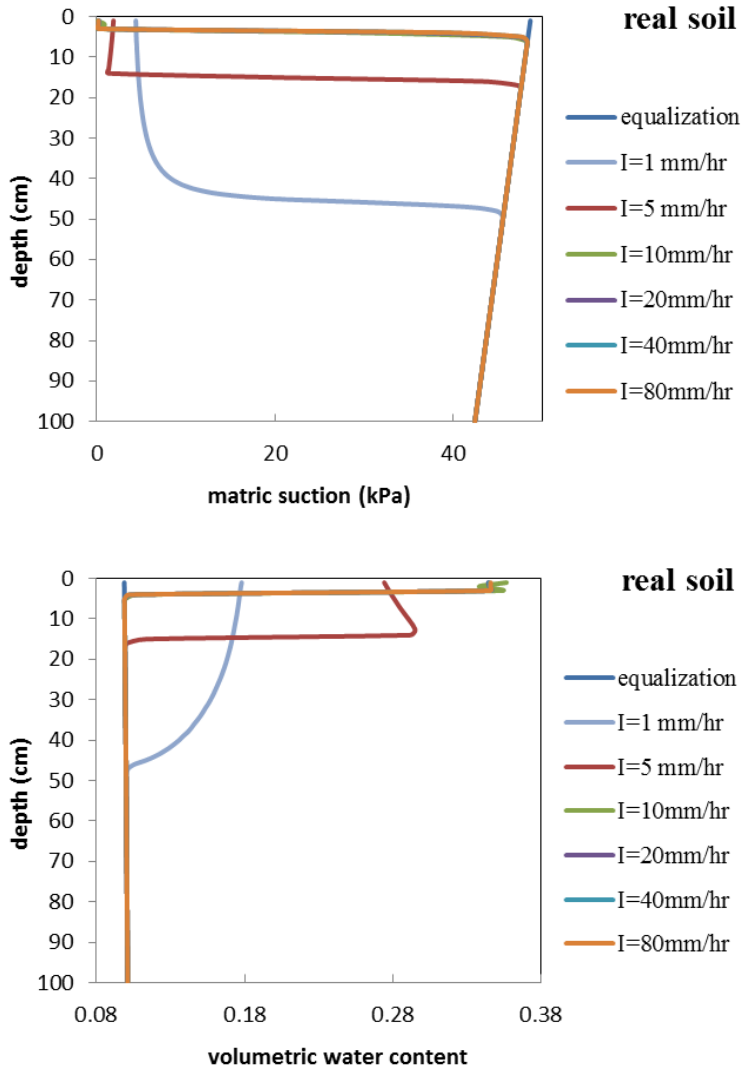

Figure E. 6. The matric suction and volumetric water content profiles at the time of failure for base angle of 50°.

Table E. 6. Results of analyses for base angle of 50°.

base angle=50°					
I (mm/hr)	f. depth(cm)	f. time(min)	Ψ_failure (kPa)	θ_failure	f. type
1	36	1267.6	0.75	0.335	M
5	13	244.8	1.34	0.295	W
10	2	49.7	0.89	0.338	E
20	2	44.2	0.21	0.345	E
40	2	42.0	0.20	0.345	E
80	2	41.0	0.19	0.346	E

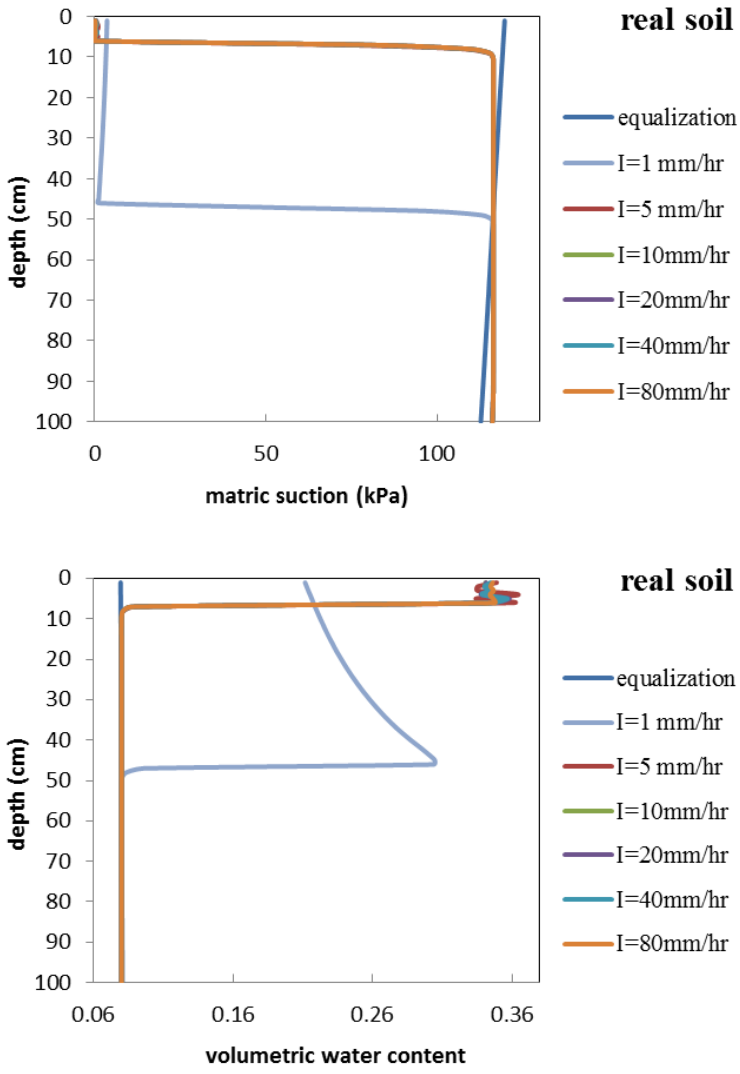

Figure E. 7. The matric suction and volumetric water content profiles at the time of failure for initial volumetric water content of 0.08.

Table E. 7. Results of analyses for initial volumetric water content of 0.08.

$\theta_{initial}$ = 0.08					
I (mm/hr)	f. depth(cm)	f. time(min)	Ψ_failure (kPa)	θ_failure	f. type
1	45	3065.1	1.21	0.305	M
5	5	365.5	1.01	0.334	E
10	5	358.4	0.14	0.347	E
20	5	355.6	0.10	0.358	E
40	5	354.4	0.10	0.357	E
80	5	353.9	0.16	0.347	E

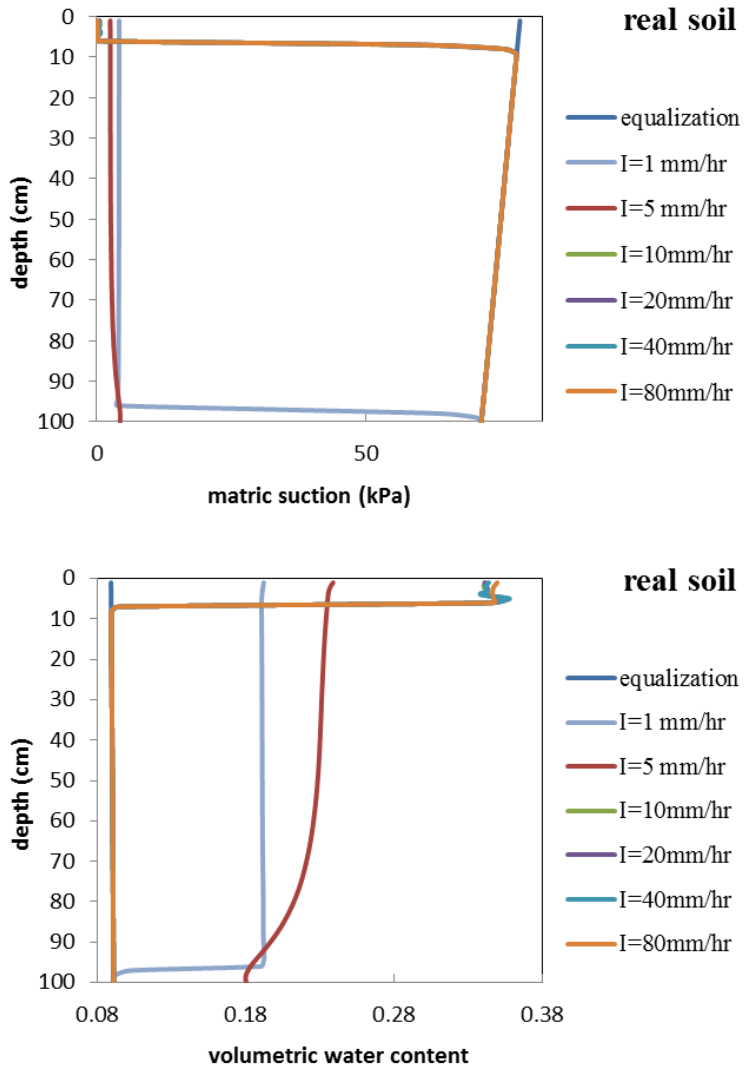

Figure E. 8. The matric suction and volumetric water content profiles at the time of failure for initial volumetric water content of 0.09.

Table E. 8. Results of analyses for initial volumetric water content of 0.09.

$\theta_{initial}$ = 0.09					
I (mm/hr)	f. depth(cm)	f. time(min)	Ψ_failure (kPa)	θ_failure	f. type
1	95	3808.1	3.86	0.192	M
5	99	873.6	4.38	0.180	M
10	5	215.4	0.11	0.353	E
20	5	213.0	0.10	0.357	E
40	5	211.8	0.10	0.358	E
80	5	211.4	0.15	0.347	E

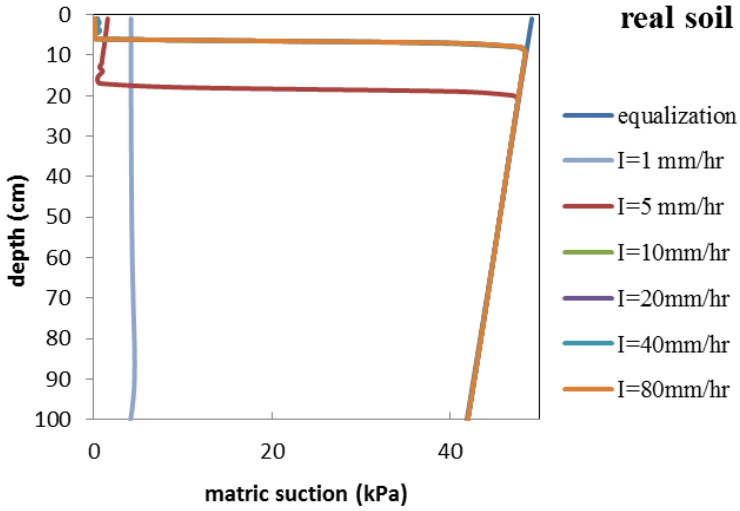

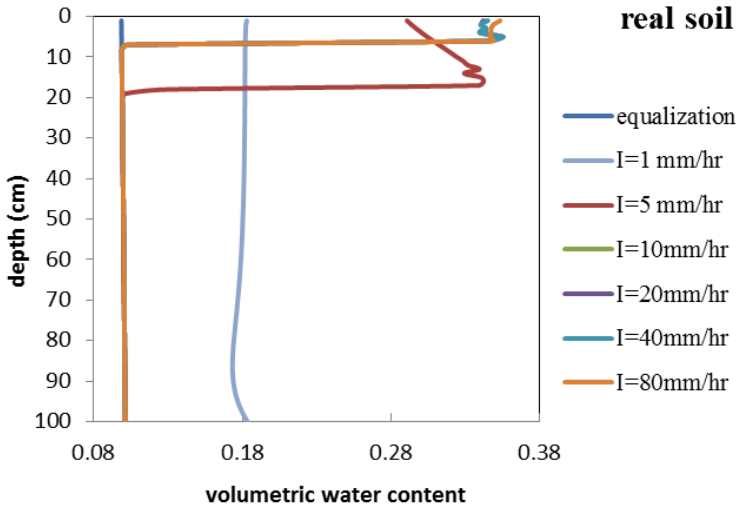

Figure E. 9. The matric suction and volumetric water content profiles at the time of failure for initial volumetric water content of 0.10.

Table E. 9. Results of analyses for initial volumetric water content of 0.09.

$\theta_{initial}$ = 0.10					
I (mm/hr)	f. depth(cm)	f. time(min)	Ψ_failure (kPa)	θ_failure	f. type
1	99	3101.3	4.20	0.182	M
5	13	245.7	0.19	0.345	W
10	5	96.0	0.12	0.349	E
20	5	93.4	0.11	0.355	E
40	5	92.3	0.10	0.355	E
80	5	92.0	0.17	0.346	E

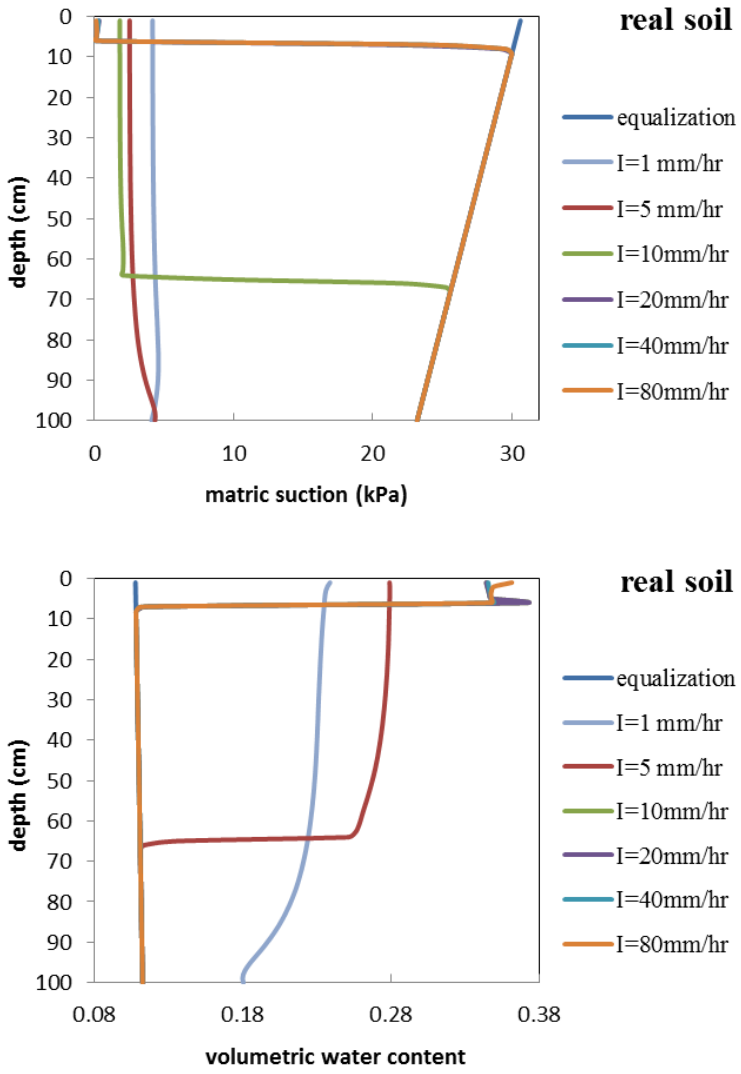

Figure E. 10. The matric suction and volumetric water content profiles at the time of failure for initial volumetric water content of 0.11.

Table E. 10. Results of analyses for initial volumetric water content of 0.11.

$\theta_{initial}$ = 0.11					
I (mm/hr)	f. depth(cm)	f. time(min)	Ψ_failure (kPa)	θ_failure	f. type
1	99	2772.5	4.18	0.184	M
5	99	873.6	4.38	0.180	M
10	63	409.8	2.04	0.255	M
20	5	39.0	0.14	0.347	E
40	5	37.2	0.15	0.347	E
80	5	36.8	0.15	0.347	E

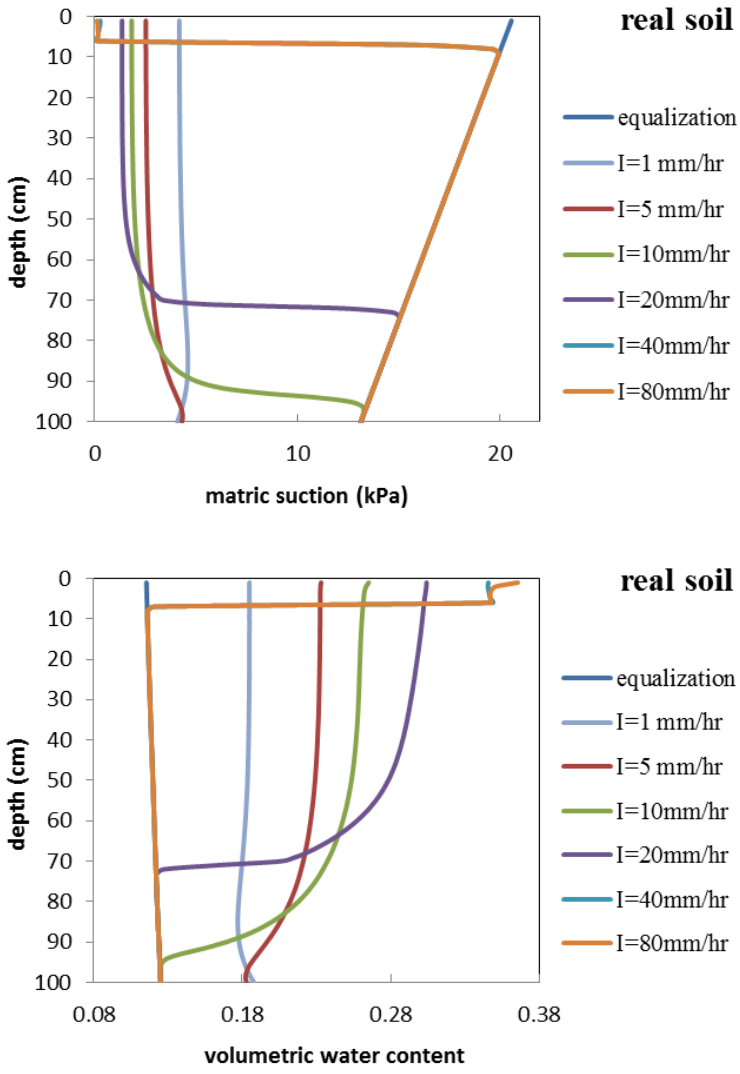

Figure E. 11. The matric suction and volumetric water content profiles at the time of failure for initial volumetric water content of 0.12.

Table E. 11. Results of analyses for initial volumetric water content of 0.12.

$\theta_{initial}$ = 0.12					
I (mm/hr)	f. depth(cm)	f. time(min)	Ψ_failure (kPa)	θ_failure	f. type
1	99	2447.3	4.16	0.186	M
5	99	796.3	4.35	0.182	M
10	75	447.4	2.64	0.229	M
20	56	224.9	1.72	0.268	M
40	5	19.0	0.16	0.347	E
80	5	18.6	0.17	0.347	E

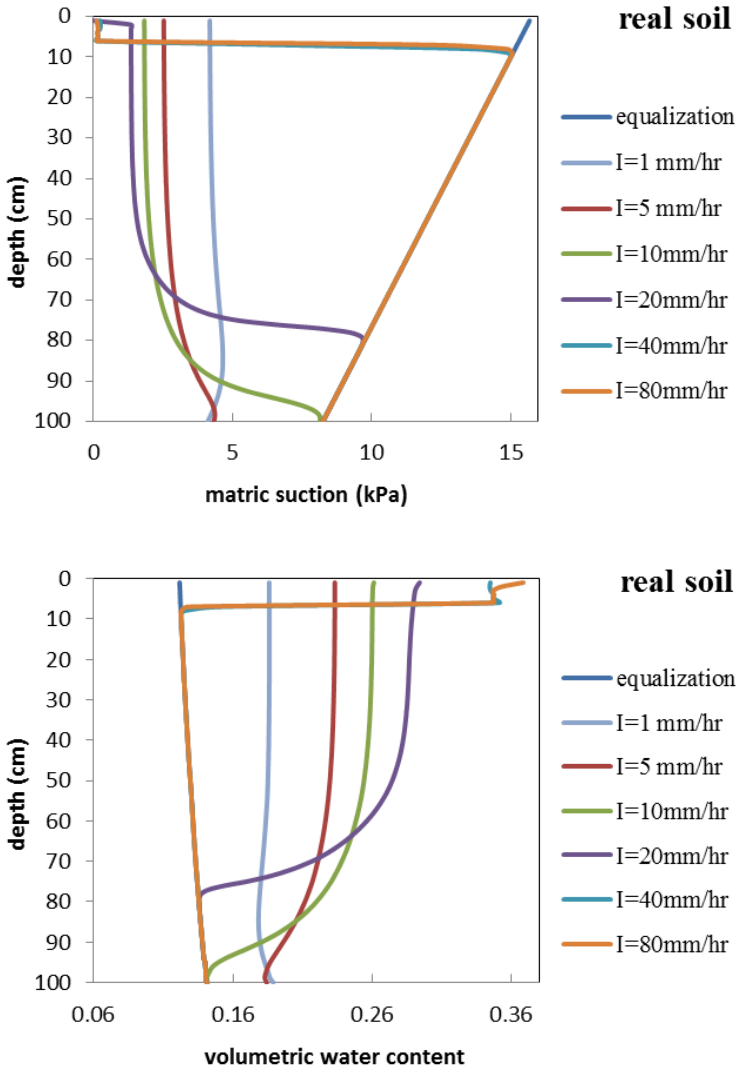

Figure E. 12. The matric suction and volumetric water content profiles at the time of failure for initial volumetric water content of 0.13.

Table E. 12. Results of analyses for initial volumetric water content of 0.13.

$\theta_{initial}$ = 0.13					
I (mm/hr)	f. depth(cm)	f. time(min)	Ψ_failure (kPa)	θ_failure	f. type
1	99	2772.5	4.18	0.184	M
5	99	873.6	4.38	0.180	M
10	63	409.8	2.04	0.255	M
20	5	39.0	0.14	0.347	E
40	5	37.2	0.15	0.347	E
80	5	36.8	0.15	0.347	E

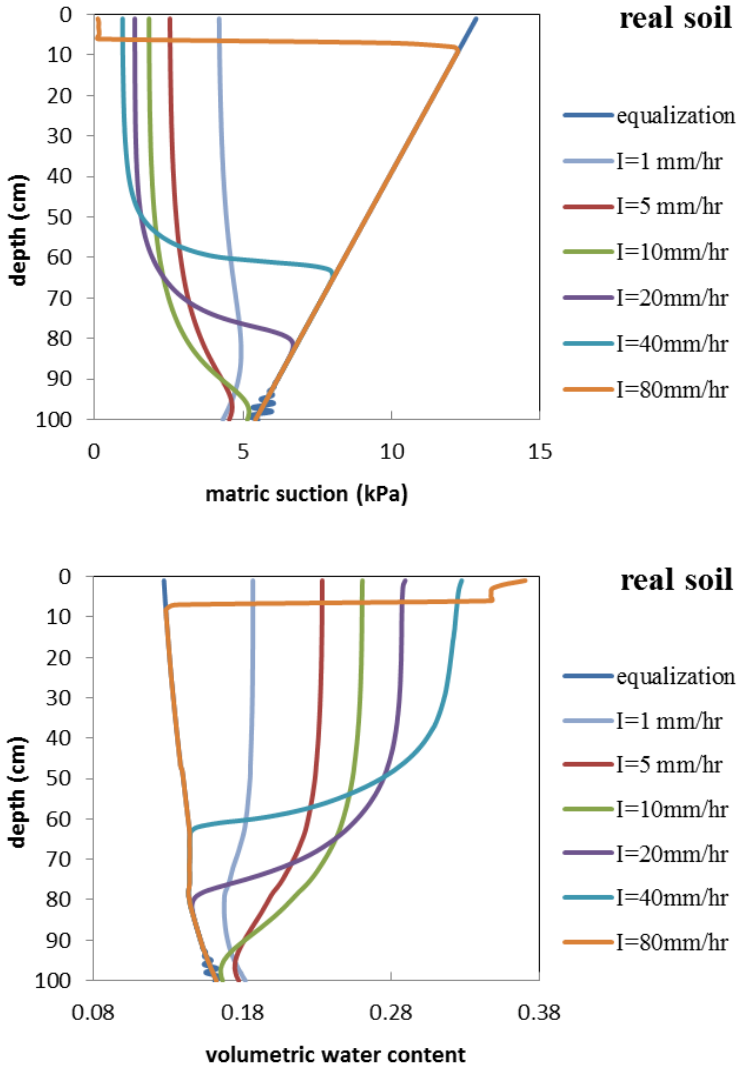

Figure E. 13. The matric suction and volumetric water content profiles at the time of failure for initial volumetric water content of 0.14.

Table E. 13. Results of analyses for initial volumetric water content of 0.14.

$\theta_{initial}$ = 0.14					
I (mm/hr)	f. depth(cm)	f. time(min)	Ψ_failure (kPa)	θ_failure	f. type
1	99	1609.7	4.39	0.180	M
5	99	609.9	4.59	0.176	M
10	78	382.6	2.92	0.218	M
20	57	198.3	1.79	0.264	M
40	45	97.7	1.30	0.292	M
80	5	8.3	0.15	0.347	E

APPENDIX F

MATLAB CODE

```
clc
clear

rint=80;        % rainfall intensity (mm/hr)
bint=0;         %bottom seepage intensity (m/sec)
dur=2;          %analysis duration (hr)
dz=0.01;        %height increment (m)
dt=0.5;         %time increment (sec)"
height=1;       %height of slope (m)
area=1;          %area of slice (m^2)
gs=2.75;        %specific gravity
alfa=46;        %base angle (degree)
c=0;            %cohesion (kPa)
BC=0;           %boundary condition for bottom face, BC=0 for bint "if bint=0 then
                impervious", BC=1 for %Q=0
equ_end=1;       %equalization is complete or not, 1 for completed; 0 for not
                completed
teta_i=0.08;    %initial volumetric water content
teta_r=0;       %residuel volumetric water content

%data points for hydraulic functions
%Ψ values for drying SWCC
swcc_d_s=[0.100000  0.110776   0.122713   0.135936   0.150584   0.166810
0.184785   0.204697   0.226754   0.251189   0.278256   0.308240   0.341455
0.378249   0.419008   0.464159   0.500000   0.514175   0.569581   0.630957
0.698947   0.774264   0.857696   0.950119   1.000000   1.052500   1.165914
1.250000   1.291550   1.430723   1.584893   1.755676   1.944862   2.154435
2.386590   2.500000   2.643761   2.928645   3.244226   3.593814   3.981072
4.410059   4.885274   5.000000   5.411695   5.994843   6.640828   7.356423
8.149127   9.027252   10.000000   11.077569   12.271252   13.593564   15.058364
16.681005   18.478498   20.000000   20.469683   22.675431   25.118864   27.825594
30.823992   34.145489   37.824899   41.900791   46.415888   50.000000   51.417518
56.958108   63.095734   69.894732   77.426368   85.769590   95.011851
```

100.000000 105.250029 116.591440 129.154967 143.072299 158.489319
175.567629 194.486244 200.000000 215.443469 238.658979 264.376119
292.864456 324.422608 359.381366 398.107171 441.005945 488.527357
541.169527 599.484250 664.082785 735.642254 814.912747 902.725178
1000.000000];
%θ values for drying SWCC
swcc_d_t=[0.439527 0.439111 0.438698 0.438288 0.437883 0.437486
0.437097 0.436720 0.436355 0.436005 0.435671 0.435355 0.435060
0.434786 0.434535 0.434310 0.434164 0.434112 0.433909 0.433610
0.433114 0.432324 0.431142 0.429468 0.428415 0.427198 0.424107
0.421357 0.419848 0.414114 0.406677 0.397314 0.385801 0.371918
0.355440 0.347049 0.336175 0.314498 0.291285 0.267431 0.243828
0.221371 0.200954 0.196699 0.183375 0.168669 0.156498 0.146525
0.138411 0.131818 0.126407 0.121875 0.118066 0.114856 0.112125
0.109750 0.107609 0.106037 0.105581 0.103580 0.101592 0.099614
0.097642 0.095672 0.093700 0.091723 0.089737 0.088285 0.087737
0.085717 0.083665 0.081568 0.079413 0.077186 0.074875 0.073684
0.072468 0.069965 0.067382 0.064733 0.062035 0.059301 0.056548
0.055795 0.055308 0.054637 0.053967 0.053296 0.052626 0.051956
0.051285 0.050615 0.049945 0.049274 0.048604 0.047933 0.047263
0.046593 0.045922 0.045252];
%Ψ values for wetting SWCC
swcc_w_s=[0.100000 0.110776 0.122713 0.135936 0.150584 0.166810
0.184785 0.204697 0.226754 0.251189 0.278256 0.308240 0.341455
0.378249 0.419008 0.464159 0.500000 0.514175 0.569581 0.630957
0.698947 0.774264 0.857696 0.950119 1.000000 1.052500 1.165914
1.250000 1.291550 1.430723 1.584893 1.755676 1.944862 2.154435
2.386590 2.500000 2.643761 2.928645 3.244226 3.593814 3.981072
4.410059 4.885274 5.000000 5.411695 5.994843 6.640828 7.356423
8.149127 9.027252 10.000000 11.077569 12.271252 13.593564 15.058364
16.681005 18.478498 20.000000 20.469683 22.675431 25.118864 27.825594
30.823992 34.145489 37.824899 41.900791 46.415888 50.000000 51.417518
56.958108 63.095734 69.894732 77.426368 85.769590 95.011851
100.000000 105.250029 116.591440 129.154967 143.072299 158.489319
175.567629 194.486244 200.000000 215.443469 238.658979 264.376119
292.864456 324.422608 359.381366 398.107171 441.005945 488.527357
541.169527 599.484250 664.082785 735.642254 814.912747 902.725178
1000.000000];
%θ values for wetting SWCC
swcc_w_t=[0.348000 0.347533 0.347065 0.346598 0.346131 0.345664
0.345197 0.344730 0.344263 0.343797 0.343330 0.342864 0.342399
0.341933 0.341468 0.341003 0.340665 0.340537 0.339933 0.338812
0.336764 0.333382 0.328259 0.320987 0.316417 0.311204 0.299600
0.291551 0.287908 0.277152 0.267144 0.257589 0.248189 0.238648
0.228669 0.223918 0.217972 0.206566 0.194715 0.182695 0.170780

0.159246 0.148365 0.146017 0.138390 0.129383 0.121315 0.114154
0.107873 0.102440 0.097826 0.093986 0.090815 0.088195 0.086006
0.084129 0.082445 0.081199 0.080834 0.079221 0.077615 0.076041
0.074519 0.073073 0.071724 0.070496 0.069409 0.068721 0.068486
0.067726 0.067079 0.066495 0.065922 0.065307 0.064599 0.064194
0.063748 0.062739 0.061597 0.060347 0.059015 0.057624 0.056202
0.055811 0.055324 0.054653 0.053983 0.053312 0.052641 0.051971
0.051300 0.050630 0.049959 0.049289 0.048618 0.047947 0.047277
0.046606 0.045936 0.045265];
%conductivity values for HCF
hcf_k=[1.724819E-05 1.708414E-05 1.691656E-05 1.674055E-05 1.655143E-
05 1.640108E-05 1.634481E-05 1.612151E-05 1.589148E-05 1.566513E-
05 1.545230E-05 1.535891E-05 1.526195E-05 1.509540E-05 1.494730E-
05 1.481233E-05 1.468536E-05 1.465919E-05 1.456179E-05 1.443952E-
05 1.431760E-05 1.419514E-05 1.407782E-05 1.407125E-05 1.394666E-
05 1.382741E-05 1.372043E-05 1.363247E-05 1.358668E-05 1.356964E-
05 1.350152E-05 1.333967E-05 1.299597E-05 1.239726E-05 1.205672E-
05 1.150230E-05 1.037273E-05 9.134954E-06 7.895182E-06 6.729729E-
06 6.555947E-06 5.684462E-06 4.777287E-06 4.009645E-06 3.373614E-
06 2.905483E-06 2.856151E-06 2.437266E-06 2.087405E-06 1.784720E-
06 1.358119E-06 1.270564E-06 1.048421E-06 8.503096E-07 6.771790E-
07 5.290519E-07 4.806385E-07 4.051159E-07 3.042924E-07 2.247126E-
07 1.635320E-07 1.175523E-07 1.134671E-07 8.364289E-08 5.897317E-
08 4.123226E-08 2.860926E-08 2.091757E-08 1.971483E-08 1.351634E-
08 9.260754E-09 6.372290E-09 4.425341E-09 3.605299E-09 3.116842E-
09 2.233666E-09 1.631253E-09 1.215773E-09 9.260617E-10 8.538369E-
10 7.215735E-10 5.728476E-10 4.603068E-10 3.719018E-10 3.001268E-
10 2.967119E-10 2.405664E-10 1.913521E-10 1.511194E-10 1.185543E-
10 9.745580E-11 9.243760E-11 7.179826E-11 5.589964E-11 4.391922E-
11 3.505675E-11 3.140525E-11 2.861447E-11 2.392437E-11 2.043041E-
11 1.776472E-11 1.568000E-11 1.520525E-11 1.400593E-11 1.262721E-
11 1.146366E-11 1.045568E-11 9.558462E-12];
%Ψ values for HCF
hcf_s=[1.0000000E-01 1.0797752E-01 1.1659144E-01 1.2589254E-01
1.3593564E-01 1.4384499E-01 1.4677993E-01 1.5848932E-01 1.7113283E-01
1.8478498E-01 1.9952623E-01 2.0691381E-01 2.1544347E-01 2.3263051E-01
2.5118864E-01 2.7122726E-01 2.9286446E-01 2.9763514E-01 3.1622777E-01
3.4145489E-01 3.6869451E-01 3.9810717E-01 4.2813324E-01 4.2986623E-01
4.6415888E-01 5.0118723E-01 5.4116953E-01 5.8434141E-01 6.1584821E-01
6.3095734E-01 6.8129207E-01 7.3564225E-01 7.9432823E-01 8.5769590E-01
8.8586679E-01 9.2611873E-01 1.0000000E+00 1.0797752E+00
1.1659144E+00 1.2589254E+00 1.2742750E+00 1.3593564E+00
1.4677993E+00 1.5848932E+00 1.7113283E+00 1.8329807E+00
1.8478498E+00 1.9952623E+00 2.1544347E+00 2.3263051E+00
2.6366509E+00 2.7122726E+00 2.9286446E+00 3.1622777E+00

```
3.4145489E+00   3.6869451E+00   3.7926902E+00   3.9810717E+00
4.2986623E+00   4.6415888E+00   5.0118723E+00   5.4116953E+00
5.4555948E+00   5.8434141E+00   6.3095734E+00   6.8129207E+00
7.3564225E+00   7.8475997E+00   7.9432823E+00   8.5769590E+00
9.2611873E+00   1.0000000E+01   1.0797752E+01   1.1288379E+01
1.1659144E+01   1.2589254E+01   1.3593564E+01   1.4677993E+01
1.5848932E+01   1.6237767E+01   1.7113283E+01   1.8478498E+01
1.9952623E+01   2.1544347E+01   2.3263051E+01   2.3357215E+01
2.5118864E+01   2.7122726E+01   2.9286446E+01   3.1622777E+01
3.3598183E+01   3.4145489E+01   3.6869451E+01   3.9810717E+01
4.2986623E+01   4.6415888E+01   4.8329302E+01   5.0118723E+01
5.4116953E+01   5.8434141E+01   6.3095734E+01   6.8129207E+01
6.9519280E+01   7.3564225E+01   7.9432823E+01   8.5769590E+01
9.2611873E+01   1.0000000E+02];

d_point=zeros(1,length(swcc_w_t));

alfa=pi*alfa/180;       %base angle in radians

rint=rint/1000/3600*cos(alfa);          %q_boundary

% equalization stage

if equ_end==0

%initial suction (suction_i)
for m=1:1:length(swcc_d_s)-1
   if teta_i<=swcc_d_t(m) && teta_i>=swcc_d_t(m+1)

suction_i=10^(log10(swcc_d_s(m))+(log10(swcc_d_s(m+1)/swcc_d_s(m)))/(swcc_d
_t(m+1)-swcc_d_t(m))*(teta_i-swcc_d_t(m)));
      break
   end
end


a=dur*3600/dt;          %# of elements in time domain
b=height/dz;            %# of elements in space domain

s=zeros(b,a);           %suction matrix
t=zeros(b,a);           %volumetric water content matrix
k=zeros(b,a);            %hydraulic conductivity matrix
q=zeros(b-1,a);         %flow matrix

multiplier=dt/dz/area;
```

```
discarded=zeros(1,a);          %surface runoff matrix

t_target=zeros(1,b);           %matrice defines maximum vol. water content through
                               wetting path
for i=1:1:b
   t_target(i)=swcc_w_t(1)+(swcc_d_t(1)-swcc_w_t(1))/(swcc_d_t(1)-teta_r)*(t(i,1)-
teta_r);
end
t_target=t_target';

s(:,1)=suction_i;

d_point=abs(swcc_d_s-suction_i);
[~, m]=min(d_point);
d_point(1,m)=100000;
[~,mm]=min(d_point);
teta_i=swcc_d_t(mm)+(swcc_d_t(m)-
swcc_d_t(mm))/log10(swcc_d_s(m)/swcc_d_s(mm))*log10(suction_i/swcc_d_s(mm
));
t(:,1)=teta_i;

for m=1:1:length(hcf_s)-1
    if suction_i>=hcf_s(m) && suction_i<=hcf_s(m+1)
      k(:,1)=10^(log10(hcf_k(m))+(log10(hcf_k(m+1))-
log10(hcf_k(m)))/(log10(hcf_s(m+1))-log10(hcf_s(m)))*(log10(suction_i)-
log10(hcf_s(m))));
       break
    end
end

%initial flux
for i=1:1:(b-1)
     q(i,1)=(2*k(i,1)*k(i+1,1))/(k(i,1)+k(i+1,1))*(-(s(i,1)-
s(i+1,1))/9.807+dz*cos(alfa))/dz*area;
end


for j=2:1:a
for i=1:1:b
if j == 2
if i==1
    t(i,j)=t(i,j-1)+(-q(i,j-1)*dt)/dz/area;
elseif i==b
  if BC==1
```

```
    t(i,j)=2*t(i-1,j)-t(i-2,j); %Q=0 'zero unit flux' boundary condition
  else
    t(i,j)=t(i,j-1)+(q(i-1,j-1)*dt-bint*area*dt)/dz/area;
  end
else
    t(i,j)= t(i,j-1)+(-q(i,j-1)+q(i-1,j-1))*multiplier;
end
else
    t(:,j)=t3;
end

d_point=abs(swcc_w_t-t(i,j));
   [~, m]=min(d_point);
   d_point(1,m)=10;
   [~,mm]=min(d_point);

psiw=10^(log10(swcc_w_s(m))+(log10(swcc_w_s(mm)/swcc_w_s(m)))/(swcc_w_t(
mm)-swcc_w_t(m))*(t(i,j)-swcc_w_t(m)));

   if t(i,j)>swcc_w_t(1)
      psiw=swcc_w_s(1);
   end
   d_point=abs(swcc_d_t-t(i,j));
   [~, m]=min(d_point);
   d_point(1,m)=10;
   [~,mm]=min(d_point);

psid=10^(log10(swcc_d_s(m))+(log10(swcc_d_s(mm)/swcc_d_s(m)))/(swcc_d_t(m
m)-swcc_d_t(m))*(t(i,j)-swcc_d_t(m)));

   d_point=abs(swcc_w_t-t(i,j-1));
   [~, m]=min(d_point);
   d_point(1,m)=10;
   [~,mm]=min(d_point);

psiw_old=10^(log10(swcc_w_s(m))+(log10(swcc_w_s(mm)/swcc_w_s(m)))/(swcc_
w_t(mm)-swcc_w_t(m))*(t(i,j-1)-swcc_w_t(m)));

   if t(i,j-1)>swcc_w_t(1)
      psiw_old=swcc_w_s(1);
   end

   d_point=abs(swcc_d_t-t(i,j-1));
   [~, m]=min(d_point);
   d_point(1,m)=10;
```

```
    [~,mm]=min(d_point);

psid_old=10^(log10(swcc_d_s(m))+(log10(swcc_d_s(mm)/swcc_d_s(m)))/(swcc_d_
t(mm)-swcc_d_t(m))*(t(i,j-1)-swcc_d_t(m)));

    if t(i,j)>=t(i,j-1)
    s(i,j)=exp(log(psiw)+log(s(i,j-
1)/psiw_old)/log(psid_old/psiw_old)*log(psid/psiw)*((t_target(i)-t(i,j))/(t_target(i)-
t(i,j-1)))^3);
    else
    s(i,j)=exp(log(psid)-log(psid_old/s(i,j-
1))/log(psid_old/psiw_old)*log(psid/psiw)*((t(i,j)-teta_r)/(t(i,j-1)-teta_r))^3);
    end
    if isnan(s(i,j)) || isinf(s(i,j))
        s(i,j)=s(i,j-1);
    end

    d_point=abs(-hcf_s+s(i,j));
    [~, m]=min(d_point);
    d_point(1,m)=10;
    [~,mm]=min(d_point);
    k(i,j)=10^(log10(hcf_k(m))+(log10(hcf_k(mm))-
log10(hcf_k(m)))/(log10(hcf_s(mm))-log10(hcf_s(m)))*(log10(s(i,j))-
log10(hcf_s(m))));
    if isnan(k(i,j))
        k(i,j)=k(i,j-1);
    end
end

    k1=[k(:,j); 0];k2=[0; k(:,j)]; k3=(2*k1.*k2)./(k1+k2);k3(1)=[];k3(length(k3))=[];

    s1=[s(:,j); 0];s2=[0; s(:,j)];s3=s1-s2;s3(1)=[];s3(length(s3))=[];

    q(:,j)=(k3).*(s3/9.807+dz*cos(alfa))/dz*area;

    q1=[q(:,j);0];q2=[0;q(:,j)];q3=q2-q1;q3(1)=(-q(1,j));
    if BC==0
        q3(length(q3))=(q(b-1,j)-bint);
    else
        q3(length(q3))=((2*t(b-1,j-1)-t(b-2,j-1))-t(b,j-1))/multiplier;
    end
    q3=q3*multiplier;

    t3=t(:,j)+q3;
```

```
   %excess water distribution algorithm
   excess=t3-swcc_d_t(1);
   excess(excess(:)<0)=0;
   if excess(1)>0
      t3(1)=swcc_d_t(1);
      discarded(j)=excess(1);
      excess(1)=0;
   end
   distributed=sum(excess);
   distributed_kk=0;

      if distributed>0
      detect=find(excess>0);
      for nn=length(detect):-1:1  %nn=index of overflowing slices
            for kk=detect(nn)-1:-1:1 %kk=slices above each overflowing slice
               if kk==detect(nn)-1
               t3(kk+1)=swcc_d_t(1);  %kk+1=overflow slice
               distributed_kk=distributed_kk+excess(kk+1);
               end

               distributed_kk=distributed_kk+excess(kk);

               if distributed_kk>0
                     if distributed_kk-(-t3(kk)+swcc_d_t(1))>=0
                     distributed_kk=distributed_kk-(-t3(kk)+swcc_d_t(1));
                     t3(kk)=swcc_d_t(1);
                     if kk==1
                        discarded(j)=discarded(j)+distributed_kk; %surface run_off;
                        distributed_kk=0;
                     end
                     else
                     t3(kk)=t3(kk)+distributed_kk;
                     distributed_kk=0;
                     end
               else
               break
               end
            end
      end
      end
end

s_equ_end=s(:,a);
t_equ_end=t(:,a);
dlmwrite('s_equ_end.txt',s_equ_end);%export initial condition data
```

```
dlmwrite('t_equ_end.txt',t_equ_end);
plot(s(:,a));
end

if equ_end==1

a=dur*3600/dt;          %# of elements in time domain
b=height/dz;            %# of elements in space domain

s=zeros(b,a);            %suction matrice
t=zeros(b,a);           %volumetric water content matrice
k=zeros(b,a);           %hydraulic conductivity matrice
q=zeros(b-1,a);          %flow matrice

multiplier=dt/dz/area;

discarded=zeros(1,a);

%initial suction&volumetric water content&conductivity
s_equ_end=dlmread('s_equ_end.txt');%import initial condition data
t_equ_end=dlmread('t_equ_end.txt');%import initial condition data
s(:,1)=s_equ_end;
t(:,1)=t_equ_end;

for i=1:b
for m=1:1:length(hcf_s)-1
    if s(i,1)>=hcf_s(m) && s(i,1)<=hcf_s(m+1)
      k(i,1)=10^(log10(hcf_k(m))+(log10(hcf_k(m+1))-
log10(hcf_k(m)))/(log10(hcf_s(m+1))-log10(hcf_s(m)))*(log10(s(i,1))-
log10(hcf_s(m))));
      break
    end
end
end
%initial flux
for i=1:1:(b-1)
     q(i,1)=(2*k(i,1)*k(i+1,1))/(k(i,1)+k(i+1,1))*(-(s(i,1)-
s(i+1,1))/9.807+dz*cos(alfa))/dz*area;
end

t_target=zeros(1,b);            %matrice defines maximum vol. water content through
                                wetting path
for i=1:1:b
   t_target(i)=swcc_w_t(1)+(swcc_d_t(1)-swcc_w_t(1))/(swcc_d_t(1)-teta_r)*(t(i,1)-
teta_r);
```

```
end
t_target=t_target';

% infiltration  process
for j=2:1:a      %temporal index
for pc=1:2       %counter for predictor-corrector solution
for i=1:1:b      %spatial index
if j==2
if i==1
    if t(i,j-1)+(rint*dt*area-q(i,j-1)*dt)/dz/area>t_target(1)
    t(i,j)=t_target(1);
    discarded(j)=t(i,j-1)+(rint*dt*area-q(i,j-1)*dt)/dz/area-t_target(1);
    else
    t(i,j)=t(i,j-1)+(rint*dt*area-q(i,j-1)*dt)/dz/area;
    end
elseif i==b
 if BC==1
    t(i,j)=2*t(i-1,j)-t(i-2,j);              %Q=0 'zero unit flux' boundary condition
 else
    t(i,j)=t(i,j-1)+(q(i-1,j-1)*dt-bint*area*dt)/dz/area;
 end
else
   t(i,j)= t(i,j-1)+(-q(i,j-1)+q(i-1,j-1))*multiplier;
end
else
   t(:,j)=t3;
end
   d_point=abs(swcc_w_t-t(i,j));
   [~, m]=min(d_point);
   d_point(1,m)=10;
   [~,mm]=min(d_point);

psiw=10^(log10(swcc_w_s(m))+(log10(swcc_w_s(mm)/swcc_w_s(m)))/(swcc_w_t(
mm)-swcc_w_t(m))*(t(i,j)-swcc_w_t(m)));

   if t(i,j)>swcc_w_t(1)
      psiw=swcc_w_s(1);
   end
   d_point=abs(swcc_d_t-t(i,j));
   [~, m]=min(d_point);
   d_point(1,m)=10;
   [~,mm]=min(d_point);

psid=10^(log10(swcc_d_s(m))+(log10(swcc_d_s(mm)/swcc_d_s(m)))/(swcc_d_t(m
m)-swcc_d_t(m))*(t(i,j)-swcc_d_t(m)));
```

```
    d_point=abs(swcc_w_t-t(i,j-1));
    [~, m]=min(d_point);
    d_point(1,m)=10;
    [~,mm]=min(d_point);

psiw_old=10^(log10(swcc_w_s(m))+(log10(swcc_w_s(mm)/swcc_w_s(m)))/(swcc_
w_t(mm)-swcc_w_t(m))*(t(i,j-1)-swcc_w_t(m)));

    if t(i,j-1)>swcc_w_t(1)
        psiw_old=swcc_w_s(1);
    end

    d_point=abs(swcc_d_t-t(i,j-1));
    [~, m]=min(d_point);
    d_point(1,m)=10;
    [~,mm]=min(d_point);

psid_old=10^(log10(swcc_d_s(m))+(log10(swcc_d_s(mm)/swcc_d_s(m)))/(swcc_d_
t(mm)-swcc_d_t(m))*(t(i,j-1)-swcc_d_t(m)));

    if t(i,j)>=t(i,j-1)
    s(i,j)=exp(log(psiw)+log(s(i,j-
1)/psiw_old)/log(psid_old/psiw_old)*log(psid/psiw)*((t_target(i)-t(i,j))/(t_target(i)-
t(i,j-1)))^3);
    else
    s(i,j)=exp(log(psid)-log(psid_old/s(i,j-
1))/log(psid_old/psiw_old)*log(psid/psiw)*((t(i,j)-teta_r)/(t(i,j-1)-teta_r))^3);
    end
    if isnan(s(i,j)) || isinf(s(i,j))
        s(i,j)=s(i,j-1);
    end

    d_point=abs(-hcf_s+s(i,j));
    [~, m]=min(d_point);
    d_point(1,m)=10000;
    [~,mm]=min(d_point);
    k(i,j)=10^(log10(hcf_k(m))+(log10(hcf_k(mm))-
log10(hcf_k(m)))/(log10(hcf_s(mm))-log10(hcf_s(m)))*(log10(s(i,j))-
log10(hcf_s(m))));
    if isnan(k(i,j))
        k(i,j)=k(i,j-1);
    end
end
```

```
k1=[k(:,j); 0];k2=[0; k(:,j)]; k3=(2*k1.*k2)./(k1+k2);k3(1)=[];k3(length(k3))=[];
if pc==1
k3_predictor=k3;
else
k3_corrector=k3;
end

s1=[s(:,j); 0];s2=[0; s(:,j)];s3=s1-s2;s3(1)=[];s3(length(s3))=[];
if pc==1
s3_predictor=s3;
else
s3_corrector=s3;
end
if pc==1
q(:,j)=(k3).*(s3/9.807+dz*cos(alfa))/dz*area;
else
k3=(k3_predictor+k3_corrector)/2;
s3=(s3_predictor+s3_corrector)/2;
q(:,j)=(k3).*(s3/9.807+dz*cos(alfa))/dz*area;
end
q1=[q(:,j);0];q2=[rint;q(:,j)];q3=q2-q1;
if BC==0
   q3(length(q3))=(q(b-1,j)-bint);
else
   q3(length(q3))=((2*t(b-1,j)-t(b-2,j))-t(b,j))/multiplier;
end
q3=q3*multiplier;

t3=t(:,j)+q3;
%water distribution algorithm for wetting
excess=t3-t_target;
excess(excess(:)<0)=0;
if excess(1)>0
   t3(1)=t_target(1);
   discarded(j)=excess(1);
   excess(1)=0;
end
distributed=sum(excess);
distributed_kk=0;

   if distributed>0
   detect=find(excess>0);
   for nn=length(detect):-1:1              %nn=index of overfilled slices
         for kk=detect(nn)-1:-1:1          %kk=slices above each overfilled slice
            if kk==detect(nn)-1
```

```
            t3(kk+1)=t_target(kk+1);                %kk+1=overfilled slice
            distributed_kk=distributed_kk+excess(kk+1);
            end

            distributed_kk=distributed_kk+excess(kk);

            if distributed_kk>0
                if distributed_kk-(-t3(kk)+t_target(kk))>=0
                distributed_kk=distributed_kk-(-t3(kk)+t_target(kk));
                t3(kk)=t_target(kk);
                if kk==1
                   discarded(j)=discarded(j)+distributed_kk;      %surface run_off;
                   distributed_kk=0;
                end
                else
                t3(kk)=t3(kk)+distributed_kk;
                distributed_kk=0;
                end
            else
            break
            end
          end
    end
    end

end

end
```

%slope stability analysis

```
gamai=zeros(b,a);           %unit weight matrice
weight=zeros(b,a);          %weight matrice
r=zeros(b-1,a);             %resistant force matrice
fs=zeros(b-1,a);            %factor of safety matrice

%gamad=gs*(1-swcc_d_t(1))*9.807;%dry unit weight
gamad=13.85;
%fi=pi*(96.076518*(0.43953-swcc_d_t(1))+30.3)/180; %friction angle (radian),
proposed by NAVFAC
fi=37*pi/180;

for j=1:1:a
   for i=1:1:b
      gamai(i,j)=gamad*(1+t(i,j)/(gamad/9.807));
      if i==1
```

```
        weight(i,j)=gamai(i,j)*area*dz;
      else
        weight(i,j)=weight(i-1,j)+gamai(i,j)*area*dz;
      end
      if i<b

r(i,j)=area*(c+weight(i,j)*(cos(alfa))^2/area*tan(fi)+(s(i,j)*s(i+1,j))^0.5*tan(fi)*((t(i,
j)*t(i+1,j))^0.5/2-teta_r)/(t_target(i)-teta_r));%vanapalli equation

fs(i,j)=r(i,j)/weight(i,j)/sin(alfa)/cos(alfa);
      end
   end
end

for j=2:1:a
   for i=1:1:b-1                    %critical slip surface depth is, therefore, 1 cm
   if fs(i,j)-1<=0
      failuretime=(j-1)*dt/60;      %failure time in minutes
      failuredepth=i*dz*100;        %failure depth in cm
      s_failure=s(i,j-1);           %suction value at failure depth on failure time
      t_failure=t(i,j-1);           %vol. water content value at failure depth on
                                    failure time
      fs_failure=fs(i,j-1);
      results=[failuretime failuredepth s_failure t_failure fs_failure];
      %dlmwrite('0.5AEV',results);%export initial condition data
   break
   end
   end
   if fs(i,j)-1<=0
      break
   end
end
end
```

In case of simulation of evaporation, following section can be replaced by "infiltration process" algorithm.

%evaporation process

```
eva_q=zeros(1,a);
eva_q(1,1)=k(1,1)*((80000-s(1,1))/9.807-dz*cos(alfa))/dz*area;
flux_eva=0.75*0.833*(4.57*25+43.3)/30/24/60/60/1000;          %USBR formula
for lake surface evaporation coef. .75 used for ground surface

if eva_q(1,1)>flux_eva
   eva_q(1,1)=flux_eva;
```

```
end

for j=2:1:a
for pc=1:2
for i=1:1:b
if j==2
if i==1
    t(i,j)=t(i,j-1)+(-eva_q(1,j-1)*dt*area-q(i,j-1)*dt)/dz/area;
elseif i==b
 if BC==1
    t(i,j)=2*t(i-1,j)-t(i-2,j); %Q=0 'zero unit flux' boundary condition
 else
    t(i,j)=t(i,j-1)+(q(i-1,j-1)*dt-bint*area*dt)/dz/area;
 end
else
   t(i,j)= t(i,j-1)+(-q(i,j-1)+q(i-1,j-1))*multiplier;
end
else
   t(:,j)=t3;
end

   d_point=abs(swcc_w_t-t(i,j));
   [~, m]=min(d_point);
   d_point(1,m)=10;
   [~,mm]=min(d_point);
   psiw=((swcc_w_s(mm)/swcc_w_s(m))^((t(i,j)-swcc_w_t(m))/(swcc_w_t(mm)-
swcc_w_t(m))))*swcc_w_s(m);

   d_point=abs(swcc_d_t-t(i,j));
   [~, m]=min(d_point);
   d_point(1,m)=10;
   [~,mm]=min(d_point);
   psid=((swcc_d_s(mm)/swcc_d_s(m))^((t(i,j)-swcc_d_t(m))/(swcc_d_t(mm)-
swcc_d_t(m))))*swcc_d_s(m);

   d_point=abs(swcc_w_t-t(i,j-1));
   [~, m]=min(d_point);
   d_point(1,m)=10;
   [~,mm]=min(d_point);
   psiw_old=((swcc_w_s(mm)/swcc_w_s(m))^((t(i,j-1)-
swcc_w_t(m))/(swcc_w_t(mm)-swcc_w_t(m))))*swcc_w_s(m);

   d_point=abs(swcc_d_t-t(i,j-1));
   [~, m]=min(d_point);
   d_point(1,m)=10;
```

```
    [~,mm]=min(d_point);
    psid_old=((swcc_d_s(mm)/swcc_d_s(m))^((t(i,j-1)-
swcc_d_t(m))/(swcc_d_t(mm)-swcc_d_t(m))))*swcc_d_s(m);

    if t(i,j)>=t(i,j-1)
    s(i,j)=exp(log(psiw)+log(s(i,j-
1)/psiw_old)/log(psid_old/psiw_old)*log(psid/psiw)*((t_target(i)-t(i,j))/(t_target(i)-
t(i,j-1)))^3);
    else
    s(i,j)=exp(log(psid)-log(psid_old/s(i,j-
1))/log(psid_old/psiw_old)*log(psid/psiw)*((t(i,j)-teta_r)/(t(i,j-1)-teta_r))^3);
    end
    if isnan(s(i,j)) || isinf(s(i,j))
        s(i,j)=s(i,j-1);
    end

    d_point=abs(-hcf_s+s(i,j));
    [~, m]=min(d_point);
    d_point(1,m)=10;
    [~,mm]=min(d_point);
    k(i,j)=((hcf_k(mm)/hcf_k(m))^((s(i,j)-hcf_s(m))/(hcf_s(mm)-
hcf_s(m))))*hcf_k(m);
    if isnan(k(i,j))
        k(i,j)=k(i,j-1);
    end
end

    eva_q(1,j)=k(1,j)*((80000-s(1,j))/9.807-dz*(cos(alfa))^2)/dz*area;
    if eva_q(1,j)>flux_eva
    eva_q(1,j)=flux_eva;
    end

    k1=[k(:,j); 0];k2=[0; k(:,j)]; k3=(2*k1.*k2)./(k1+k2);k3(1)=[];k3(length(k3))=[];
    if pc==1
    k3_predictor=k3;
    else
    k3_corrector=k3;
    end

    s1=[s(:,j); 0];s2=[0; s(:,j)];s3=s1-s2;s3(1)=[];s3(length(s3))=[];
    if pc==1
    s3_predictor=s3;
    else
    s3_corrector=s3;
    end
```

```
if pc==1
q(:,j)=(k3).*(s3/9.807+dz*cos(alfa))/dz*area;
else
k3=(k3_predictor+k3_corrector)/2;
s3=(s3_predictor+s3_corrector)/2;
q(:,j)=(k3).*(s3/9.807+dz*cos(alfa))/dz*area;
end
q1=[q(:,j);0];q2=[-eva_q(1,j);q(:,j)];q3=q2-q1;
if BC==0
   q3(length(q3))=(q(b-1,j)-bint);
else
   q3(length(q3))=((2*t(b-1,j)-t(b-2,j))-t(b,j))/multiplier;
end
q3=q3*multiplier;

t3=t(:,j)+q3;

%water distribution algorithm for drying
excess=-t3+teta_r;
excess(excess(:)<0)=0;
distributed=sum(excess);
if distributed>0
   detect=find(excess>0);
   distributed_kk=0;
   for nn=1:length(detect)
      for kk=detect(nn):b
         if kk==b
         t3(kk)=teta_r;
         break
         end
         if kk==detect(nn)
         t3(kk)=teta_r;
         distributed_kk=distributed_kk+excess(nn);
         end
         if distributed_kk>0
         if t3(kk+1)-distributed_kk>=teta_r
         t3(kk+1)=t3(kk+1)-distributed_kk;
         distributed_kk=0;
         break
         else
         distributed_kk=distributed_kk-t3(kk+1)+teta_r;
         t3(kk+1)=teta_r;
         end
         end
      end
```

```
      end
    end

end
end
```